2017

Spatial and Temporal Compressive Sensing for Vibration-based Monitoring: Fundamental Studies with Beam Vibrations

Vaahini Ganesan
University of Central Florida

SPATIAL AND TEMPORAL COMPRESSIVE SENSING FOR VIBRATION - BASED MONITORING: FUNDAMENTAL STUDIES WITH BEAM VIBRATIONS

by

VAAHINI GANESAN
B.E. Electrical and Electronics Engineering, Anna University, India, 2011
M.S. Mechanical Engineering, University of Central Florida, USA, 2014

A dissertation submitted in partial fulfilment of the requirements
for the degree of Doctor of Philosophy
in the Department of Mechanical and Aerospace Engineering
in the College of Engineering and Computer Science
at the University of Central Florida
Orlando, Florida

Summer Term
2017

Major Professor: Tuhin K. Das & Jeffrey L. Kauffman

ABSTRACT

Vibration data from mechanical systems carry important information that is useful for characterization and diagnosis. Standard approaches rely on continually streaming data at a fixed sampling frequency. For applications involving continuous monitoring, such as Structural Health Monitoring (SHM), such approaches result in high data volume and require powering sensors for prolonged duration. Furthermore, adequate spatial resolution, typically involves instrumenting structures with a large array of sensors. This research shows that applying Compressive Sensing (CS) can significantly reduce both the volume of data and number of sensors in vibration monitoring applications. Random sampling and the inherent sparsity of vibration signals in the frequency domain enables this reduction. Additionally, by exploiting the sparsity of mode shapes, CS can also enable efficient spatial reconstruction using fewer spatially distributed sensors than a traditional approach. CS can thereby reduce the cost and power requirement of sensing as well as streamline data storage and processing in monitoring applications. In well-instrumented structures, CS can enable continuous monitoring in case of sensor or computational failures.

The scope of this research was to establish CS as a viable method for SHM with application to beam vibrations. Finite element based simulations demonstrated CS-based frequency recovery from free vibration response of simply supported, fixed-fixed and cantilever beams. Specifically, CS was used to detect shift in natural frequencies of vibration due to structural change using considerably less data than required by traditional sampling. Experimental results using a cantilever beam provided further insight into this approach. In the experimental study, impulse response of the beam was used to recover natural frequencies of vibration with CS. It was shown that CS could discern changes in natural frequencies under modified beam parameters. When the basis functions were modified to accommodate the effect of damping, the performance of CS-based recovery further improved. Effect of noise in CS-based frequency recovery was also studied. In

addition to incorporating damping, formulating noise-handling as a part of the CS algorithm for beam vibrations facilitated detecting shift in frequencies from even fewer samples. In the spatial domain, CS was primarily developed to focus on image processing applications, where the signals and basis functions are very different from those required for mechanical beam vibrations. Therefore, it mandated reformulation of the CS problem that would handle related challenges and enable the reconstruction of spatial beam response using very few sensor data. Specifically, this research addresses CS-based reconstruction of deflection shape of beams with fixed boundary conditions. Presence of a fixed end makes hyperbolic terms indispensable in the basis, which in turn causes numerical inconsistencies. Two approaches are discussed to mitigate this problem. The first approach is to restrict the hyperbolic terms in the basis to lower frequencies to ensure well conditioning. The second, a more systematic approach, is to generate an augmented basis function that will combine harmonic and hyperbolic terms. At higher frequencies, the combined hyperbolic terms will limit each other's magnitude, thus ensuring boundedness. This research thus lays the foundation for formulating the CS problem for the field of mechanical vibrations. It presents fundamental studies and discusses open-ended challenges while implementing CS to this field that will pave way for further research.

I dedicate this work to my mother, Vimala Devi and father, Ganesan. Thank you for giving me a dream and making it possible. I am also dedicating this work to my husband and best friend, Janardan. I will always be grateful for your unwavering support.

ACKNOWLEDGMENTS

PhD is a long interesting journey that demands dedication, patience and presents not just challenges, but surprising twists - some of them, pleasant. At different points during this journey, I've had the opportunity to get to know very knowledgeable, helpful and supportive people, without whom this day would not have been possible.

I would like to thank my advisors, Dr. Tuhin K Das and Dr. Jeffrey L Kauffman for their unwavering support throughout my PhD. I will always be grateful for your valuable time and efforts in helping me build my career. I would also like to thank my committee members Dr. Alain Kassab and Dr. Nazanin Rahnavard for their valuable time and suggestions during my PhD. I would also like to acknowledge the late Dr. Suhada Jayasuriya, who was the primary source of inspiration for this work.

My family has always been my wall of support and I am forever grateful to them. I want to acknowledge my parents, Vimala Devi and Ganesan, my husband, Janardan and his family, my sister, Poornima, my brother-in-law Prasath and my niece, Pratya. Thank you for the encouragement and standing by me throughout this journey.

My labmates have played an integral role throughout my PhD. Thank you Singith, Paty, Sadaf, Bilal, Amjad and Dhanushka for the invaluable support and most importantly, for creating a great environment that will always be a cherished memory. I would also like to acknowledge Jeanine, Lynn and the other MAE staff that have helped me out throughout my PhD. Thank you for tirelessly answering all my questions and for being the great team that you are.

This acknowledgement would be incomplete without thanking my friends at UCF, who have made every moment of this endeavor a wonderful memory.

TABLE OF CONTENTS

LIST OF FIGURES

LIST OF TABLES

CHAPTER 1: INTRODUCTION

Detecting and locating changes in structures is an important field of research, as it has a direct impact on safety and reliability. During their service lifetime, structural components undergo changes in their characteristics [1]. Over a period of time, these changes accumulate and may result in damage or failure of the component. The aging infrastructure of the United States, that continues to experience an ever-increasing demand on performance and reliability is a case in point [2]. Failure of machinery or their components result in huge monetary losses for industries as well. Early detection and location of these changes is therefore important and it enables prolonged performance of the components or of the structure. In this regard, the literature is very elaborate and encompasses several approaches to addressing the problem. Non- Destructive Evaluation techniques such as Guided Wave Testing (GWT), eddy current methods, etc. are some common methods that are used to identify and locate changes in structural characteristics [3,4]. There are 2 basic approaches to GWT - (i) Pulse echo and (ii) Pulse catch. The pulse echo system consists of an actuator that generates a narrow bandwidth pulse of guided wave, which propagates through the structure, detects a discontinuity and is reflected back to the sensor. The latter is a simpler approach where the signal generated by the actuator is detected and analyzed by a sensor on the other end after its propagation through the structure. Damages are identified based on changes in the features of this propagated pulse [5]. Vibration-based monitoring is another well-established approach in detecting and locating structural changes [6] and is heavily invested in exploring sensing systems and damage indicating signatures that are the most accurate and robust. In this quest for accuracy, the over-burdening of data acquisition systems is ignored, which results in the generation of a large volume of data that is arguably redundant. The focus of this research is therefore to develop an elegant vibration - based monitoring scheme that would allow to work with fewer data and minimal number of sensors without compromising on accuracy of detecting and locating changes in

structural characteristics. A brief insight into vibration based techniques is provided in the next section.

Vibration Based Monitoring

Vibration-based condition monitoring of machines and mechanical structures is an established method [7, 8] and it has found applications in Structural Health Monitoring (SHM) in recent years. Mechanical components such as shafts, wind turbine blades, etc. inevitably undergo vibrations in their operating environment. These vibrations inherently carry signatures in temporal and spatial domains which reflect changes in structural characteristics, thus enabling detection and localization of these changes [3, 4]. Vibration-based detection methods are also popular in civil engineering structures such as bridges [9–11], for monitoring their structural health. When excited by some force, the response of any structure or component can be measured as a function of time as well as of space. Consequently, based on the domain in which the response is obtained, vibration-based monitoring approaches are broadly classified into two categories - (i) Temporal and (ii) Spatial.

Temporal methods include analysis of modal parameters such as natural frequencies of vibration, Frequency Response Function (FRF) and other performance comparison parameters that are derived from comparing modified vibration responses in the time domain against baseline (undamaged) response. Measuring and monitoring the transmissibility function between the DOFs of a structure, modeled as a multi-DOF system, is another time domain method for vibration based monitoring. Correlation coefficients between the time histories of strain data is another useful parameter that can help in this regard. While temporal techniques are effective in detecting changes in structural characteristics, localizing these changes calls for examination of these vibration responses in the spatial domain. The problem of identifying and localizing changes therefore becomes spatio-temporal in nature. Modeshape, quite literally ‘shape of a mode’ is the spatial

counterpart of a natural frequency. Changes in structural characteristics, in addition to shifting natural frequencies, may therefore reflect changes in modeshapes which constitute the vibration response in the spatial domain. To enhance sensitivity to change in structural characteristics, the first or second derivative of modeshapes may be used as well. Concentration of modal strain energy to a specific mode as a result of change is called mode localization, which is another damage indicator worth mentioning. Other such indicators in this domain include Modal Assurance Criterion (MAC) and Coordinate Modal Assurance Criterion (COMAC), both of which are obtained from measuring modeshapes before and after change. Operation deflection shapes (ODS) is typically a mixture of several modes and is the physical pattern the structure takes while undergoing vibration. Hence, it is an important and direct spatial attribute that may indicate and localize damage. For this reason, this research adopts ODS as a potential candidate for investigating changes in structural characteristics. A detailed analysis of both temporal and spatial approaches is provided in Section 2. Although vibration based monitoring is widely practiced, for greater reliability and accuracy, it requires greater amount of data. Hence, the effectiveness of such an approach comes at the expense of the data acquisition system.

Drawbacks of Vibration Based Monitoring

As mentioned in the previous section, while a plethora of techniques are available for vibration-based monitoring, they mostly involve instrumenting a given structure with as many sensors as possible. Thereafter, data extraction follows the traditional approach of Nyquist-Shannon's sampling theorem, which states that for good frequency recovery and subsequent signal reconstruction, the sampling rate has to be at least twice the highest frequency content of the signal [12]. In addition, fourier transform methods such as FFT (Fast Fourier Transform) set a requirement on the duration of data capture. Further, advancements in sensor systems and the drop in their costs have led to sensing proliferation as well. The immediate consequence is generation of large volumes of

data that in turn contributes to computational burden and increased power requirement, [13]. Because conventional signal reconstruction methods show a better performance with greater amount of data, in both time and space, spatial distribution of sensors are also dense. In most cases in literature, these projects are implemented on a research or experimental level, thereby eliminating the need to consider financial impact. To make a vibration based monitoring system commercially viable, it would be very important to reduce the amount of data generated as a function of time and in spatial distribution as well.

A thorough literature-review of existing vibration-based monitoring and diagnostic techniques used in SHM are discussed in Chapter 2. The problem statement for this research and proposed solution are explained in Chapter 3. A detailed background of beam vibration and compressive sensing is provided in Chapter 4, which prepares the reader to understand the problem formulation for this research and presents the rationale for proposing a CS based monitoring scheme for detection and localization of structural changes. Primary results achieved thus far are presented in Chapter 5 and this lays the groundwork for future scope of the project presented in Chapter 6. Finally concluding remarks are made and references are provided.

CHAPTER 2: LITERATURE REVIEW

Vibration-based SHM employs suitable in-situ active or passive transducers in order to analyze the characteristics of the structure in time, frequency, and modal domains [14–18]. Earliest approaches to this type of SHM involved comparison of modal properties of the damaged structure against an undamaged baseline of the same structure. Areas of application include structures such as bridges and wind turbines, [4, 9, 10, 19]. All vibration-based SHM methods rely heavily on time-history response of a structure that can be acquired using sensors such as accelerometers, strain gauges, etc. Modal parameters are then extracted by transforming the response into frequency domain, [20].

Looking more closely, detecting changes in the natural frequencies of a structure remains important in vibration-based SHM, [6]. Although theoretically sound, it was shown that with increasing severity of damage, natural frequencies exhibited a more distributed shift as opposed to localized shift, [16, 21, 22]. The effect of the geometry of damage on the shift was studied in [23, 24]. Sensitivity of frequency shifts to damage and ambient variations has also been of interest, [25, 26]. In addition, experimental validations have been conducted on actual structures, [27–29]. Frequency Response Functions (FRF) have been utilized to determine natural frequencies and their shifts, [30–32]. Here, fault localization is suggested by collecting the FRF from multiple sensors at different locations of the structure. However, as mentioned earlier, FRF accuracy will depend on the number and location of sensors, [14, 33, 34]. Analyzing transmissibility function between the degrees of freedom and measuring the transmission coefficient for detecting structural change have been explored also, [35]. The review indeed confirms that while the shifting of natural frequencies is an indicator of structural change, it is not an effective means of locating the same. This brings the topic of spatial characterization in SHM.

As explained in Section 1, the spatial counterpart of natural frequency may help in localization

of structural change. Therefore, modeshape extraction from the response of structures, for detection and localization of damage, became popular, [20, 36]. One technique is measuring similarity between a specific mode shape of a structure in its healthy and damaged states using Modal Assurance Criterion (MAC), [37]. A MAC value of 0 indicates complete dissimilarity and hence severe damage, while a value of 1 indicates complete similarity between the two compared mode shapes. Coordinate Modal Assurance Criterion (COMAC), an advancement of MAC, measures the difference between the two mode shapes point-to-point and hence clearly locates the damage. Like the MAC, this method again takes values between 0 and 1 to indicate the presence and severity of damage [38, 39]. A disadvantage of mode shapes based SHM is the large amount of data that is required in order to make reliable and accurate detection [14]. Additionally, mode shape data is polluted by noise and measurement errors that affect their sensitivity to damage. A solution to by-pass this problem can be to measure the first (slope) or second (curvature) derivatives of the mode shape itself, [40]. Nevertheless, the mode shape based SHM method is widely studied and applied in experiments as well, [14, 41–51].

Mode localization is a phenomenon in which the modal strain energy is confined to a specific mode due to damage or change in structural characteristics. This energy concentration is another feature that can be beneficial to detect as well as locate damage in a structure [15,49,52–54]. Measurement of correlation coefficients between time histories of strain data of a structure before and after damage can be a useful tool for damage detection as well its localization [55]. Quite similar to the MAC and COMAC, the correlation coefficient takes values between $+1$ and -1, with $+1$ indicating highest correlation or no damage and -1 indicating maximum severity of damage. Another related method of extracting spatial information is by reconstructing the Operational Deflection Shapes (ODS), [56]. ODS are superposition of mode shapes and provide a physical view of the vibration of a structure, [14, 57]. Any change in structural characteristics will therefore distort the vibration pattern of the structure or component, which will be a clear indicator of damage and may help

in locating the change as well. Other related techniques for structural monitoring include Guided Wave Testing (GWT) [5], imaging and pattern recognition, [58], and Wavelet transforms, [59–63].

Spatial wavelet analysis for damage detection and localization is a recent approach that has gained popularity. However, inherent distortions in wavelet transform induces the possibility that damages near the boundaries of structures may be undetectable. In [64], the authors address this drawback by employing a novel padding method to the vibration response while using Continuous Wavelet Transform. Ultimately, all vibration-based monitoring methods necessitate acquiring a large amount of data which, as previously explained, limits their commercial viability.

CHAPTER 3: RESEARCH FOCUS AND MOTIVATION

The problem statement for this research work and the significance of addressing the issue are discussed in this section. In addition, a potential solution is laid out, the details of which are presented in the rest of the dissertation.

Problem Statement

From literature, it is evident that vibration based monitoring encompasses several approaches, both in the temporal and spatial domains, all of which share one requirement in common - *bulk amount of data*. In the temporal domain, this translates to large time histories of data, while in the spatial domain, this implies instrumenting a given structure with a large number of sensors. This is a major setback for vibration based monitoring techniques that needs to be addressed. To reiterate, it is important to develop a vibration based monitoring system that would operate on fewer data without compensating on reliability and accuracy of results. This becomes the focus of this research.

Impacts of Large Data Requirement

Requiring large volume of data has undesirable impacts on many levels. First of all, it increases the storage and computational burden on data acquisition systems. Greater amount of data requires greater number of sensors, that contributes to elevation of power requirement thereby adding to operational cost. Although sensor systems today are well developed and efficient, instrumenting a structure with a large number of sensors compromises on the ease of installation, maintenance and repair or modification processes. Owing to these practical constraints, most of the approaches

discussed in the literature have not progressed beyond laboratory stages.

While considering cutting down on amount of data gathered, the first question to answer would be *'How much data is really required?'*. Considering that most of the data is redundant and is only required because of the algorithm for signal recovery and reconstruction, it would be prudent to examine the literature for a reconstruction scheme that would perform better than conventional methods and with lesser data. One such sampling technique is Compressive Sensing, that allows for signal reconstruction from randomly placed reduced number of samples, provided the signal is sparse, i.e. has very few significant coefficients when expressed in a suitable domain. The details of this approach and the rationale to employ it for analyzing beam vibrations are discussed in the sections to come.

Proposed Solution

Simply put, compressively sampled vibration based monitoring is proposed as a potential solution to the research problem. As mechanical and civil engineering structures become more complicated and their performance standards are raised, monitoring and diagnostics will increasingly become more challenging. Hence, in spite of faster computational speeds and superior sensor technologies, it is imperative that the efficiency of condition monitoring be improved. Higher efficiency of monitoring implies reduced sensing requirement, low computational burden, and a greater flexibility of sensing.

In [65], the authors recognized the importance of down-sampling and investigated its effect on damage detection in the spatial domain. In this paper, the application of Compressive Sensing (CS) to vibration-based monitoring, [66], is proposed in order to achieve reduced sensing. While this approach is still in its nascent stages, an important related work in literature is [67], where the authors evaluated the ability of CS to compress vibration data from civil structures. In [68],

spatial interpolation of the impulse response of a vibrating plate using sub-Nyquist sampling was investigated. Spatial sparsity may also be exploited for source localization of acoustic waves [69], [70].

In vibration- based monitoring, these attributes can be incorporated by applying Compressive Sensing [66]. For data reduction, the combination of vibration-based monitoring and Compressive Sensing (CS) is optimal, since the former offers sparsity which the latter fundamentally requires. The approach is also less reliant on mathematical modeling and model-based computations. This research develops the foundation for CS based monitoring for lateral vibration of beams and intends to extend it further to incorporating related issues such as handling noisy data, quantifying structural changes and damage signatures, compensation for non-synchronized time data and development of a combined spatio-temporal framework.

CHAPTER 4: FUNDAMENTALS OF BEAM VIBRATION AND COMPRESSIVE SENSING

Background on the fundamentals of lateral beam vibrations and the effect of structural changes are provided in this section. Using simulations, the use of CS in detecting change in natural frequencies and spatial reconstruction of deflection shape for detecting and locating structural changes are demonstrated in this chapter. Sparsity of beam vibrations and the rationale for using CS in vibration-based monitoring are introduced here also.

Beams are continuous mechanical systems that can be used to represent different kinds of structural components such as shafts, wind turbine blades, building structures, etc. The vibration characteristics of beams in their operating environment change with progression of faults or other introduced structural changes. In the next two sections, we discuss the basics of beam vibrations and demonstrate how structural changes in the beam produces changes in vibration characteristics through simulations.

Lateral Vibration Response as Weighted Sum of Modeshapes

The equation of motion of a uniform *Euler-Bernoulli Beam* is given by Eq.(4.1), [7]:

$$EI\frac{\partial^4 y(x,t)}{\partial x^4} + \rho A\frac{\partial^2 y(x,t)}{\partial t^2} = f(x,t) \tag{4.1}$$

where, $y(x,t)$ is the lateral response of the beam, $f(x,t)$ represents forcing on the beam, E is the elastic modulus, I is the second moment of area, ρ is the density of the material and A is the area of cross section in m^2, all expressed in appropriate units. The response of the beam can be expressed

as a weighted sum of its modeshapes as shown below,

$$y(x,t) = \sum_{q=1}^{\infty} T_q(t) W_q(x). \tag{4.2}$$

Here, the q^{th} mode is represented by its mode shape $W_q(x)$, with principal co-ordinate $T_q(t)$, attached to it. In its most general form, $T_q(t)$ is influenced by both transient (free) and forced vibration components and can be expressed as, [7]:

$$\begin{gathered} T_q(t) = A_q \cos(\omega_q t) + B_q \sin(\omega_q t) + \tfrac{1}{\rho A b \omega_q} \int_0^t Q_q(\tau) \sin(\omega_n (t-\tau)) d\tau \\ b = \int_0^L W_q^2(x) dx, \quad Q_q(t) = \int_0^L f(x,t) W_q(x) dx \end{gathered} \tag{4.3}$$

In Eq.(4.3), A_q and B_q are constants obtained from initial conditions, L is the length of the beam, and ω_q is the q^{th} natural frequency of vibration. Therefore, in effect, both free as well as forced vibration responses of a beam can be expressed as a weighted sum of mode shapes. Specifically, from Eqs.(4.2) and (4.3), the general structure of free vibration response of a beam is

$$y(x,t) = \sum_{q=1}^{\infty} \left[A_q \cos(\omega_q t) + B_q \sin(\omega_q t) \right] W_q(x) = \sum_{q=1}^{\infty} \left[\bar{A}_q(x) \cos(\omega_q t) + \bar{B}_q(x) \sin(\omega_q t) \right], \tag{4.4}$$

where ω_q, $q = 1, 2, \cdots$, are the natural frequencies, $W_q(x)$ is the q^{th} mode shape, $\bar{A}_q(x) = A_q W_q(x)$ and $\bar{B}_q(x) = B_q W_q(x)$. As expressed in Eq.(4.4), theoretically, the free vibration response of the beam is a combination of all its modes ($q = 1, 2 ... \infty$). However, given an initial deflection profile, $y(x,0)$, the modes present in that profile are manifested in the response. Similarly, the response of a beam to harmonic forcing $f = f_0 \sin(\omega_f t)$, applied at location x, takes the form

$$y(x,t) = \sum_{q=1}^{\infty} \left[D_q(\omega_q, \omega_f) f_0 \sin(\omega_f t) \right] W_q(x) = \sin(\omega_f t) \sum_{q=1}^{\infty} \bar{D}_q(\omega_q, \omega_f, f_0) W_q(x). \tag{4.5}$$

The expression $\sum_{q=1}^{\infty} \bar{D}_q(\omega_q, \omega_f, f_0) W_q(x)$ is the Operational Deflection Shape (ODS). The ODS is a constant shape that is maintained at any time when the operational forcing frequency remains unchanged. Furthermore, it is a linear combination of mode shapes $W_q(x)$ and predominantly contains those modes that lie in close proximity to the forcing frequency. Vibration response of a beam carries two types of signatures, namely: (i) the natural frequencies ω_q in time domain, and (ii) the mode shapes $W_q(x)$ in the spatial domain. A change in a beam's characteristics, for instance due to damage or deterioration, causes these signatures to change. Vibration-based monitoring of structures rely on detecting and quantifying these changes. The next section illustrates how structural changes or faults are manifested in natural frequencies of vibration and ODS.

Identifying Structural Change Using Vibrational Signatures

A finite-element (FEM) simulation of a simply supported beam illustrates changes in vibrational characteristics. The structural parameters for the beam are assumed to be: $EI = 1$, $\rho A = 1$, $L = 5$ in consistent units. The beam is modeled using 100 elements and simulated with boundary conditions of $y(0,t) = y(L,t) = y''(0,t) = y''(L,t) = 0$. A schematic is shown in Fig.4.1(a).

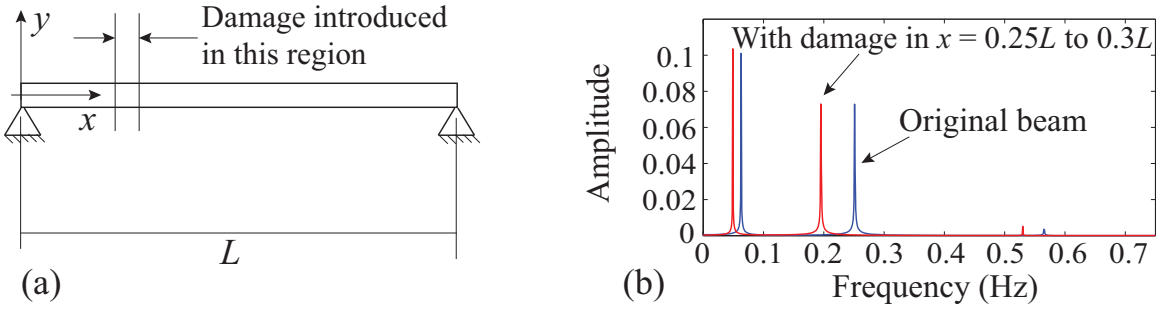

Figure 4.1: (a) Uniform simply-supported beam, (b) Shift in natural frequencies due to damage

To demonstrate the change in characteristics, the value of EI was reduced from 1 to 0.1 in elements $25 - 30$, to simulate a damage. Shifts in natural frequencies were extracted from free vibration response of the point $x = 0.75L$ using Fast Fourier Transform (FFT), and are shown in Fig.4.1(b). Frequency shifts can be initial indicators of a developing change or damage in a beam. However, they are not a direct indicator of the location of the damage. The question of localizing a damage can be addressed by the Operational Deflection Shapes (ODS). To demonstrate this, the response of the simply-supported beam under a harmonic forcing of $f = \sin(0.5t)$ applied at $a = L/5$, as shown in Fig.4.2(a), was simulated. Faults were introduced at different segments along the span of the beam. The resulting ODS, shown in Fig.4.2(b), were generated for each damage scenario. The figure shows that the distortion in the ODS can be used to determine the location of a damage.

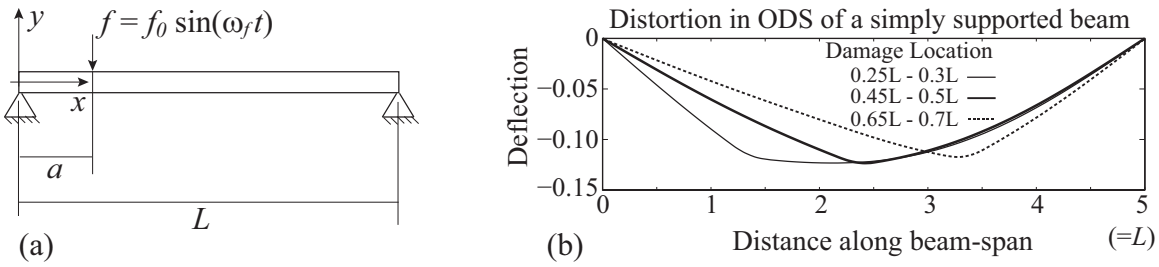

Figure 4.2: (a) Uniform simply-supported beam under harmonic forcing, (b) ODS of beam showing distortions

Compressive Sensing

Compressive Sensing (CS) deals with frequency recovery and reconstruction of an under-sampled signal from random, linear and non-adaptive measurements when the signal is sparsely represented in a proper basis, [66]. The CS problem refers to finding a sparse solution $\hat{s} \in R^n$, with sparsity k

(i.e. with $\leq k$ nonzero entries), of the equation

$$\Phi s = z, \tag{4.6}$$

given a vector of measurements $z \in R^m$ and a measurement matrix $\Phi \in R^{m \times n}$ with $m < n$. The sparsest solution of the aforementioned under-determined set of equations is obtained from the l_0 minimization of s, which is NP-Hard to compute, [66]. An alternative that is less computationally intensive is the ℓ_1 minimization of s, which is given as

$$\hat{s} = argmin \|s\|_{\ell_1} : \quad \text{subject to} \quad \Phi s = z, \tag{4.7}$$

where $\|s\|_{\ell_1} = \sum_{i=1}^{n} |s_i|$. The equivalence of the ℓ_1 solution to ℓ_0 is guaranteed under an additional condition on Φ, namely the ***Restricted Isometry Property (RIP)*** [71], which will be discussed in the sections to come. The ℓ_1 minimization is a convex optimization problem [72], and therefore easier to solve computationally. When the number of measurements m is of the order [73],

$$m \simeq O\left(k \ ln(n/k)\right), \tag{4.8}$$

a carefully designed Φ satisfies RIP of order $2k$, thus allowing for the sparse solution to be obtained with overwhelming probability. In Eq.(4.8), k is the number of non-zero entries in s and hence represents its sparsity. While this result was originally derived for random matrices mostly, CS maybe extended to recovery of signals that have other types of expansions as well [73]. In the application to beam vibration, Φ is determined based on the beam response equation in temporal and spatial domains.

An example of frequency recovery using compressive sampling, from a given signal in time domain, is discussed next.

An Example of Compressive Sensing

Consider a signal $y(t)$ that can be expressed as $y(t) = \sum_{i=1}^{n} a_i \sin(\omega_i t)$. Further, assume that the vector $s = [a_1\, a_2 \cdots a_n]^T$ is k-sparse, i.e. only $k(< n)$ entries of s are non-zero. Let the corresponding frequency range for y be denoted by $\Omega_n \in [\omega_1, \omega_n]$. The CS problem, Eq.(4.6), can be posed as: *find the k-sparse solution $\hat{s}$ from m measurements of y, i.e. from $z_j = y(t_j)$, where* $j = 1, 2, \cdots m$. The vector $z = [z_1\, z_2 \cdots z_m]^T$ consists of measurements made at random instants, and $\Phi \in R^{m \times n}$ is constructed as $\Phi_{j,i} = \sin(\omega_i t_j)$. A lower bound on m is obtained from Eq.(4.8). Thus, Eq.(4.6) takes the form

$$z = \Phi s \quad \Rightarrow \quad \begin{bmatrix} z_1 \\ z_2 \\ \vdots \\ z_m \end{bmatrix} = \begin{bmatrix} \sin(\omega_1 t_1) & \sin(\omega_2 t_1) & \cdots & \sin(\omega_n t_1) \\ \sin(\omega_1 t_2) & \sin(\omega_2 t_2) & \cdots & \sin(\omega_n t_2) \\ \vdots & \vdots & \cdots & \vdots \\ \sin(\omega_1 t_m) & \sin(\omega_2 t_m) & \cdots & \sin(\omega_n t_m) \end{bmatrix} \begin{bmatrix} a_1 \\ a_2 \\ \vdots \\ a_n \end{bmatrix}.$$

For this example, the following signal is considered, y(t) = $\sin(\pi t) - 0.5 \sin(4\pi t)$. In posing the CS problem, the frequency range considered is $\Omega_n \in [0,\, 2.5]$Hz, $k = 2$, the frequency resolution chosen is $\Delta f = 0.1$Hz, implying $n = 26$. Using the lower bound obtained from Eq.(4.8), we choose $m = 7$. In Φ shown above, $\omega_i = (2\pi f_i)$rads^{-1}, where $f_i = [0,\, 0.1,\, 0.2 \ldots 2.4,\, 2.5]$Hz. Figure 4.3 illustrates two trials of frequency recovery using random sampling. The first trial is shown in Figs.4.3(a) and (b), while the second one is depicted in Figs.4.3(c) and (d). In each trial, the samples are arbitrarily chosen and the ℓ_1 minimization is carried out using the ℓ_1-magic code available as open source from statweb.stanford.edu. It can be observed that the desired frequencies are recovered at exact amplitudes in both the trials, irrespective of sample distribution.

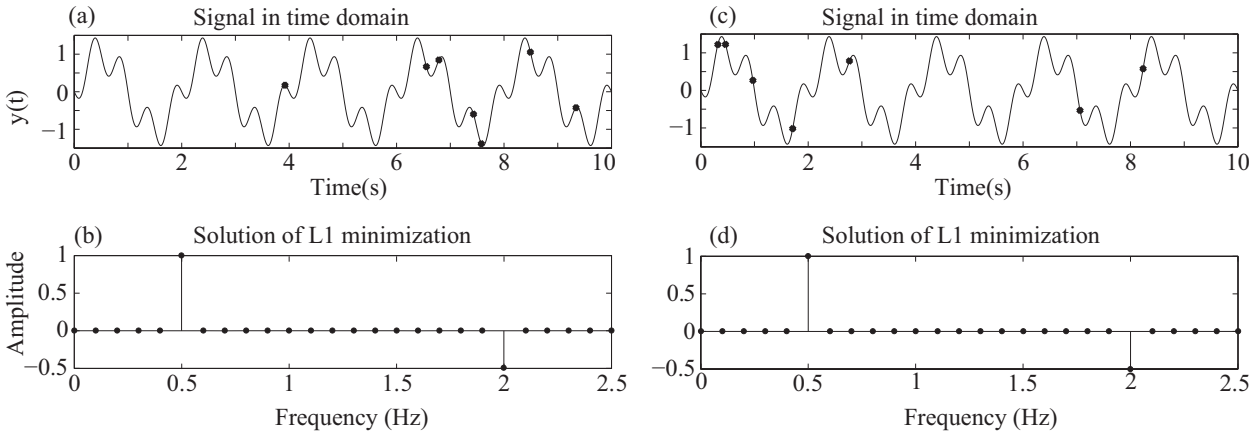

Figure 4.3: Frequency recovery using Compressive Sampling from 2 Sets of Random Samples

As mentioned above, the design of Φ is important for CS to be effective. To this end, Φ must satisfy a *Restricted Isometry Property*, explained in the next section.

Restricted Isometry Property (RIP)

The reconstruction of an under-sampled signal (without loss of important information) requires the design of a suitable measurement matrix Φ and that the signal be represented in a proper basis where it is k-sparse. For a high probability of reconstruction, Φ needs to satisfy the Restricted Isometry Property (RIP). In addition, as stated earlier, satisfying RIP also guarantees that the ℓ_1 minimization solution coincides with that ℓ_0. A matrix Φ is said to satisfy RIP of order k if its *Restricted Isometric Constant* δ_k satisfies $0 < \delta_k < 1$. The constant δ_k is defined as the smallest value satisfying

$$(1 - \delta_k) \leq \frac{\|\Phi v\|_2^2}{\|v\|_2^2} \leq (1 + \delta_k), \tag{4.9}$$

for all vectors v with sparsity $\leq k$, [66]. Satisfying the RIP implies that all the column sub-matrices of Φ are well conditioned. These attributes lead to high probability of signal recovery by

CS, [66, 71]. For a given k, δ_k for a matrix $\Phi \in R^{m\times n}$ can be determined numerically by applying the condition

$$(1-\delta_k) \leq \lambda_{min}(\Phi_T'\Phi_T) \leq \lambda_{max}(\Phi_T'\Phi_T) \leq (1+\delta_k) \tag{4.10}$$

for all sub-matrices $\Phi_T \in R^{m\times p}$ that can be formed from any p columns of Φ, with $1 \leq p \leq k$. In practice, however, $\delta_k \geq 1$ is not forbidden; it would simply mean that the stability of recovery under noise and the closeness of the ℓ_1 solution to ℓ_0 solution may not be well guaranteed, [74]. In order to quantify RIP better, consider the example of Section 4. Since $k = 2$ in this example, we need to determine δ_2. For the given $m \times n$ (7×26) Φ matrix, we determined $\delta_2 = 0.95$. Thus $\delta_2 < 1$, and frequency recovery was reliable with high probability. Increasing the number of measurements m to 20 yielded $\delta_2 = 0.63$, which is expected. A third scenario, with $n = 16$ and $m = 7$, yielded $\delta_2 = 0.84$.

Sparsity in Beam Vibration: The Rationale for Adopting Compressive Sensing

Consider the problem of recovering the natural frequencies and ODS from vibration data of beams. This is of significance for detecting and locating structural damages. Traditionally, the vibration characteristics can be reconstructed from data using the Nyquist-Shannon Sampling Theorem, [12]. According to this theorem, for good reconstruction of any given signal, the sampling frequency (f_s) has to be at least twice the highest frequency (f_b) contained in the signal, i.e., $f_s \geq 2f_b$. In practice, usually a much higher sampling rate is chosen, i.e. $f_s >> 2f_b$. Traditional reconstruction algorithms such as the FFT relies on this sampling paradigm and results in high data volume when high frequencies are involved and high frequency-resolution are needed. On the other hand, Compressive Sensing can allow signal reconstruction with significantly lower amount of data. It relies on sparsity of the signal in appropriate domain(s), a feature that is inherent in vibration of continuous systems.

Temporal Sparsity

Free vibration of any location on a beam is sparse in the frequency domain, since it only contains natural frequency harmonics. This is evident from Eq.(4.4). To illustrate sparsity, consider a beam vibrating with a combination of the first two natural frequencies ω_α and ω_γ. Their values are considered unknown but are known to lie in a range $\Omega_r = [0, \omega_r]$. Consider the task of recovering these frequencies from vibration data $z_i = y(\bar{x}, t_i)$ collected at a location $\bar{x}$ on the beam using a series solution, i.e.

$$z_i = \sum_{j=1}^{n} \left[a_j \cos(\omega_j t) + b_j \sin(\omega_j t) \right], \quad \omega_j = \omega_r (j-1)/(n-1). \tag{4.11}$$

Conventionally, to determine a_j, b_j, $j = 1, 2, \cdots, n$, we need $2n$ equations and hence $2n$ data points, implying $z = [z_1\, z_2\, \cdots z_{2n}]^T$. Assuming that at indices $j = p$ and $j = p'$, $\omega_p = \omega_\alpha$ and $\omega_{p'} = \omega_\gamma$, we expect $a_j = b_j = 0\ \forall\ j \neq p,\, p'$. Thus, the vector $s = [a_0\, a_1\, \cdots\, a_n\, b_0\, b_1\, \cdots\, b_n]^T$ has a sparsity of $k = 4$. Fundamentally, this sparsity implies that data lesser than $2n$ should be sufficient to determine the constants $a_p, b_p, a_{p'}, b_{p'}$. Compressive sensing capitalizes on this general idea of sparsity. By knowing that a signal is k-sparse, compressive sensing uses randomized and undersampled data, coupled with an ℓ_1 minimization algorithm, to find the sparse solution. This will be discussed in greater detail in Section 4.

Spatial Sparsity

As discussed in Section 4, ODS can be used to locate a damage/change in a beam. This requires spatial vibration data. ODS of beams also show sparsity, but in spatial-frequency domain. To explain this, note that the ODS $\sum_{q=1}^{\infty} \bar{D}_q(\omega_q, \omega_f, f_0) W_q(x)$, identified in Eq.(4.5), is a function of the mode shapes $W_q(x)$ only. The modes shapes in turn are functions of the spatial parameter β_q that

are uniquely related to the natural frequencies ω_q. For instance, for uniform beams under lateral vibration $\omega_q = \beta_q^2\sqrt{EI/\rho A}$, and a general expression of a mode-shape is $W_q = C_q \sin(\beta_q x) + F_q \cos(\beta_q x) + G_q \sinh(\beta_q x) + H_q \cosh(\beta_q x)$, satisfying appropriate boundary conditions. The ODS thus takes the form

$$y_{ODS}(x) = \sum_{q=1}^{\infty} \bar{D}_q(\omega_q, \omega_f, f_0) W_q(x) = \sum_{q=1}^{\infty} \bar{C}_q \sin(\beta_q x) + \bar{F}_q \cos(\beta_q x) + \bar{G}_q \sinh(\beta_q x) + \bar{H}_q \cosh(\beta_q x), \tag{4.12}$$

which has a similar structure as Eq.(4.4), except it is in spatial domain with spatial frequencies β_q. The ODS, Eq.(4.12), is sparse in spatial-frequency since $\beta_q = f(\omega_q)$ and sparsity exists in the temporal frequency (i.e. ω) domain. This is the rationale for applying compressive sensing to ODS reconstruction, which amounts to requiring fewer spatially distributed sensors. In addition to the ODS, free vibration of beams also shows spatial sparsity. This can be shown from Eq.(4.4). However, the deflection shape of free vibration varies with time. Thus, ODS is deemed a preferred candidate for spatial reconstruction, and for comparison with baseline data to locate faults.

Quantitative Comparison of CS and Nyquist-Shannon Sampling Theorem

For a quantitative comparison between CS and the traditional sampling, we consider the reconstruction of the following signal: y(t) = $\sin(0.3\, 2\pi t) + 0.5 \sin(1.7\, 2\pi t)$. In posing the CS problem, the frequency range considered is $\Omega_r \in [0,\ 2.5]$Hz, $k = 2$, and the frequency resolution chosen is $\Delta f = 0.1$Hz, implying $n = 26$. Using the lower bound obtained from Eq.(4.8), we choose $m = 10$. In Φ shown above, $\omega_i = (2\pi f_i)$rads^{-1}, where $f_i = [0,\ 0.1,\ 0.2 \ldots 2.4,\ 2.5]$Hz. Figure 4.4(a) illustrates the signal and the random samples. The ℓ_1 minimization was carried out using the ℓ_1-magic code. Frequency recovery through ℓ_1 minimization is shown in Fig.4.4(b). It can be observed that correct frequencies and amplitudes are recovered from only 10 samples.

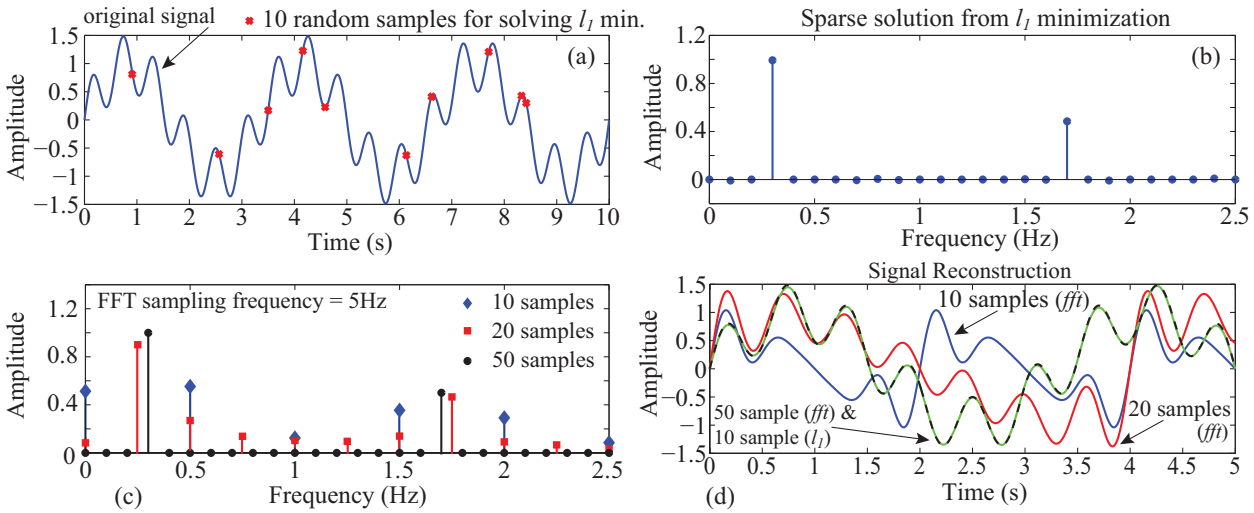

Figure 4.4: (a) Signal and random samples, (b) Sparse solution from ℓ_1 optimization, (c) FFT of the signal with different number of samples, (d) Signal recovery with compressive sensing and FFT

To compare with traditional sampling, the above signal was sampled at 5Hz, (so that Nyquist Frequency, 2.5Hz, is greater than the highest signal frequency 1.7Hz, [71]). Three sets of data, i.e. 10, 20 and 50 samples, were used to carry-out DFT (using the FFT algorithm). The consequent signal reconstruction in each of the three cases is achieved using those frequency components whose amplitudes are significantly above the noise level. The results are shown in Fig.4.4(c) and (d). While the ℓ_1 minimization gave accurate reconstruction with 10 samples, the reconstruction had significant errors when traditional sampling technique was used, even with 20 samples. The accuracy of ℓ_1-based reconstruction with 10 samples is at the same level as that of the reconstruction from FFT components with 50 samples. The main differences between CS and FFT based (i.e. traditional sampling) approaches are briefly explained in the following subsection.

Differences Between CS and Traditional Sampling Approaches

1. Uniform vs. Random Sampling:

The random sampling in CS effectively allows the data to be *richer* in information with fewer samples compared to regular sampling in FFT. In FFT this *richness* is achieved by increasing frequency and duration of sampling.

2. Exact vs. Probabilistic Solution:

The FFT solution is exact in the sense that the quantity of data and the number of unknowns match. In contrast, ℓ_1 optimization fundamentally relies on sparsity and solves an under-determined system iteratively. This, combined with randomness of data, can assure recovery with a certain probability, albeit a very high one if *RIP* is satisfied by Φ.

3. Volume of Data:

FFT fundamentally relies on high sampling rate for recovering a wide frequency-band and relies on high sampling duration for obtaining adequate resolution between neighboring frequencies. Both individually increase the data requirement proportionally. In CS, the data requirement is considerably more moderate, since it increases only with sparsity and in a logarithmic manner with the number of frequency components in Φ, Eq.(4.8).

4. Signal Sparsity:

The ℓ_1 optimization relies on sparsity, and hence for sparse signals CS out-performs FFT. If signal sparsity is weak, the two methods may show comparable performance.

CHAPTER 5: RESULTS AND DISCUSSION

In chapter 4, free and forced vibration responses of a beam were discussed. Changes in natural frequencies and distortions in ODS were noted for changes in structural characteristics and the sparsity of spatio-temporal vibration was discussed also. With that background, this chapter delves into the formulation of a novel CS-based vibration monitoring system, wherein the fundamentals characteristics of mechanical beam vibrations are employed to formulate the CS problem. Furthermore, it attempts to address some of the challenges that emerge from exploring the compatibility between CS and vibration based monitoring.

As a first step, temporal (natural) frequency recovery to detect changes in structural characteristics of standard mechanical beams is demonstrated. Preliminary experimental validation of these FEM-based simulation results are also presented. Next, the more complicated problem of localizing structural changes is examined. Spatial frequency recovery, the consequent ODS reconstruction and related challenges in the spatial domain are explored in detail. Furthermore, the effects of noise formulation and incorporating boundary conditions while formulating the CS-based vibration problem is also discussed [75], [76].

Frequency Recovery from Beam Vibration

Drawing background from Chapter 4, this section presents the formulation of the CS-based vibration problem for detecting structural changes in mechanical beams. Initial investigations are FEM based simulation results, that explore the recovery of distinct (natural) frequencies before (baseline) and after introducing changes by employing CS to demonstrate the feasibility of using reduced and random samples for detecting structural changes. The following sections develop this method for simply supported and cantilever beams.

A simply supported (SS) beam has both its ends pinned and is constrained to have no displacement or bending moment on either ends, as shown in Fig.5.1(a). We show the application of CS in detecting changes in its natural frequencies from free vibration data. A beam of length L is modeled with N_{el} finite elements, rigidity modulus EI, and mass density ρA_r. The free vibration response is simulated by providing an initial deflection profile $y(x,0)$. With the theoretical knowledge of baseline characteristics, the parameters for compressive sampling problem are set up following Section 4. The beam response thus obtained is compressively sampled to obtain baseline and modified natural frequencies ω_q, $q = 1, 2, \cdots$, and the shift in these frequencies allow detection of change in characteristics. From Eq.(4.4), considering that the q^{th} mode shape of an SS beam is $W_q(x) = \sin\frac{q\pi x}{L}$, and referring to Fig.5.1(a), the free vibration response at a specified distance $\bar{x}$ is given by

$$\begin{aligned} y(\bar{x},t) &= \sum_{q=1}^{\infty}(A_q\cos(\omega_q t) + B_q\sin(\omega_q t))\,W_q(\bar{x}) = \sum_{q=1}^{\infty}(A_q\cos(\omega_q t) + B_q\sin(\omega_q t))\,\sin\tfrac{q\pi\bar{x}}{L} \\ &= \sum_{q=1}^{\infty}(\bar{A}_q(\bar{x})\cos(\omega_q t) + \bar{B}_q(\bar{x})\sin(\omega_q t)), \end{aligned} \tag{5.1}$$

where $\bar{A}_q(\bar{x}) = A_q\sin\frac{q\pi\bar{x}}{L}$ and $\bar{B}_q(\bar{x}) = B_q\sin\frac{q\pi\bar{x}}{L}$. The measurement point, $\bar{x}$, is chosen such that it does not fall at the nodal point (zero displacement point) of the response. In a realistic scenario, since multiple sensors will be spatially distributed, if a sensor location coincides with a node, alternate sensors can be used for CS based recovery. Consider the goal of recovering the natural frequencies ω_q using CS, within a frequency range of $\Omega_r \in [0, \omega_r]$. Further, consider a frequency recovery resolution $\Delta\omega$. The measurement vector $z \in R^m$ is generated from m random measurements $z_j = y(t_j)$, $j = 1, 2, \cdots m$, and the matrix Φ is constructed using *sine* and *cosine* basis functions, Eq.(5.1). Since each frequency is represented by two basis functions, we expect even-sparsity in the solution of $s = [A_1\ A_2\ \cdots\ A_n\ B_1\ B_2\ \cdots\ B_n]^T$, $n = (\omega_r/\Delta\omega) + 1$, obtained

from the ℓ_1 minimum solution of Eq.(4.6). In this case, Eq.(4.6) takes the form

$$z = \Phi s \quad \Rightarrow \quad \begin{bmatrix} z_1 \\ z_2 \\ \vdots \\ z_m \end{bmatrix} = \begin{bmatrix} \cos(\omega_1 t_1) & \cdots & \cos(\omega_n t_1) & \sin(\omega_1 t_1) & \cdots & \sin(\omega_n t_1) \\ \cos(\omega_1 t_2) & \cdots & \cos(\omega_n t_2) & \sin(\omega_1 t_2) & \cdots & \sin(\omega_n t_2) \\ \vdots & \vdots & \vdots & \vdots & \vdots & \vdots \\ \cos(\omega_1 t_m) & \cdots & \cos(\omega_n t_m) & \sin(\omega_1 t_m) & \cdots & \sin(\omega_n t_m) \end{bmatrix} s$$

$$\text{where} \quad s = [A_1 \ A_2 \ \cdots \ A_n \ B_1 \ B_2 \ \cdots \ B_n]^T . \tag{5.2}$$

In Eq.(5.2), ω_i, with $i = 1, 2, \cdots, n$, represent the spanning frequencies of the range Ω_r, i.e. $\omega_i = \Delta\omega(i-1)$, $\omega_0 = 0$ and $\omega_n = \omega_r$.

To demonstrate CS, an SS beam is considered with the following specifications: $L = 1$, $\rho A_r = 1$, $EI = 1$. The natural frequencies ω_q are $[\pi^2,\ 4\pi^2,\ 9\pi^2\ \cdots]$ in rad/s, and the corresponding mode-shapes are $[\sin(\pi x),\ \sin(2\pi x),\ \sin(3\pi x), \cdots]$, [7]. Free vibration is simulated using a discrete model consisting of $N_{el} = 500$ beam elements. It is given an initial deflection profile of $y(x, 0) = 0.6\sin(\pi x/L) + 0.4\sin(2\pi x/L)$, which is a combination of the first two mode-shapes. This causes the first two natural frequencies to be manifested in the free vibration response. Typically, the proposed method can be applied to a wide variety of initial conditions and the corresponding modes will be manifested in the response. Change is introduced by reducing EI from 1 to 0.1 over elements $200 - 250$. The time domain response of the beam, before and after change, is measured at $\bar{x} = 3L/4$. The ℓ_1 minimization problem of Eq.(5.2) is setup with $\omega_r = 7$Hz $= 14\pi$rad/s and $\Delta\omega = 0.01$Hz $= 0.02\pi$rad/s. This yields $n = 701$ and we choose $m = 15$ random measurements. This is comparable to $m = 20$ suggested by Eq.(4.8), which is based on a sparsity of four for the first two natural frequencies. Note that the frequency range $\Omega \in [0, 7]$ is chosen to cover the first

two natural frequencies $\omega_q = \pi/2$Hz, 2πHz. The solutions of the two ℓ_1 minimization problems, namely before and after making changes in EI, are shown in Fig.5.1. A schematic of the beam is shown in Fig.5.1(a). Frequency recovery from data collected at $\bar{x} = 3L/4 = 0.75$ is shown in Fig.5.1(b).

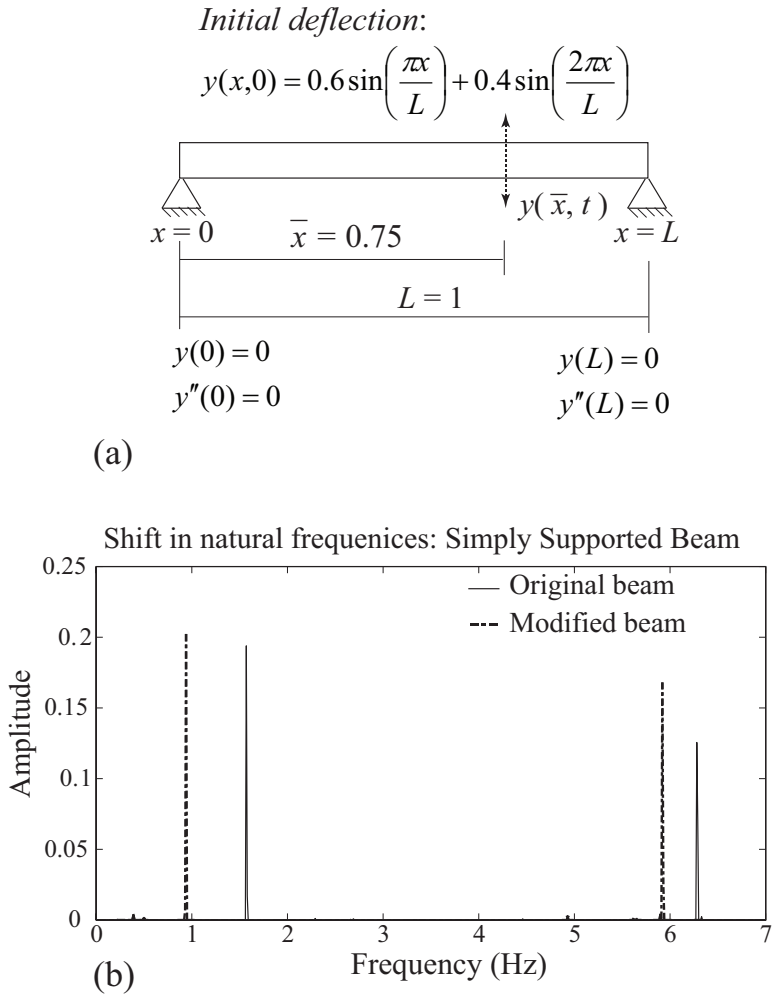

Figure 5.1: (a) Schematic: Simply supported beam (b) Shift in natural frequencies: Recovery by CS from 15 random samples for each scenario

The original natural frequencies $\omega_q = \pi/2$Hz, 2πHz are correctly predicted by the ℓ_1 minimum solution. The amplitudes plotted are $\sqrt{A_i^2 + B_i^2}$, since each frequency ω_i has a combined basis

function $[A_i \sin(\omega_i t) + B_i \cos(\omega_i t)]$, as evident from Eqs.(5.1) and (5.2). Figure 5.1(b) also shows the shift in frequencies due to the change in EI. They were also determined by solving the same ℓ_1 minimization problem. The reduction in frequencies is expected since change was introduced in the form of reduction in EI (stiffness/rigidity).

To study the effectiveness of ℓ_1 minimization, we plot the accuracy of recovery as a function of the number of measurements m. The plot is shown in Fig.5.2. The contour $k = 2$ represents quality of recovery when only the 1^{st} natural frequency $\frac{\pi}{2}$Hz was present in the free vibration. The contour $k = 4$ represents recovery when the 2^{nd} natural frequency 2πHz was superimposed with the 1^{st}. The contours $k = 8$ and 16 similarly show the quality of recovery when the first 4 and first 8 natural frequencies respectively are present.

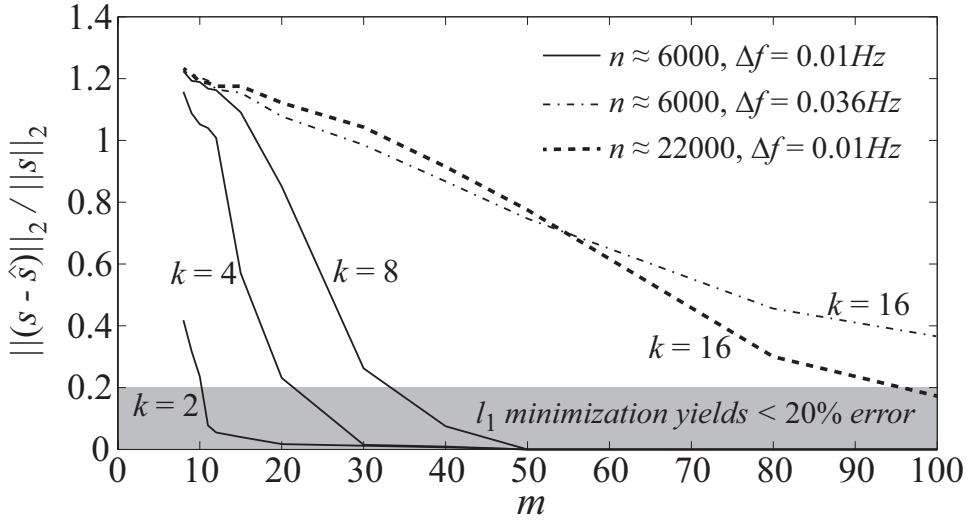

Figure 5.2: Error analysis of ℓ_1 minimization as a function of measurements m for different signal sparsity

Nominally $n \approx 6000$ and $\Delta f = 0.01$Hz was chosen, thus the frequency range of recovery was 60Hz. This range contains the first six natural frequencies (recall that the n^{th} natural frequency is

$(n^2\pi/2)$Hz). For $k = 16$, the natural frequency $\omega_q = 32\pi > 60$Hz, and hence Δf was increased to 0.036 Hz. For comparison n was increased to $n \approx 22000$, to restore $\Delta f = 0.01$Hz. This improved the quality of recovery, as is evident in Fig.5.2. Also, the number of measurements required to achieve higher accuracy of reconstruction increases with an increase in the number of frequencies to be recovered from the response. This is in accordance with Eq.(4.8). Because the number of measurements m, is affected by the natural logarithm of the original length of the signal n, for a given value of sparsity k, m remains a modest value for increasing n. In addition, it may be observed from Fig.5.2 that the recovery error is reduced around this lower bound on m.

Detecting Natural Frequencies of a Cantilever Beam using CS

A cantilever beam has one fixed end and one free end. The fixed end is constrained to have no displacement or slope during vibration. The free end experiences no bending moment or shear force. Similar to Section 5, here we show the application of CS in recovering the natural frequencies from vibration data collected from a single location. By detecting shifts in the frequencies, CS is used to predict changes in structural characteristics, such as damage. In this section, the approach is demonstrated using simulations. A cantilever beam is illustrated in Fig.5.3(a). Its q^{th} mode-shape is given by

$$\begin{gathered} W_q(x) = [\sin(\beta_q x) - \sinh(\beta_q x)] - \alpha_q \left[\cos(\beta_q x) - \cosh(\beta_q x)\right] \\ \cos(\beta_q L) \cdot \cosh(\beta_q L) = -1,\ \alpha_q = \tfrac{\sin(\beta_q L) + \sinh(\beta_q L)}{\cos(\beta_q L) + \cosh(\beta_q L)}. \end{gathered} \tag{5.3}$$

The solutions of β_q, from the above equation, are: $\beta_q L = [1.875,\ 4.694,\ 7.855,\ \cdots]$, [7]. The free vibration response at a distance $\bar{x}$, as indicated in Fig.5.3(a), is given by

$$y(\bar{x}, t) = \sum_{q=1}^{\infty} (A_q \cos(\omega_q t) + B_q \sin(\omega_q t))\, W_q(\bar{x}) = \sum_{q=1}^{\infty} (\bar{A}_q(\bar{x}) \cos(\omega_q t) + \bar{B}_q(\bar{x}) \sin(\omega_q t)), \tag{5.4}$$

where $\bar{A}_q(\bar{x}) = A_q W_q(\bar{x})$ and $\bar{B}_q(\bar{x}) = B_q W_q(\bar{x})$, and the natural frequencies ω_q satisfy $\omega_q = \beta_q^2 \sqrt{EI/\rho A_r}$. The structure of Eq.(5.4) is similar to that in Eq.(5.1) and thus Eq.(5.2) is applicable to setup the ℓ_1 minimization problem for CS-based frequency recovery.

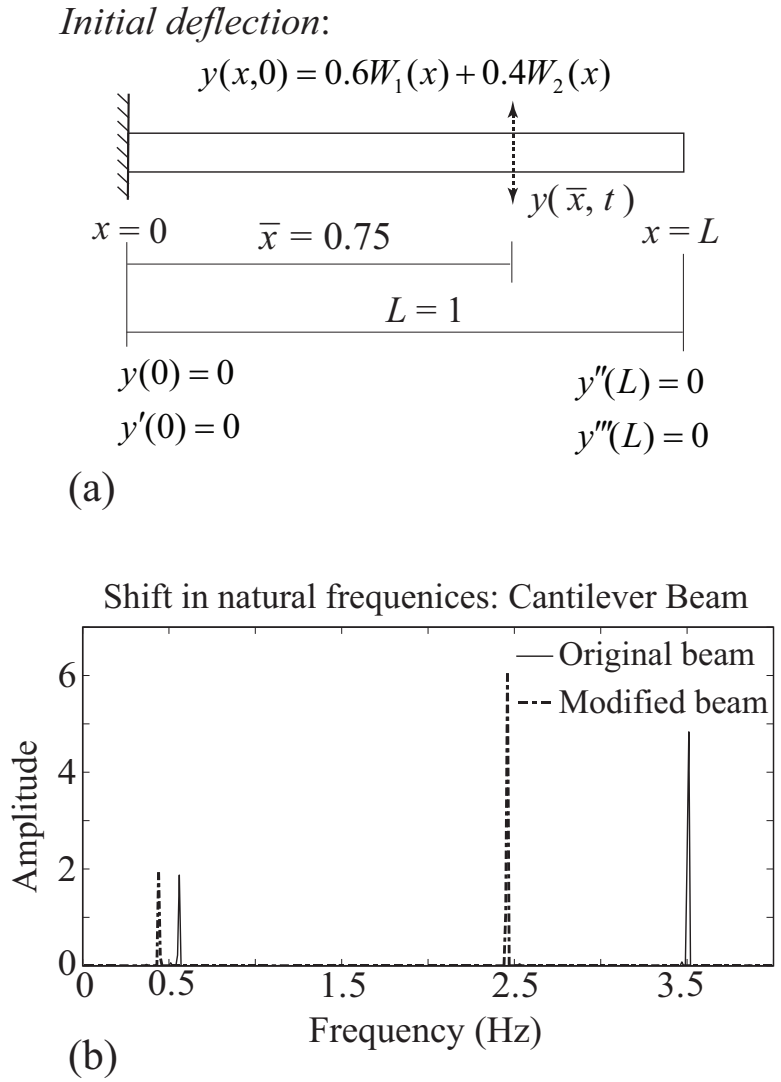

Figure 5.3: (a) Schematic: Cantilever beam (b) Shift in natural frequencies: Recovery by CS from 15 random samples from each scenario

The specifications of the cantilever beam are identical to that of the simply-supported beam in Section 5, i.e. $L = 1$, $\rho A_r = 1$, $EI = 1$. The natural frequencies ω_q are $[3.52,\ 22.03,\ 61.7,\ \cdots]$

in rad/s. Free vibration is simulated using a discrete model consisting of $N_{el} = 500$ beam elements. It is given an initial deflection profile of $y(x, 0) = 0.6W_1(x) + 0.4W_2(x)$, i.e. a combination of the first two mode-shapes. This causes the first two natural frequencies to be manifested in the free vibration response.

Change is introduced by reducing EI from 1 to 0.1 over elements $200 - 250$. The time domain response of the beam, before and after change, is measured at $\bar{x} = 3L/4$ and random measurements are made. The ℓ_1 minimization problem is setup with $\omega_r = 4$Hz $= 8\pi$rad/s and $\Delta\omega = 0.01$Hz $= 0.02\pi$rad/s. This yields $n = 401$ and we choose $m = 15$ random measurements. This is comparable to $m = 18$ suggested by Eq.(4.8), which is based on $k = 4$ for recovering two natural frequencies. Successful recovery of the vibrational frequencies using the CS methodology can be seen in Fig.5.3(b). Reducing EI led to reduction of natural frequencies from $\omega_1 = 0.56$Hz and $\omega_2 = 3.51$Hz to $0.44Hz$ and $2.45Hz$ respectively. This was first determined numerically using the finite-element beam model. Subsequently, it was confirmed that the changes were reflected in ℓ_1 solution, as evident in Fig.5.3(b).

Preliminary Experimental Validation

The previous section laid the foundation for devising a CS-based vibration monitoring system, specifically to detect changes in structural characteristics of mechanical beams. FEM-based simulation results were used to demonstrate the feasibility of using reduced and randomly placed samples to identify when changes are introduced in simply supported and cantilever beams. This section provides preliminary experimental validation for using reduced random sampling to detect shift in natural frequencies of vibration of mechanical beams, thereby detecting their structural changes. It also provides an insight into some practical difficulties in the practical implementation of such a system. Specifically, the problem is formulated for a cantilever beam setup.

Experimental Setup for Detecting Structural Change - Cantilever Beam

The experimental setup used for the experimental validation is explained in this section. It is shown in Fig. 5.4(a), (b) and (c). The DAQ, amplifier and cantilever beam used in the setup are a part of an educational control systems module from QUANSER, which is used to study control concepts related to vibration analysis. For this experiment, the setup solely serves to acquire free vibration impulse response of the cantilever beam.

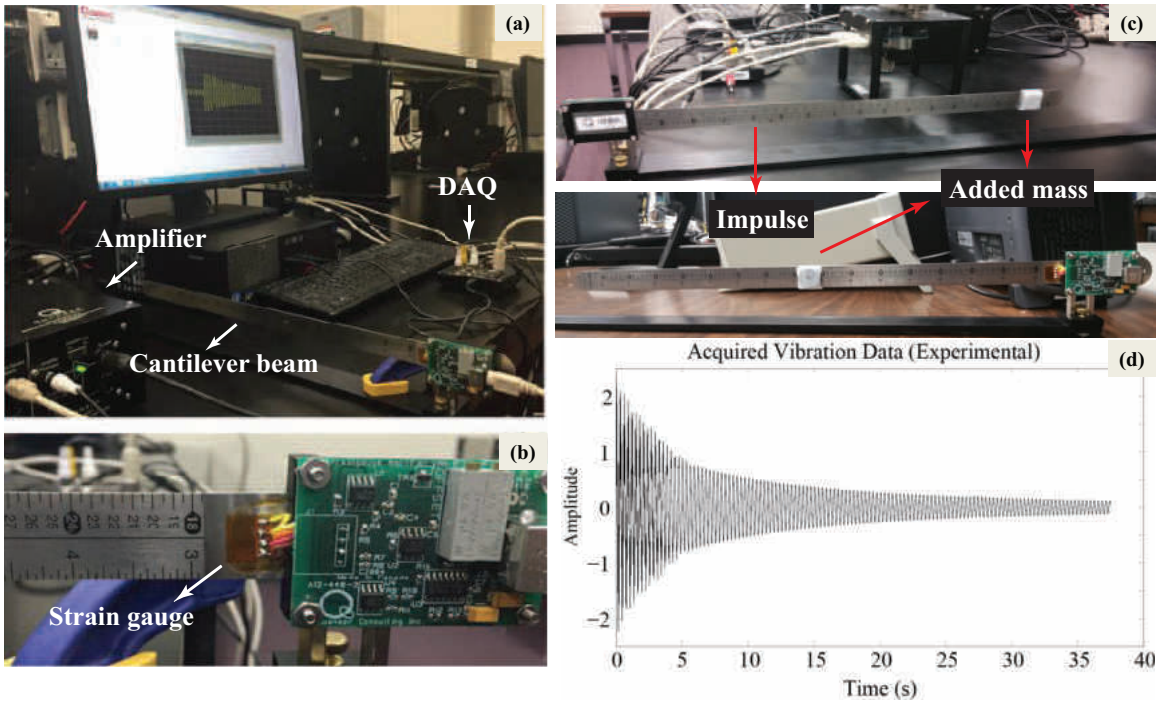

Figure 5.4: (a) Experimental setup with all components (b) Strain gauge on beam (c) Point of application of impulse and added mass on beam (d) Acquired data from cantilever setup when no mass is added

The cantilever beam used is of mass $m = 0.065$kg, length $L = 0.419$m, width $b = 0.02$m and stiffness $K_{stiff} = 1.66\text{kgm}^2\text{(rad/s)}^2$. As indicated in Fig.5.4(b), the beam consists of a strain gauge mounted at one end to measure the deflection when an impulse is experienced near the base

(see Fig.5.4(c)). The strain gauge used has a measurement range of -5V to $+5$V. Fig.5.4(c) also shows an added mass that is used to introduce change in the beam characteristics. The details these changes will be discussed in the sections to come.

Detecting Structural Change in the Cantilever Beam Setup

This section examines the process of detecting structural change by obtaining the natural frequencies of vibration of the cantilever beam that deviate from its baseline characteristics. Therefore, as a first step, the baseline characteristics of the beam were established. The cantilever beam was subjected to free vibration as a result of an impact near its base as indicated in Fig. 5.4(c). The free vibration response of the unmodified cantilever beam at a sampling frequency of 1000Hz is presented in Fig.5.4(d). Theoretically, this response will consist of all the natural frequencies (modes) of vibration. In practice, the lower modes are predominantly present in the free vibration response. This pattern of energy concentration in the lower modes (1^{st} and 2^{nd}) was observed in the experimental results. These frequency components from the free response were recovered using Fast Fourier Transform that uses traditional sampling approach. The baseline recovery problem was setup as follows:

- Duration of data capture $0 - 37.5$s
- Sampling frequency 1kHz
- Number of data points 37500 at regular intervals

The resulting first and second natural frequencies were 3.387Hz and 21.25Hz respectively (The first natural frequency was also verified against the value specified in the data sheet of the cantilever beam setup from the vendor). Thus, the original natural frequencies of vibration, i.e. of the unmodified beam were identified. Once these were established as a known (baseline) quantity, the beam characteristics were deliberately changed to investigate a shift in these natural frequencies.

This change was incorporated by adding mass sets at two locations of the beam, each considered as an independent configuration as shown in Fig.5.4(c): (i) Tip of the beam (ii) Mid length of the beam.

In each configuration, 6 cases were investigated, each with a different value of added mass. As in the case of obtaining baseline natural frequencies, after the mass is added, the beam was again subjected to impulse force near its base and the free vibration response of the modified beam was extracted. The frequency components from these responses were extracted using both the traditional sampling as well as CS methods. Addition of masses introduced shift in natural frequencies of vibration, an effect similar to that produced when damage develops in a structure. Therefore, adding different values of masses may be analogous to varying levels of damage. The values of added mass, modified frequencies and percentage reduction for tip mass and mass at mid-length are listed in Table 5.1 and Table 5.2 respectively.

Table 5.1: Recovered natural frequencies of the cantilever beam with tip mass

Added mass	% m increase	ω_1	% ω_1 drop	ω_2	% ω_2 drop
No mass added (Case 1)	-	3.387Hz	-	21.25Hz	-
$2.4g$ (Case 2)	3.7	3.17Hz	6.3	20.67Hz	2.7
$4.9g$ (Case 3)	7.5	2.99Hz	11.7	20.29Hz	4.5
$6g$ (Case 4)	9.2	2.91Hz	14.2	20.16Hz	5.1
$9.8g$ (Case 5)	15.1	2.72Hz	19.7	19.73Hz	7.1
$15.2g$ (Case 6)	23.4	2.48Hz	26.8	19.25Hz	9.4
$30.4g$ (Case 7)	46.8	2.053Hz	39.4	18.64Hz	12.3

Table 5.2: Recovered natural frequencies of the cantilever beam with mass at mid length

Added mass	% m increase	ω_1	% ω_1 drop	ω_2	% ω_2 drop
No mass added (Case 1)	-	3.387Hz	-	21.25Hz	-
$2.4g$ (Case 2)	3.7	3.36Hz	0.8	20.29Hz	4.5
$4.9g$ (Case 3)	7.5	3.33Hz	1.7	19.52Hz	8.1
$6g$ (Case 4)	9.2	3.32Hz	1.98	19.31Hz	9.1
$9.8g$ (Case 5)	15.1	3.307Hz	2.4	18.24Hz	14.2
$15.2g$ (Case 6)	23.4	3.2Hz	5.5	17.23Hz	18.9
$30.4g$ (Case 7)	46.8	3.12Hz	7.9	15.09Hz	28.99

In accordance with theory that increase in mass reduces the natural frequency of vibration, in each scenario, a left-shift was observed in the recovered frequencies (see Fig.5.5 (a),(b)). The specifications of the problem setup for FFT-based frequency recovery is the same as that for obtaining baseline characteristics. From the experimental data, it was observed that although addition of masses did result in a reduction in the natural frequencies, the effect was not uniformly pronounced in every mode. For instance, as listed in Table 5.2, it may be observed that when mass sets were added at mid length of the beam, the reduction in second natural frequency was more evident than the first. Therefore, only the shift in ω_2 is shown for this case. When the mass sets were added near the tip of the beam however, the shift in the first natural frequency was quite evident.

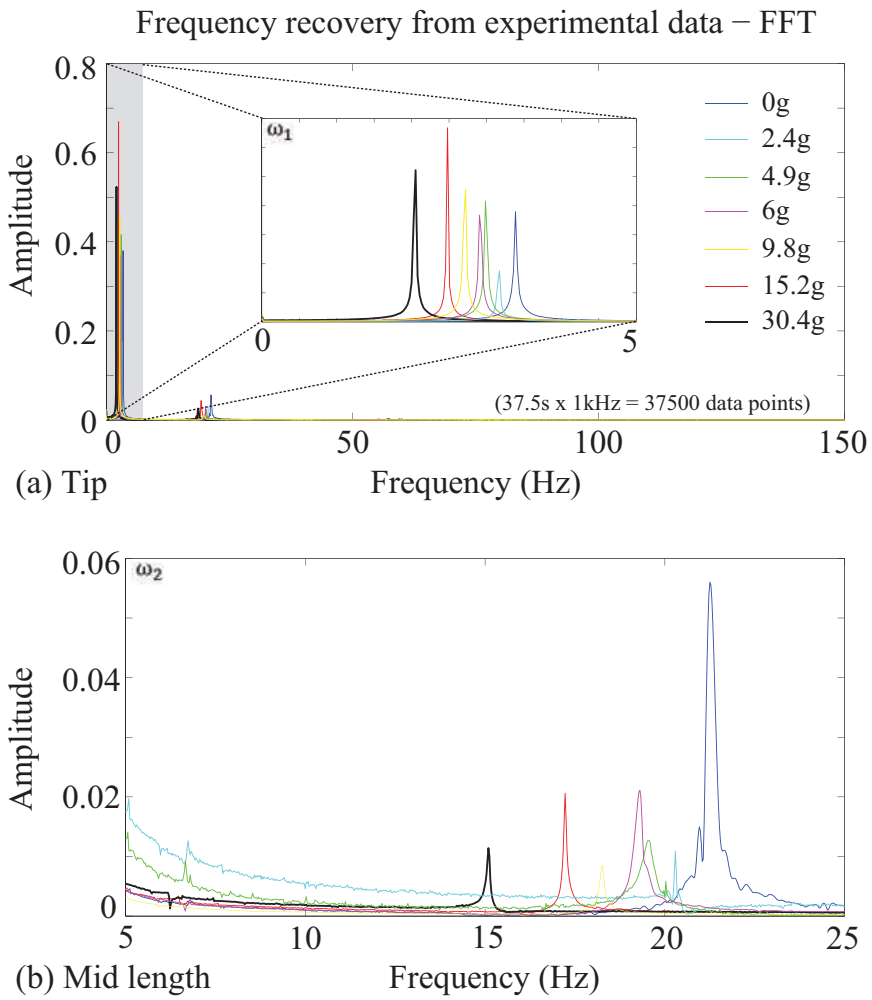

Figure 5.5: Frequency recovery from experimental data of cantilever beam using FFT (a) Tip mass (ω_1 & ω_2) (b) Mass at mid length (ω_2)

Fig.5.6 illustrates compressive sensing based frequency recovery from the same free vibration responses for all the cases listed in Table 5.1 and Table 5.2. The specifications of the CS problem setup were as follows:

- Duration of data capture $0 - 37.5$s
- Frequency range in Hz, $N = 0 : 0.01 : 30$
- Number of data points 200 (randomly spaced in time)

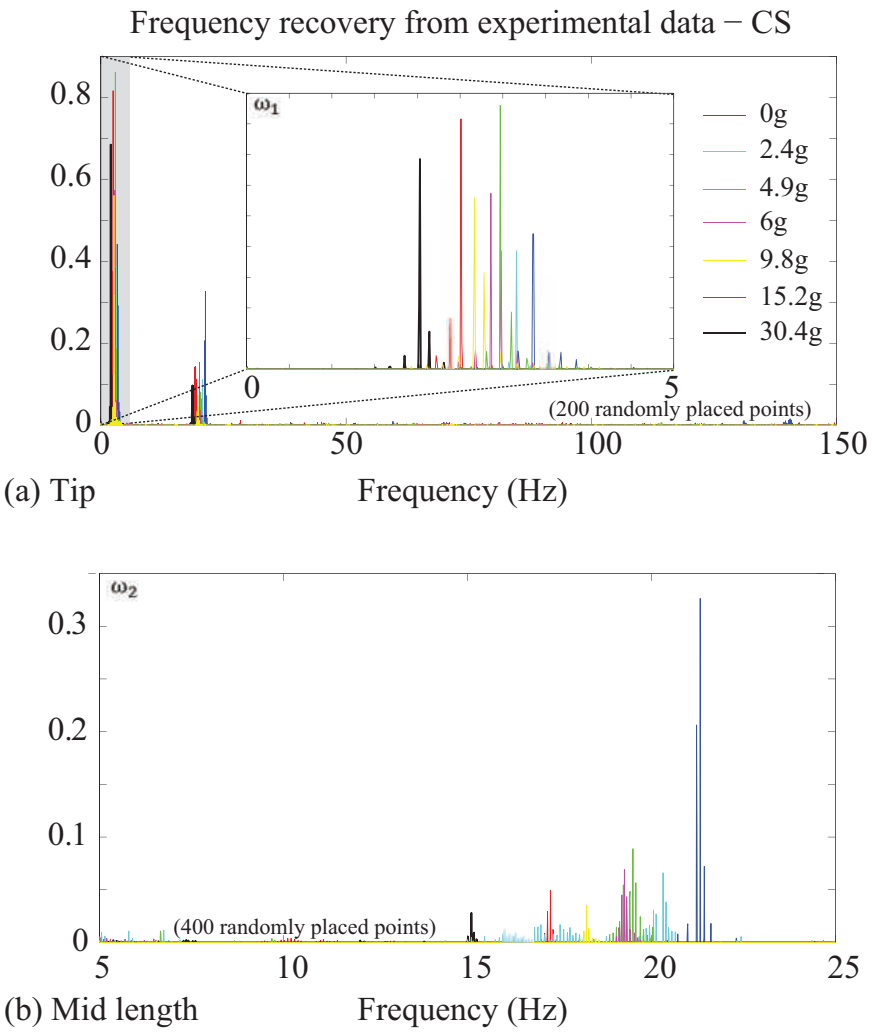

Figure 5.6: Frequency recovery from experimental data of cantilever beam using CS (a) Tip mass (ω_1 & ω_2) (b) Mass at mid length (ω_2)

When mass sets were added at mid length of the beam, recovery of the second natural frequencies were harder with just 200 data points. In order to ensure recovery of the second natural frequency, the number of random samples was increased to 400. With that said, we could possibly argue that higher modes may also be recovered with higher number of samples, which may however still remain a modest value as compared to the traditional method. However, since change in beam characteristics are indeed expected to reflect changes in all the modes, it allows for the

examination of just the lower modes. Tables 5.4 and 5.3 show the comparison between natural frequencies recovered using FFT and CS approaches. It can be observed that the frequencies recovered using both approaches coincide, thus indicating that CS-based frequency recovery may also enable damage detection from reduced number of samples.

Table 5.3: Shift in 1st natural frequency (tip mass) - FFT vs CS

FFT (37500 samples)	CS(200 samples)	% difference
21.25 Hz	21.33 Hz	0.38
20.29 Hz	20.32 Hz	0.15
19.57 Hz	19.50	0.36
19.31	19.27	0.21
18.27	18.24	0.16
17.23	17.26	0.17
15.09	15.11	0.13

Table 5.4: Shift in 2nd natural frequency (mass at mid-length) - FFT vs CS

FFT (37500 samples)	CS(200 samples)	% difference
3.39 Hz	3.36 Hz	0.88
3.17 Hz	3.16 Hz	0.32
2.99 Hz	2.97	0.67
2.91	2.86	1.72
2.72	2.67	1.84
2.48	2.51	1.21
2.05	2.03	0.98

The experimental data contained noise. However, it may be observed from the results that the signal to noise ratio (SNR) was sufficient to recover the first and second natural frequencies from reduced number of samples using CS without necessarily having to introduce noise formulation. Furthermore, these frequency values matched those listed in Table 5.1 and Table 5.2. Hence, it may be seen that CS promises to be a good candidate for reducing sensing and data requirement in vibration based monitoring of mechanical structures. As mentioned earlier, this section also attempts to look at some challenges that will emerge during the implementation of a CS-based vibration monitoring system. Non-uniform distribution of effects in mode shifts (or natural frequency shifts) is one such indispensable challenge. One way to overcome this would be using greater number of samples (but, with $m << n$) for frequency extraction. In addition, during realization of such a system in practice, the effects of noise may not be very subtle as observed during the experiment. In such situations, the effects of introducing such a noise formulation for CS may prove beneficial and it will be discussed in detail in next section.

Effects of Noise Formulation

Presence of noise in measurement data is inevitable. In order to evaluate the practical feasibility of CS-based vibration monitoring, it is therefore, imperative to gain knowledge of its performance while handling realistic data, i.e. noisy signal. It is common practice to design filters based on the expected noise features of a given type of signal. This approach of incorporating noise filtering might be straightforward in those applications that involve continuous streaming of data or continuous measurements. On the other hand, it becomes more complicated when the signal is measured at random time instants or at random spatial points. CS-based vibration monitoring is a case in point. Literature on compressive sensing presents an approach to handling noisy signals, by redefining the l_1 minimization problem to account for noise [74], [77], [78]. In this section, noise formulation is incorporated into the CS-based vibration problem in order to study how it

alters the performance of CS in detecting frequency shift from the free vibration response of mechanical beams. Specifically, this section aims to quantitatively measure the effect of using noise formulation in CS-based frequency recovery by evaluating the average l_2 error. Firstly, the problem formulation is applied to simple sinusoidal signals with multiple frequencies and later extended to free vibration response of a simply supported beam. This analysis is based on FEM simulations. As the next step, experimental data from a cantilever beam obtained in the previous sections is considered. Here, incorporating noise handling in CS helps to study its effect on the inherent noise in the experimental data.

Identifying the Regularization Parameter

Traditional approach to filtering out noise requires that data is collected continuously (stream). However, data acquisition in compressive sensing is random. In fact this *'randomness'* is the essence of compressive sensing. Hence, noise reduction is incorporated into the ℓ_1 minimization algorithm itself. To find the sparse solution from the noisy measurements, Eq. (4.7) is modified as

$$\hat{s} = argmin||s||_1 \quad s.t. \quad ||z - \Phi s||_2 < \epsilon, \tag{5.5}$$

where ϵ depends on the noise variance and can be learned through experimental data. Instead of a quadratically constrained l_1 minimization problem, it is common practice to reformulate Eq.(5.5) into a LASSO problem (Eq.(5.6)) [74] and that equivalent is used for frequency recovery.

$$\hat{s} = argmin||\Phi s - z||_2^2 + \lambda||s||_1 \tag{5.6}$$

where λ is the regularization parameter, also tuned depending on the noise level in the signal to be recovered. An advantage of using Eq.(5.6) for noise handling in CS is that λ promotes sparsity by imposing penalty on s. The rest of this section uses Eq.(5.6) while considering noise formulation.

The value of regularization parameter may vary depending on the type of signal and more importantly, the signal to noise ratio (SNR) [79]. The first step is, therefore, to identify an approximate value of λ that is most suitable for the type of signals that are dealt with in this application. Figure 5.7 illustrates the variation of average l_2 error of reconstruction for varying values of regularization constant, λ.

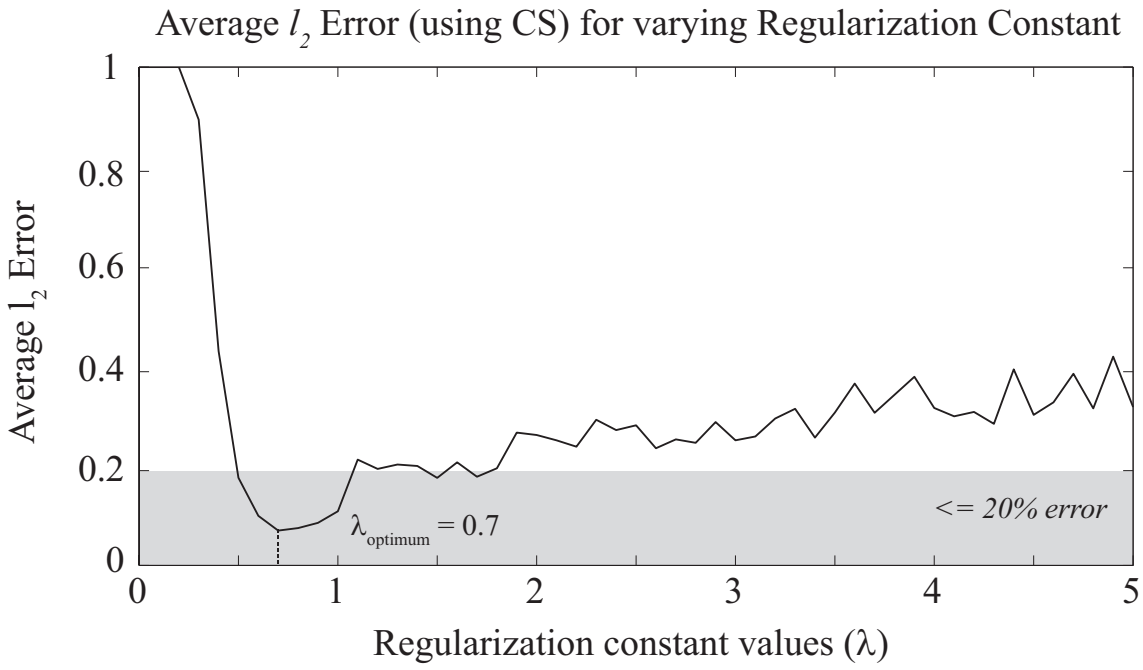

Figure 5.7: Choosing a suitable regularization constant: Variation of average l_2 error of reconstruction over varying values of regularization constant λ

In order to determine an optimal λ, a sinusoidal signal with two frequencies, $f_1 = 2$Hz and $f_2 = 5$Hz was corrupted with a noise signal whose coefficients were derived from a Gaussian distribution with mean, $M1 = 0$ and variance, $\sigma^2 = 0.1$. Frequency components were then recovered using CS with noise formulation as expressed in Eq.(5.6), with the regularization constant taking a range of values from $\lambda = 0, 0.1, 0.2, ...5$. For each value of λ, the signal was compressively sampled 100 times. From the recovered frequencies at every attempt, the sinusoid was reconstructed and

the average l_2 error was calculated between the original and reconstructed signals. The quality of reconstruction is dependent on the accuracy of frequency recovery. Hence, a lower reconstruction error implies higher accuracy of frequency recovery. Following the assumption in Fig.(5.2), the acceptable maximum recovery error could be at 20%. Scanning the range of λ values for which the recovery error was below 20%, the optimum value was chosen at $\lambda = 0.7$ for CS-based recovery and reconstruction of vibration signals. The rest of this section will discuss how the frequency recovery is affected by varying levels of noise and varying number of measurements with and without noise formulation.

Analyzing Noise Formulation in Sinusoids

In [80], the authors study the effect of noise, sampling rate and signal sparsity in order to evaluate the performance of CS-based pulse compression. Based on their approach, the following tests were developed in order to analyze the performance of CS-based frequency recovery from a sinusoidal signal with multiple frequencies. The CS problem was set up as listed in Table 5.5.

Table 5.5: Problem setup for evaluating CS performance with noise formulation - Sinusoids with multiple frequencies

Parameters	K = 2	K = 4	K = 6
No. of Frequencies	2	4	6
Frequencies (Hz)	2, 5	2, 5, 3.5, 2.5	2, 5, 3.5, 2.5, 4, 4.5
Frequency range (Hz)	0:0.01:10	0:0.01:10	0:0.01:10
Mean (M1)	0	0	0
Variance (σ^2)	0:0.01:0.5	0:0.01:0.5	0:0.01:0.5
No. of samples (m)	15	30	40

Accuracy of CS-based frequency recovery was evaluated as a measure of reconstruction error. Higher the fidelity of reconstruction, greater is the accuracy of recovered frequencies that were in fact used in the reconstruction. For each case of sparsity K, the signal reconstruction error and hence the probability of reconstruction was averaged over 100 attempts. This was done to ensure that the values obtained maybe close to accurate. Figure 5.8 illustrates the variation of average l_2 error of reconstructed sinusoids for increasing noise variance levels.

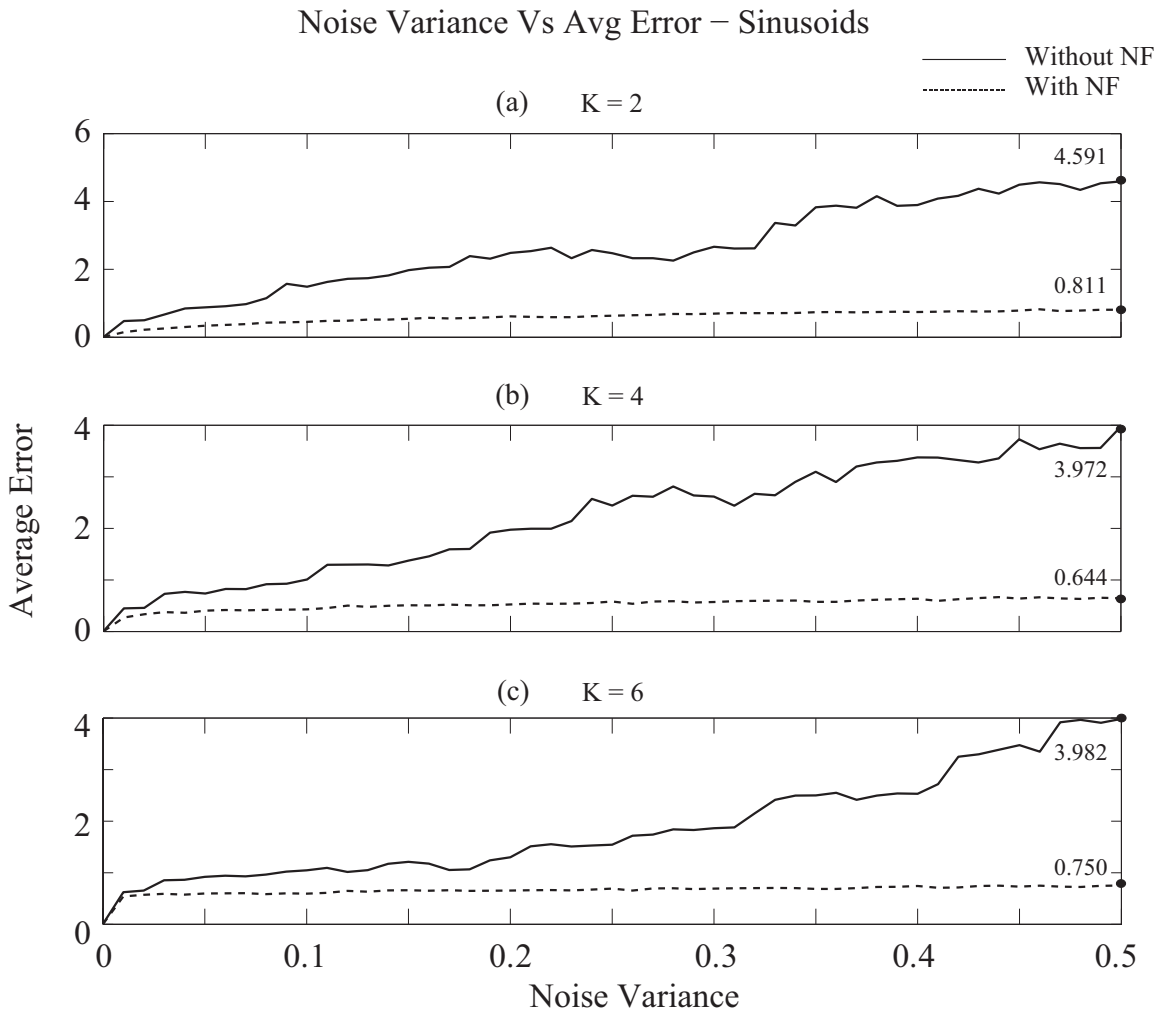

Figure 5.8: Effect of noise formulation in CS-based frequency recovery: Variation of average l_2 error for increasing noise variance - Sinusoids with multiple frequencies (a) $K = 2$ (b) $K = 4$ (c) $K = 6$

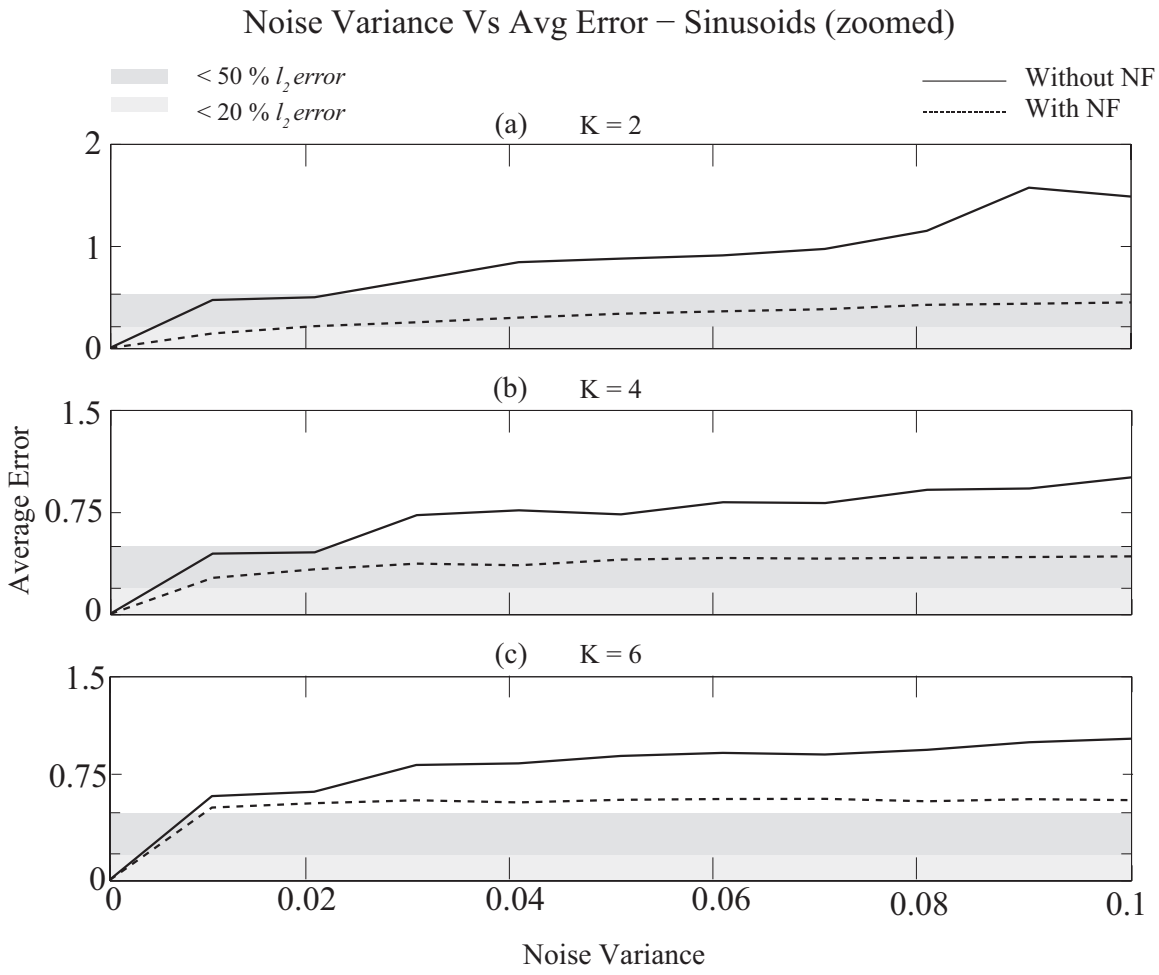

Figure 5.9: Effect of noise formulation in CS-based frequency recovery using average l_2 error over a lower range of noise variance (0 - 0.1) - Sinusoids

The value of regularization parameter used during the frequency recovery was $\lambda = 0.7$. Recall that λ in fact depends on the SNR. In order to obtain a more accurate error value, for each noise level, λ could be tuned. However, in order to study the influence of noise formulation in the CS performance and recovery error, it is not an uncommon practice to use a fixed value of λ over a range of noise level [81]. Each plot in Fig. 5.8 corresponds to a different sparsity level. Because there are only sine components for each frequency, as listed in Table 5.5, K = 2, 4 and 6 imply two, four and six frequencies to recover in each case respectively. Furthermore, each

plot indicates, for a given noise variance, the average error of reconstruction from frequencies recovered by CS with and without noise formulation. At zero noise variance, the average error of reconstruction is the least. In addition, it can also be observed that the average l_2 error values at zero noise is almost equal whether or not noise formulation was incorporated in the CS-based recovery and reconstruction. As the noise variance increases, there is a gradual increase in the error value. However, in the presence of noise formulation, the rate of increase in error is modest as compared to its rate when noise formulation was not used. Consider Fig.5.8 (a) as an example for the following discussion. In the presence of noise formulation, the l_2 error corresponding to the highest noise variance of 0.5 is 0.811. This implies a recovery error of about 81%. Although this error value is significantly lower than that in the absence of noise formulation, recovering only 20% of the signal effectively provides no valuable information about it. From a realistic viewpoint, a more useful analysis may be drawn by studying the CS based frequency recovery over a lower range of noise levels, say upto 0.1. Figure 5.9 (a), (b) and (c) illustrate performance of CS-based frequency recovery over a lower range of noise variance (0 - 0.1) using the variation of average l_2 error.

Table 5.6: Average l_2 error of reconstruction with and without noise formulation (NF) - Sinusoids with multiple frequencies

Noise	K = 2			K = 4			K = 6		
(σ)	No NF	With NF	% drop	No NF	With NF	% drop	No NF	With NF	% drop
0.02	0.502	0.219	56.37	0.458	0.333	27.95	0.654	0.571	12.69
0.04	0.846	0.303	64.18	0.766	0.363	52.61	0.863	0.576	33.26
0.06	0.912	0.365	96	0.825	0.416	49.58	0.941	0.601	56.57
0.08	1.152	0.428	62.85	0.917	0.418	54.42	0.963	0.584	39.36
0.1	1.488	0.451	69.69	1.008	0.428	57.54	1.045	0.592	43.35

Table 5.6 lists the l_2 error values for specific noise variance levels with and without noise formulation. For higher levels of noise, when noise formulation is not incorporated in the CS recovery algorithm, it can be observed that the average l_2 error is greater than unity (see Table 5.6), implying that the CS reconstruction may have failed at these high noise levels.

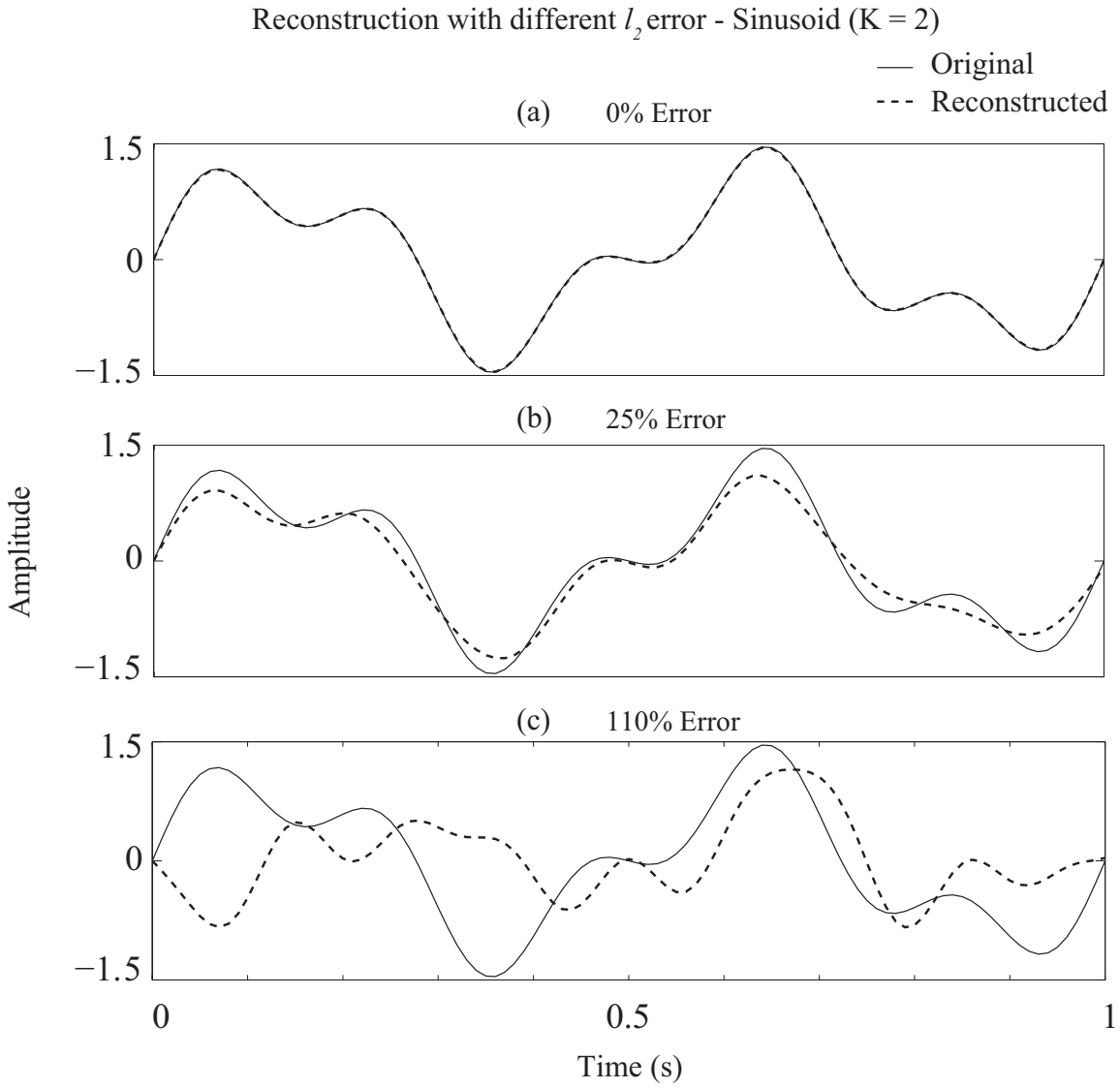

Figure 5.10: Reconstruction of dual frequency sinusoid for different values of average l_2 error

In order to gain understanding of how the reconstruction looks for different values of error, Fig. 5.10 illustrates the CS-based reconstruction of the sinusoid ($K = 2$) for different levels of reconstruction error. On the other hand, with noise formulation, the highest average l_2 error for k = 2, 4, and 6 are 0.811, 0.644 and 0.750 respectively. Figure 5.11 illustrates the variation of probability of success of reconstruction of the sinusoid signal for increasing noise variance. Essentially, it is an alternative representation of Fig.5.9. This probability reflects a qualitative representation of the accuracy of CS-based frequency recovery.

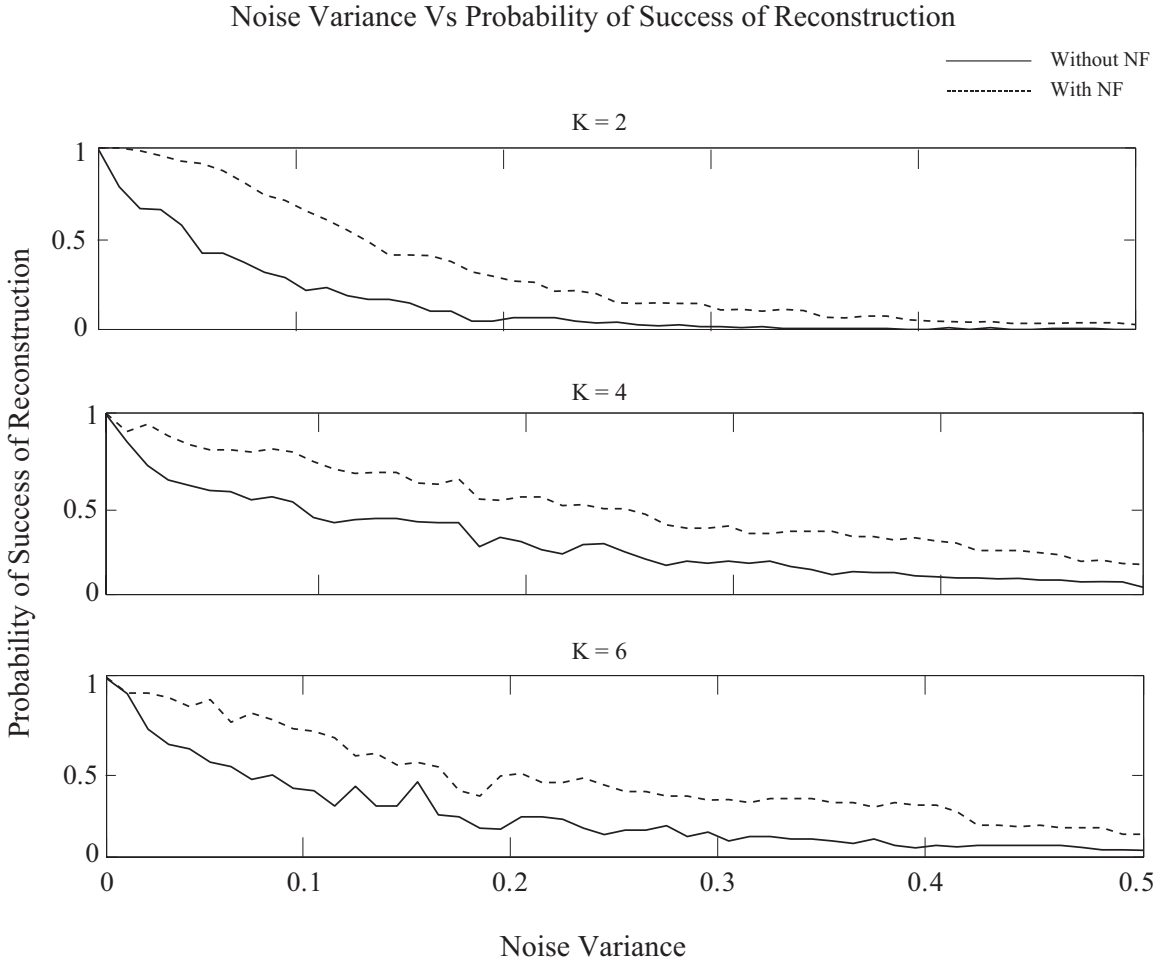

Figure 5.11: Variation of probability of reconstruction success for increasing noise variance - Sinusoids

As observed from Fig.5.11, for each case of sparsity K, the reconstructed signal has highest fidelity in the absence of any noise. As the signal to noise ratio decreases, for a given number of samples, it becomes increasingly difficult to faithfully reconstruct the signal. This is a direct indication of poor frequency recovery. Additionally, the probability of success of signal reconstruction tends to degrade at a lower rate in the presence of noise formulation in the CS problem. It may therefore be understood that incorporating noise formulation improves the recovery and reconstruction of the signal.

Analyzing Noise Formulation in Simply Supported Beam

This is a preliminary examination of the effect of formulating noise handling in the CS-based recovery of natural frequencies from beam vibrations. In this respect, the results of this study are important because higher accuracy in frequency recovery implies more accurate detectability of shift in natural frequencies. In turn, it improves the ability to detect small structural changes. In the previous section, performance of CS-based frequency recovery was studied for sinusoidal signals with multiple frequencies. This was accomplished by evaluating the variation of average l_2 error and probability of success of reconstruction for increasing noise variance. It served as a preliminary step in understanding the effect of incorporating noise formulation in CS-based frequency recovery. The analysis of results thus obtained, offered a convincing claim that for any given sparsity and suitable number of samples, the frequency recovery and subsequent signal reconstruction improved considerably in the presence of noise formulation in the CS algorithm. In this section, the performance of CS-based recovery is evaluated for the time domain free vibration response of a simply supported beam with three different initial conditions.

The details of the CS problem are listed in Table 5.7. As explained in chapter 4, the response of the beam in each case, is expected to predominantly contain only those modes that are present

in the corresponding initial condition. From Eq.(4.4), each modal frequency contains both the sine and cosine components in the beam response. It follows that the measurement matrix is also a combination of these individual components. Each modal frequency, therefore contains representation in both sine and cosine domains, which in turn implies that for one mode, there are two non-zero coefficients to recover. Therefore, the sparsity values are K = 4, 8, 12 for recovering 2, 4, and 6 frequencies respectively.

Table 5.7: Problem setup for evaluating CS performance with noise formulation - Simply Supported Beam

Parameters	K = 4	K = 8	K = 12
No. of Frequencies	2	4	6
Frequencies (Hz)	1.5, 6.28	1.5, 6.28, 14.13, 25.13	1.5, 6.28, 14.13, 25.13, 39.27, 56.55
Frequency range (Hz)	0:0.01:10	0:0.01:30	0:0.01:60
Mean (M1)	0	0	0
Variance (σ^2)	0:0.01:0.5	0:0.01:0.5	0:0.01:0.5
No. of samples (m)	30	50	80

Figure 5.12 illustrates variation of average l_2 error of reconstruction of the free vibration response of the SS beam for increasing noise variance in the signal. In turn, it indicates the effect of noise formulation in CS-based recovery of natural frequencies. Figure 5.13, presents the l_2 error variation over a lower range of noise variance. It can be observed that the plot follows a trend similar to that of Fig. 5.8. Again, in order to minimize inconsistencies, for each case of sparsity K, the signal reconstruction error and the probability of success of reconstruction were averaged over 100 attempts.

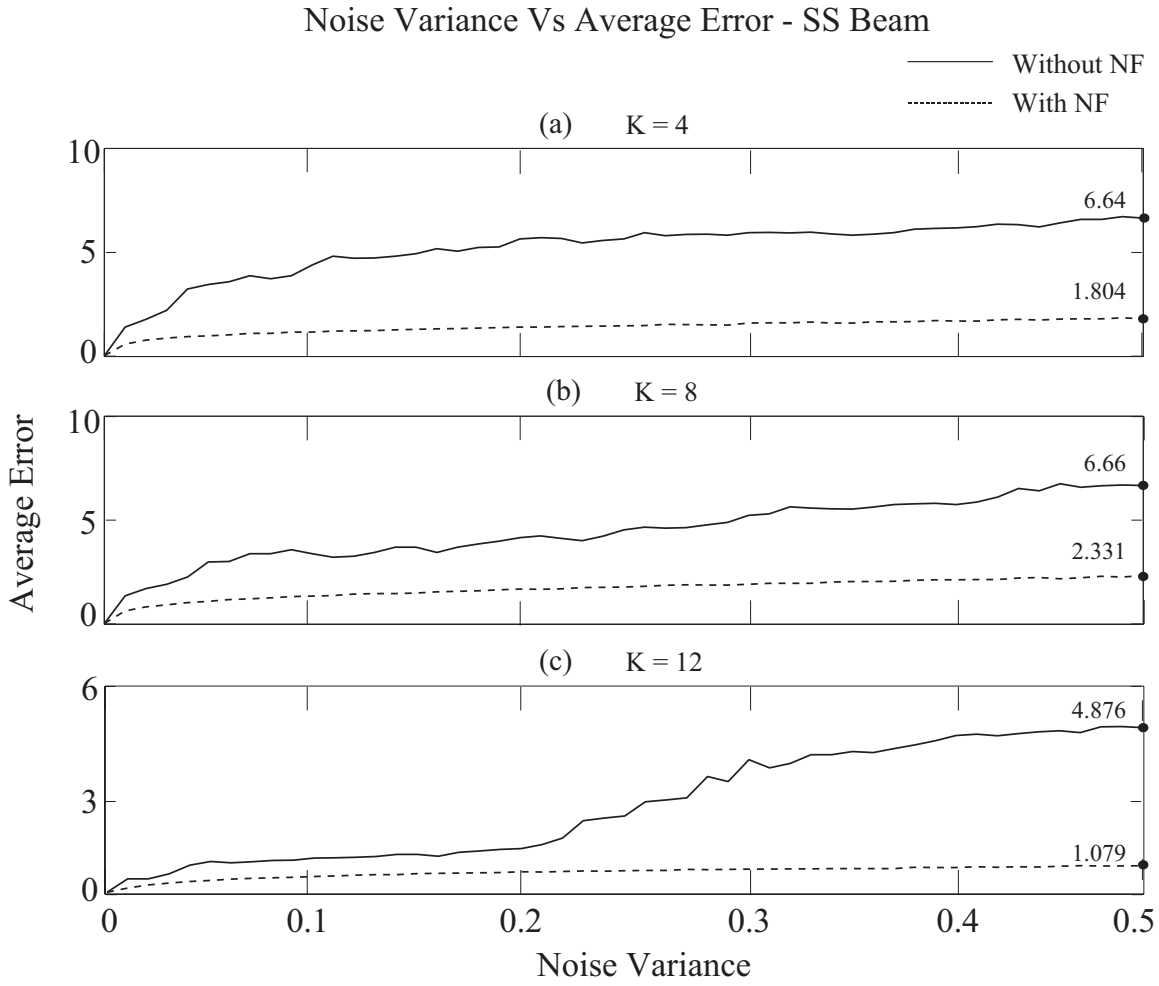

Figure 5.12: Effect of noise formulation in CS-based frequency recovery: Variation of average l_2 error for increasing noise variance - SS Beam (a) $K = 4$ (b) $K = 8$ (c) $K = 12$

When the signal is not corrupted with any noise, the l_2 error was the least (almost zero). Also, due to this negligible noise level, there is no discernible difference in reconstruction error values between using CS-based recovery with and without noise formulation. This behavior was already observed in Fig. 5.8. Similarly, there is an increase in the reconstruction error with increasing noise variance in the signal (i.e. decreasing SNR), the rate of which is significantly lowered by incorporating the noise formulation in the CS problem. As explained in the previous section, error values greater than unity indicate that the reconstructed signal is incomparable to the original.

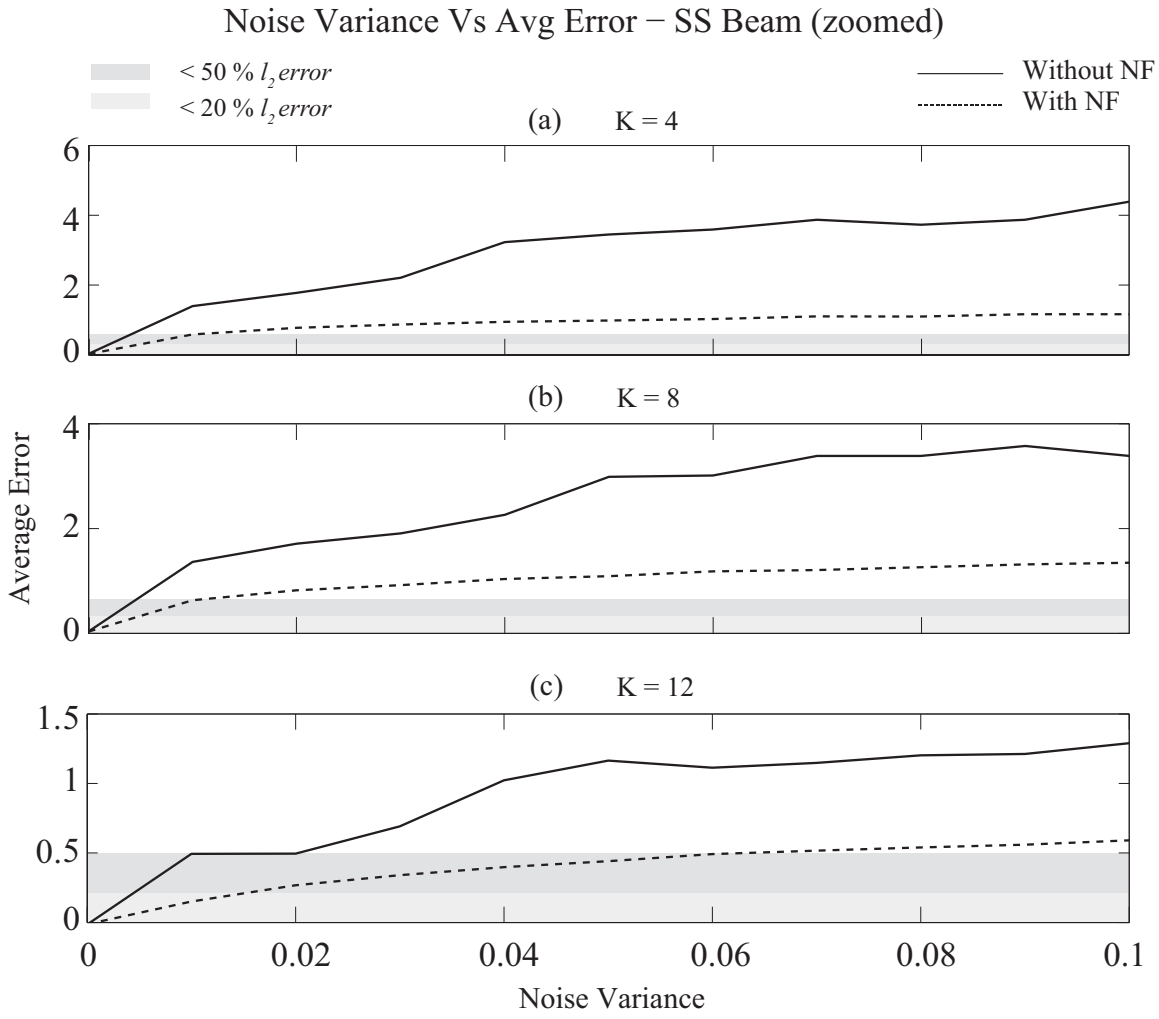

Figure 5.13: Effect of noise formulation in CS-based frequency recovery using average l_2 error over a lower range of noise variance (0 - 0.1) - SS Beam

The average l_2 error values for specific noise variance levels are listed in Table 5.8. From these results, it may be reiterated that incorporating noise handling in the CS-based frequency recovery improves its performance. Furthermore, higher accuracy in recovery guarantees improved reliability and enables detection of smaller shift in natural frequencies, i.e. smaller structural changes.

Table 5.8: Average l_2 error of reconstruction with & without noise formulation (NF) - SS Beam

Noise	K = 4			K = 8			K = 12		
(σ)	No NF	With NF	% drop	No NF	With NF	% drop	No NF	With NF	% drop
0.02	1.78	0.776	56.40	1.712	0.821	52.04	0.717	0.554	22.43
0.04	3.23	0.949	70.62	2.26	1.035	54.20	1.097	0.647	41.02
0.06	3.59	1.027	71.39	3.01	1.181	60.76	1.162	0.715	38.47
0.08	3.73	1.098	70.56	3.383	1.260	62.75	1.227	0.750	38.88
0.1	4.39	1.166	73.44	3.383	1.345	60.24	1.289	0.786	39.02

Figure 5.14 illustrates the decrease in probability of success of response reconstruction for increasing levels of noise variance with respect to the signal amplitude. Because increase in noise effectively degrades the signal, the quality of reconstruction is expected to decrease, which is captured by the trend of the plots in Fig.5.14. The probability of success of reconstruction with respect to increasing noise level, maybe seen as the qualitative representation of the performance of CS-based reconstruction. As mentioned in the previous section, this is essentially, an alternative illustration of Fig. 5.12. It is important to note that the probability of success of reconstruction may not be a well defined or quantitative indicator of the performance of CS-based recovery and reconstruction. But, it can still be observed that the performance of CS is enhanced in the presence of noise formulation. In fact, on comparing Figs. 5.12 and 5.14, it is indisputable that the average l_2 error is a better and clearer indicator of the performance of CS in the presence and absence of noise formulation. For instance, consider the trend of the plot for K = 4 in both the figures. While Fig. 5.12 shows the gradual increase in reconstruction error for increasing noise variance in the signal, in Fig. 5.14, the probability falls to almost zero and remains indiscernible beyond a noise variance of 0.2 in the absence of noise formulation and 0.1 in the presence of noise formulation.

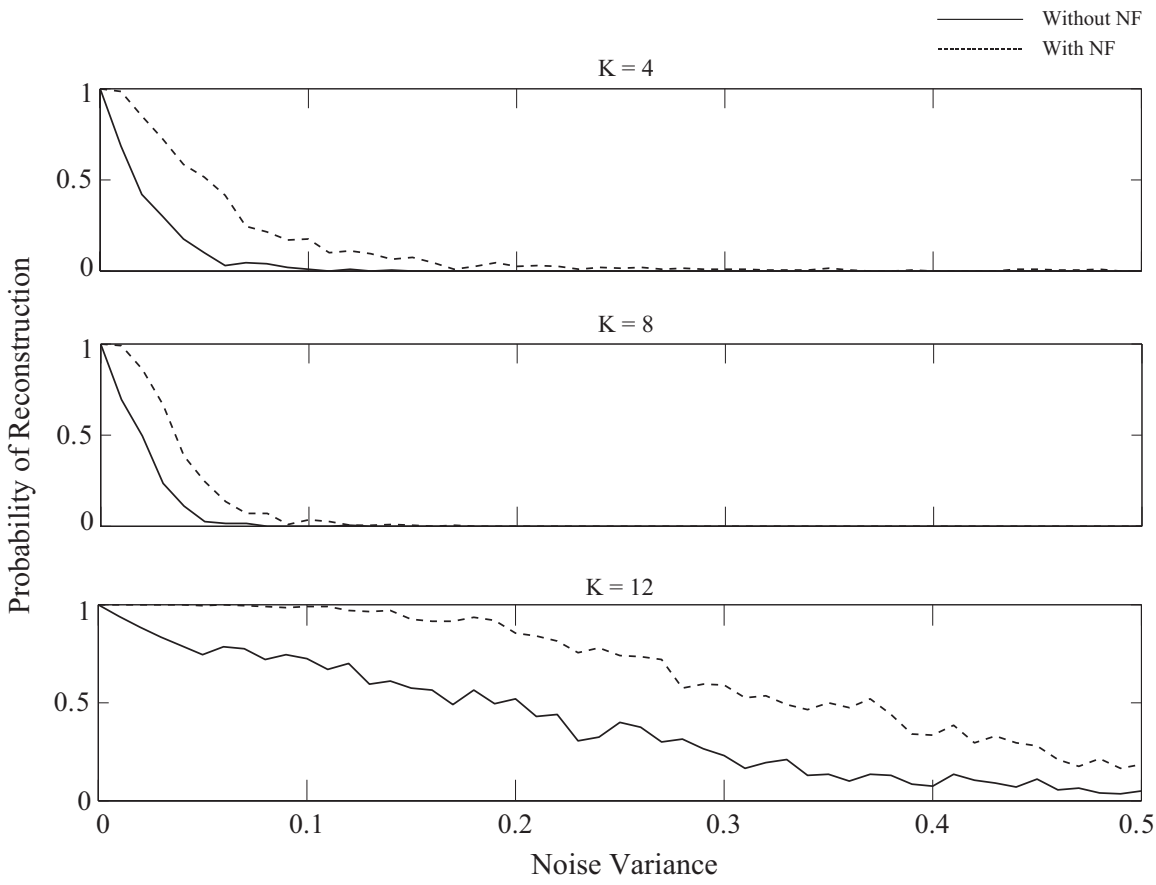

Figure 5.14: Variation of probability of reconstruction success for increasing noise variance - SS Beam

Analyzing Noise Formulation in Cantilever Beam (Experimental)

The previous two sections provided a detailed insight into how the incorporation of noise formulation in CS can help enhance its performance in frequency recovery and more importantly, in detecting smaller shift in natural frequencies. In this section, a more realistic case is examined - frequency recovery from the impulse response of a cantilever beam obtained through experiments. The free vibration response of the cantilever beam setup obtained in the preliminary experimen-

tal validation (Section 5) is used here. As explained previously, the experimental data contained noise. Although the SNR was sufficient enough to recover the first and second modes from the free vibration response using CS without explicit noise formulation, in this section, the effect of incorporating noise formulation for the same problem is studied. Furthermore, as opposed to changing noise variance in the signal, here, the number of measurements are varied to illustrate the enhancement of performance of CS in frequency recovery and ultimately, detection of structural change.

Section 5 describes the CS problem setup for detecting changes in the cantilever beam by extracting the first and second natural frequencies from its free vibration response. While the frequency recovery is a fairly straightforward process, in contrast, obtaining a quantitative measure of enhancement of this CS-based frequency recovery requires calculation of the average l_2 error. In turn, this requires the reconstruction of the beam response and its comparison to original data. This mandates certain modification in the CS problem setup, because, as opposed to simulation data (Section 5), the realistic (experimental) data includes damping. The effect of damping has to therefore be accounted for, in order to get a reconstruction that may facilitate comparison to the original response. Furthermore, successful formulation of a suitable basis that includes damping will enable reliable reconstruction of the spatial beam vibrations using CS.

Relative Decay of First and Second Modes of Vibration

In this section, the basis for formulating a modified CS problem setup for reconstructing the damped vibration response of a cantilever beam is presented. Specifically, the relative rate of decay of the first and second modes of vibration (natural frequencies) of a 2DOF system is discussed. Consider a discrete 2 DOF mass-spring-damper system shown in Fig.(5.15).

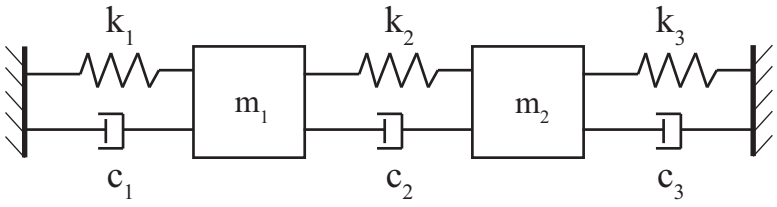

Figure 5.15: Discrete 2 - Degree of Freedom (DOF) System

The equation of motion of the above 2DOF system is expressed as,

$$M\ddot{x} + C\dot{x} + Kx = 0 \tag{5.7}$$

where, M, C and K are the mass, damping and stiffness matrices. Assuming that $m_1 = m_2 = m$, $c_1 = c_2 = c$ and $k_1 = k_2 = k$ these matrices take the form as shown in Eq.(5.8) below.

$$M = \begin{pmatrix} m & 0 \\ 0 & m \end{pmatrix} \quad C = \begin{pmatrix} 2c & -c \\ -c & 2c \end{pmatrix} \quad K = \begin{pmatrix} 2k & -k \\ -k & 2k \end{pmatrix} \tag{5.8}$$

From Eq.(5.15), the relationship between K and C matrices may be drawn as,

$$(C) = (K)\,\frac{c}{k} \tag{5.9}$$

From Eq.(5.9), we can assume that the system is proportionally damped, i.e., the damping is proportional to the stiffness of the system. Therefore, the damping coefficients (ζ_1 and ζ_2) may be expressed by the following set of equations.

$$\zeta_1 = \frac{\alpha + \beta {\omega_1}^2}{2\omega_1} \quad \zeta_2 = \frac{\alpha + \beta {\omega_2}^2}{2\omega_2} \tag{5.10}$$

Because the damping is only proportional to the stiffness (Eq.(5.9)), $\alpha = 0$ in Eq.(5.10). Therefore,

the damping coefficients can be re-written as follows.

$$\zeta_1 = \frac{\beta\omega_1}{2} \quad \zeta_2 = \frac{\beta\omega_2}{2} \implies \zeta_1 = \frac{c}{2k}\omega_1 \quad \zeta_2 = \frac{c}{2k}\omega_2 \tag{5.11}$$

Since natural frequencies increase in the order of mode number, the following set of relations hold true.

$$\omega_2 > \omega_1 \implies \zeta_2 > \zeta_1 \tag{5.12}$$

Further, since the damping ratios are dependent on ζ_1 and ζ_2,

$$\sigma_1 = \zeta_1\omega_1 \quad \sigma_2 = \zeta_2\omega_2 \implies \sigma_2 > \sigma_1 \tag{5.13}$$

We know that, the response of the 2DOF system can be expressed by Eq.(5.14).

$$x_n(t) = Ae^{-\sigma_n t}sin(\omega_{d_n}t + \phi) \qquad where, \;\; n = 1, 2 \tag{5.14}$$

From Eqs.(5.13) and (5.14), we can conclude that $x_2(t)$ decays faster relative to $x_1(t)$. Therefore, the first mode is dominant over the second mode and therefore tends to persist longer in the free vibration response of the system. Based on the understanding of the response of this 2DOF system, the CS problem formulation to recover the first and second modes of vibration and subsequently reconstruct the response of the cantilever beam is modified. These details are presented in the sections to come.

Recovering the First Mode of Vibration from Experimental Data

This section describes the CS problem formulation for recovering the first mode of vibration and reconstructing the response with and without noise formulation. In addition, in the presence of noise formulation, it examines the difference in performance when the basis function for the CS problem

include damping. Table 5.9 lists the CS problem formulation. In the free vibration response with initial deflection, each mode/natural frequency has a sine and cosine component associated with it. Therefore, for recovering the first mode (one frequency), the sparsity $K = 2$.

Table 5.9: Problem Setup for Evaluating CS performance with Noise Formulation - Cantilever Beam (Experimental - 1st mode)

Parameters	K = 2
No. of Frequencies	1
Frequencies (Hz)	3.41
Frequency range (Hz)	0:0.01:10
Duration of data capture (s)	27 - 37
No. of samples (m)	20 - 100

From previous discussion on relative decay of the first and second modes, it was understood that the second mode decays faster than the first mode. Hence, in order to extract only the first natural frequency, the relatively steady state portion of the signal was used, where the second mode and other transients are expected to be negligible ($t_1 = 27$s to $t_2 = 37$s, while the total duration of the signal was 37s). In order to study the effect of introducing noise formulation, the number of measurements is varied and the corresponding variation in average l_2 error of reconstruction is analyzed. Figure 5.16 illustrates the change in l_2 reconstruction error for varying number of measurements. It can be observed that for all the plots, the l_2 error decreases with an increase in the number of measurements. This is because, with increasing number of measurements, the probabilistic (CS) solution tends towards a more definitive solution. When noise formulation is incorporated in the CS problem, the average l_2 error is reduced for a given number of measurements. This implies that using such a formulation has the ability to further reduce the number of samples used for reconstruction. This analysis, as extended to the spatial domain then implies that

the number of sensors (spatial samples) could also potentially be reduced.

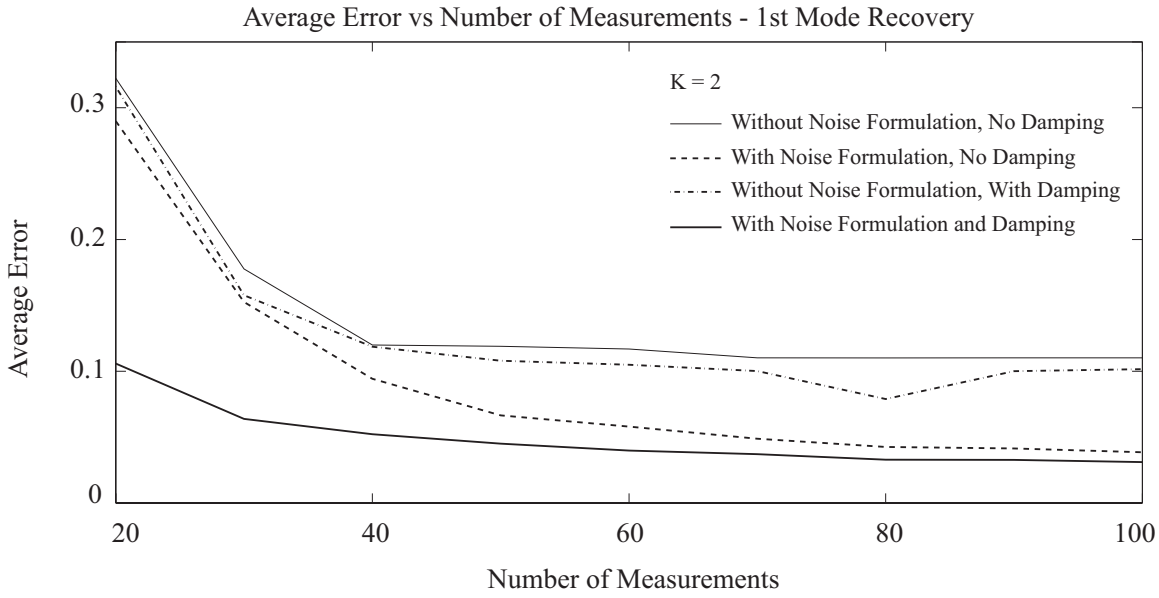

Figure 5.16: Effect of noise formulation and damping in CS-based frequency recovery: Variation of average l_2 error for increasing m - Experimental study (1st mode)

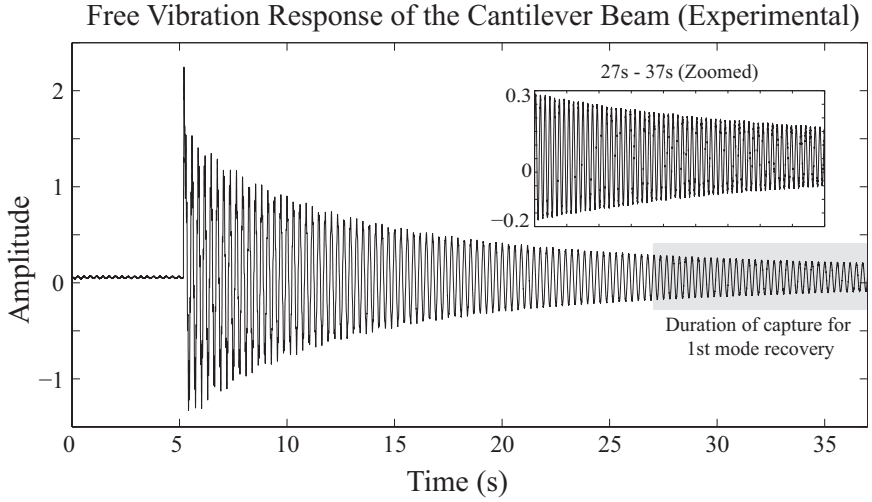

Figure 5.17: Impulse response of the cantilever beam in the experimental setup: Zoomed in view of the steady state response

Without accounting for the damping in response, the average error calculated may not reflect a true comparison between the original and reconstructed responses of the cantilever beam. Therefore, an approximation of the damping ratio for the first mode was calculated using the following set of equations, considering the part of the beam response from 27s to 37s.

Approximate calculation of ζ_1:

$$\delta = \frac{1}{n} log(\frac{P_1}{P_n}) = \frac{2\pi\zeta}{\sqrt{1-\zeta^2}} \tag{5.15}$$

where, P_1 and P_2 are the amplitudes to the first and n^{th} peaks of the signal respectively and n is the number of peaks/periods considered. Here, $P_1 = 0.2734$, $P_2 = 0.1709$ and $n = 52$. Therefore, $zeta_1 = 0.0014$. It is also important to understand how the measurement matrix was modified to accommodate for damping. The exponential component (that represents damping) is included as a part of the matrix, and is as expressed below.

$$\begin{bmatrix} e^{-\zeta_1\omega_1 t_1}\cos(\omega_1 t_1) & \cdots & e^{-\zeta_1\omega_n t_1}\cos(\omega_n t_1) & e^{-\zeta_1\omega_1 t_1}\sin(\omega_1 t_1) & \cdots & e^{-\zeta_1\omega_n t_1}\sin(\omega_n t_1) \\ e^{-\zeta_1\omega_1 t_2}\cos(\omega_1 t_2) & \cdots & e^{-\zeta_1\omega_n t_2}\cos(\omega_n t_2) & e^{-\zeta_1\omega_1 t_2}\sin(\omega_1 t_2) & \cdots & e^{-\zeta_1\omega_n t_2}\sin(\omega_n t_2) \\ \vdots & \vdots & \vdots & \vdots & \vdots & \vdots \\ e^{-\zeta_1\omega_1 t_m}\cos(\omega_1 t_m) & \cdots & e^{-\zeta_1\omega_n t_m}\cos(\omega_n t_m) & e^{-\zeta_1\omega_1 t_m}\sin(\omega_1 t_m) & \cdots & e^{-\zeta_1\omega_n t_m}\sin(\omega_n t_m) \end{bmatrix} \tag{5.16}$$

After including the damping component in the reconstruction of the response, the average l_2 error was again calculated. From Fig.5.16, it can observed that for a given number of measurements, when damping is accounted for, in addition to noise formulation, there is a significant drop in error. This result is especially important for reconstruction of the spatial response of a realistic beam where damping will be inevitable. This is however outside the scope of this dissertation, but will be addressed as a part of further work. Table 5.10 lists the percentage drop in l_2 reconstruction error for each measurement case.

Table 5.10: Drop in Average l_2 Reconstruction Error With Noise Formulation (NF) and Damping

No. of Measurements	No NF	With NF and Damping	% Drop in l_2 error
20	0.322	0.106	67.19
30	0.178	0.064	64.09
40	0.120	0.052	56.48
50	0.119	0.045	62.14
60	0.117	0.040	65.98
70	0.110	0.037	66.39
80	0.110	0.033	70.17
90	0.110	0.033	70.17
100	0.110	0.031	71.87

Recovering the First and Second Modes of Vibration from Experimental Data

The section on preliminary experimental validation, explained in detail, the process of detecting structural change in a cantilever beam by recovering the first two natural frequencies of vibration and identifying a shift in their values. Furthermore, the experimental validation suggested that change in structural characteristics may not be uniformly reflected in all the modes/natural frequencies. For instance, it was observed that when mass sets were added at mid-length of the beam, the shift in second mode was more pronounced than in the first. Therefore, depending upon the nature of change, it may mandate the recovery of frequencies higher than the first mode. This question leads into a new avenue of research - localization of energy in specific modes. Although it is beyond the scope of this dissertation, it is nevertheless, a problem that we intend to address as a part of the future work of this project.

Recovering the second natural frequency was feasible by suitably adjusting the number of measurements and frequency range. However, as discussed for the first mode in the previous section, evaluating the performance of CS in recovering the second mode will also require reconstruction of the response that should account for not only this mode, but its damping as well. Given that the second mode decays rather quickly, it dictates that the initial part of the response be used for frequency recovery and reconstruction. Table 5.11 lists the CS problem formulation. Here, the CS problem attempts to recover the first two natural frequencies from the free vibration response of the cantilever beam. Since each frequency has two (sine and cosine) components associated with it, the sparsity $k = 4$. In order to extract the second natural frequency, the initial duration of response was utilized ($t_1 = 5.2$s to $t_2 = 10.2$s, while the total duration of the signal was 37s). As mentioned earlier, the number of measurements is varied and the corresponding variation in average l_2 error of reconstruction is analyzed.

Table 5.11: Problem Setup for Evaluating CS performance with Noise Formulation - Cantilever Beam (Experimental - 1st and 2nd modes)

Parameters	K = 4
No. of Frequencies	2
Frequencies (Hz)	3.41, 21.23
Frequency range (Hz)	0:0.01:30
Duration of data capture (s)	5.2 - 10.2
No. of samples (m)	20 - 100

Figure 5.18 illustrates the change in l_2 reconstruction error for varying number of measurements. Similar to Fig.5.16, the l_2 error decreases with an increase in the number of measurements.

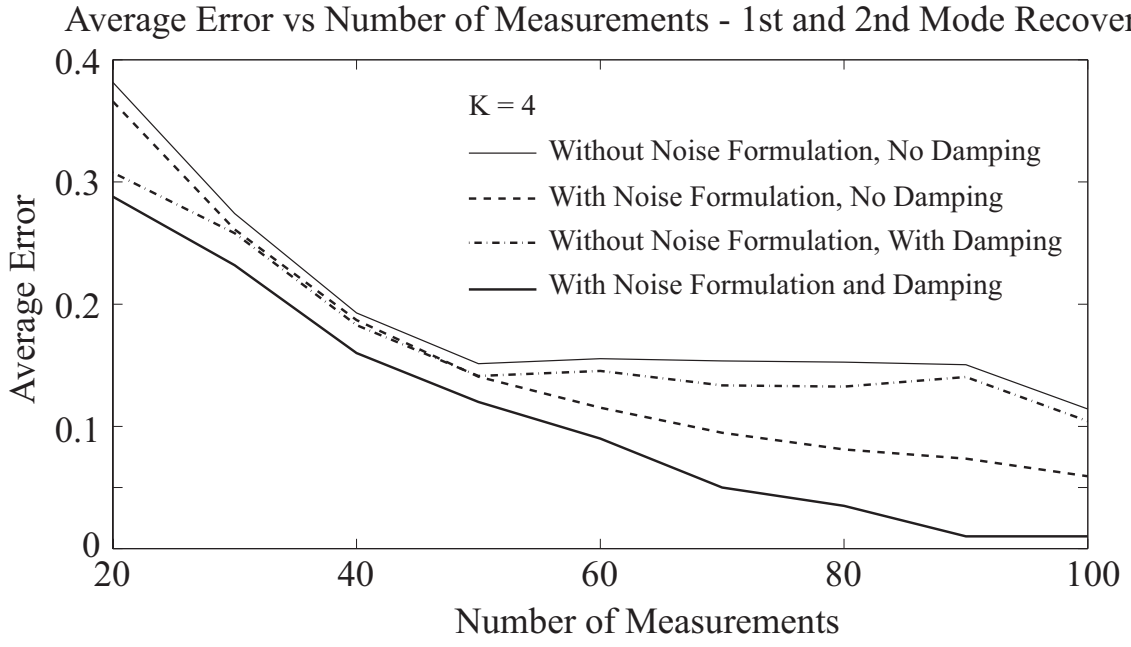

Figure 5.18: Effect of noise formulation and damping in CS-based frequency recovery: Variation of average l_2 error for increasing m - Experimental study (1st and 2nd modes)

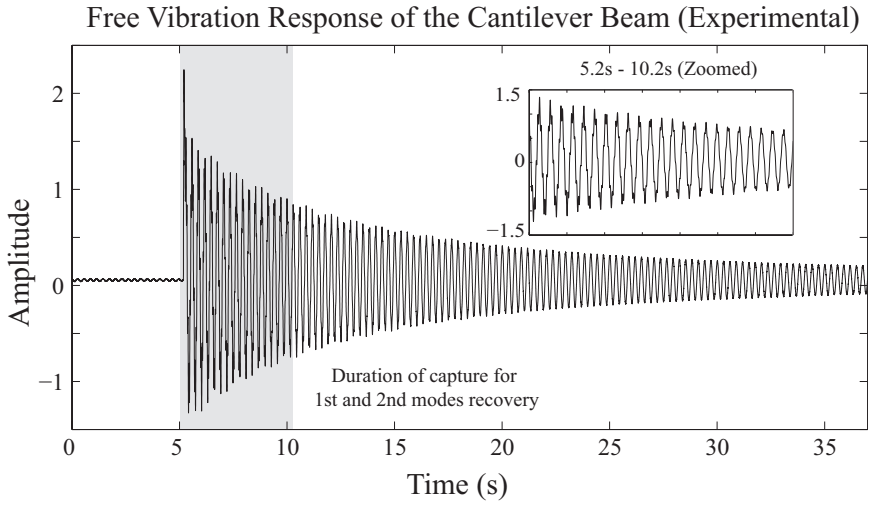

Figure 5.19: Impulse response of the cantilever beam in the experimental setup: Zoomed in view of the transient portion of response

As explained in Section 5, in order to draw a better comparison of the performance of CS without

and with the incorporation of noise formulation, it is necessary to account for damping. Figure 5.19 illustrates the portion of the response used in calculating the approximate damping ratio and subsequent signal reconstruction. Using Eq.(5.15), the approximate damping coefficient was calculated using the following values: $n = 25 \;\; P_1 = 1.533 \;\; P_2 = 0.6787 \;\; \Longrightarrow \;\; \zeta_{1,2} = 0.0052$. The measurement matrix used here is as described in Eq.(5.16). Because the initial duration of the vibration response is a combination of the first and the second modes as well as any transients, the approximate ζ calculated above is not purely associated with the second mode. It is therefore denoted by $\zeta_{1,2}$. Furthermore, because the amplitude of the second mode is comparable to other undesirable transients or noise, incorporation of noise formulation in the CS problem tends to eliminate or lower the effect of the second mode during reconstruction. As a result, although the average l_2 error exhibits an appreciable drop in the presence of noise formulation and damping, the value of the error is higher in comparison to that in Fig.5.16. The decrease in l_2 error values for varying number of measurements in this case is listed in Table 5.12.

Table 5.12: Drop in Average l_2 Reconstruction Error With Noise Formulation (NF) and Damping

No. of Measurements	No NF	With NF and Damping	% Drop in l_2 error
20	0.308	0.288	6.41
30	0.258	0.232	10.15
40	0.259	0.160	38.33
50	0.244	0.120	50.79
60	0.255	0.090	64.68
70	0.229	0.050	78.16
80	0.216	0.035	83.82
90	0.286	0.010	96.50
100	0.207	0.010	95.17

Section 4 illustrates that changes in beam characteristics produce distortions in its Operational Deflection Shape (ODS). Determining the spatial response or the ODS is key to locating these changes. This section investigates reconstruction of the ODS of a beam using compressive sensing by applying it spatially. The deflection shape of a beam under free-vibration, at an instant $\bar{t}$, can be expressed in terms of the normal modes $q = 1, 2, \cdots \infty$ as

$$\begin{aligned} y(x,\bar{t}) &= \sum_{q=1}^{\infty}[A_q\cos(\omega_q\bar{t}) + B_q\sin(\omega_q\bar{t})]W_q(x) \\ &= \sum_{q=1}^{\infty} C_q(\bar{t})W_q(x), \end{aligned} \tag{5.17}$$

where, $C_q(\bar{t}) = [A_q\cos(\omega_q\bar{t}) + B_q\sin(\omega_q\bar{t})]$ and W_q is the q^{th} mode-shape. On the other hand, the instantaneous deflection shape in response to a steady harmonic forcing $F = \sum_{i=1}^{p} f_{0,i}\sin(\omega_{f,i}t)$ takes the form

$$\begin{aligned} y(x,\bar{t}) &= \sum_{i=1}^{p}\sum_{q=1}^{\infty} D_q(\omega_q,\omega_{f,i})f_{0,i}\sin(\omega_{f,i}\bar{t})W_q(x) \\ &= \sum_{q=1}^{\infty}\bar{D}_q(\bar{t})W_q(x), \\ \bar{D}_q(\bar{t}) &\triangleq \sum_{i=1}^{p} D_q(\omega_q,\omega_{f,i})f_{0,i}\sin(\omega_{f,i}\bar{t}) \end{aligned} \tag{5.18}$$

From Eqs.(5.17) and (5.18), one distinction of the two deflection shapes is that the former is dependent on $\bar{t}$, while the other is not, provided the forcing has steady amplitudes and frequencies. Thus, deflection shapes generated by steady forced vibration are time-invariant. The rationale for formulating the deflection-shape reconstruction using compressive-sensing is that mode-shapes W_q are sparse in β_q, since β_q and ω_q are related by $\omega_q = \beta_q^2\sqrt{EI/\rho A_r}$. For instance for a simply-supported beam, $W_q = \sin\beta_q x = \sin\frac{q\pi x}{L}$ and that for a cantilever beam are given by Eq.(5.3). The following sections explain and illustrate ℓ_1 minimum solutions for reconstructing deflection shapes for simply-supported, fixed-fixed and cantilever beams. The emphasis will be on reconstruction from forced vibration response.

Spatial recovery remains similar to that of time-domain. However, sampling of the beam response is performed at one time instant from different spatial points along the length of the beam, i.e. the length axis becomes analogous to time axis. The parameters used to define the beam, L, EI and ρA_r, are the same as those in Section 5. Results of CS based recovery are validated against a finite-element model of the beam of N_{el} elements. Figure 5.20(a) illustrates the beam. From Eq.(5.18), the deflection equation for a simply supported beam can be expressed as

$$y(x,\bar{t}) = \sum_{q=1}^{\infty} \bar{D}_q(\bar{t}) W_q, \quad W_q = \sin(\beta_q x) = \sin\frac{q\pi x}{L}. \tag{5.19}$$

Thus, the basis functions are sinusoids of wavelengths $\lambda_q = 2L/q$, i.e. of spatial frequency $\xi_q = q/2L$. Consider the problem of reconstructing the deflection shape of the beam under a harmonic force with frequency $\omega_q < \omega_f < \omega_{q+1}$. The deflection shape will be dominated by the q^{th} and $(q+1)^{th}$ mode-shapes, i.e. by ξ_q and ξ_{q+1}. Consider a spatial frequency range $\Xi_r = [\xi_l, \xi_h]$, such that $(\xi_q, \xi_{q+1}) \in [\xi_l, \xi_h]$, and a measurement vector $z \in R^m$ generated by measurements y taken at m random locations along the length of the beam at an instant $\bar{t}$, $z_j = y(x_j, \bar{t})$, $j = 1, 2, \cdots m$.

$$z_j = \sum_{i}^{n} H_i \sin(2\pi\xi_i x_j), \quad \xi_i = \xi_l + (i-1)\frac{(\xi_h - \xi_l)}{n-1},\ i = 1,\ 2,\ \cdots n, \tag{5.20}$$

The deflection shape can be reconstructed by determining the ℓ_1 minimum solution of

$$z = \Phi s, \quad \Phi = \begin{bmatrix} \sin(2\pi\xi_1 x_1) & \sin(2\pi\xi_2 x_1) & \cdots & \sin(2\pi\xi_n x_1) \\ \sin(2\pi\xi_1 x_2) & \sin(2\pi\xi_2 x_2) & \cdots & \sin(2\pi\xi_n x_2) \\ \vdots & \vdots & \vdots & \vdots \\ \sin(2\pi\xi_1 x_m) & \sin(2\pi\xi_2 x_m) & \cdots & \sin(2\pi\xi_n x_m) \end{bmatrix}, \tag{5.21}$$
$$s = [H_1\, H_2\, \cdots H_n]^T.$$

In Eq.(5.21), Ξ_r forms a searching frequency-range and we expect to obtain a sparse solutions with non-zero H_i if $H_i \approx \bar{D}_q$. We note that although the deflection shape will have the presence of other mode-shapes, such as $(q-1)^{th}$ and $(q+2)^{th}$, but their influence will be minor. When the characteristics of the beam changes locally, such as due to damage, the mode-shapes W_q cease to have the analytic form of Eq.(5.19). Hence in a damaged or modified beam, the ℓ_1 solution will show a lower sparsity. However, an indicator of the location of a damage will be the reconstructed deflection shape itself rather than the non-zero coefficients of the sparse solution.

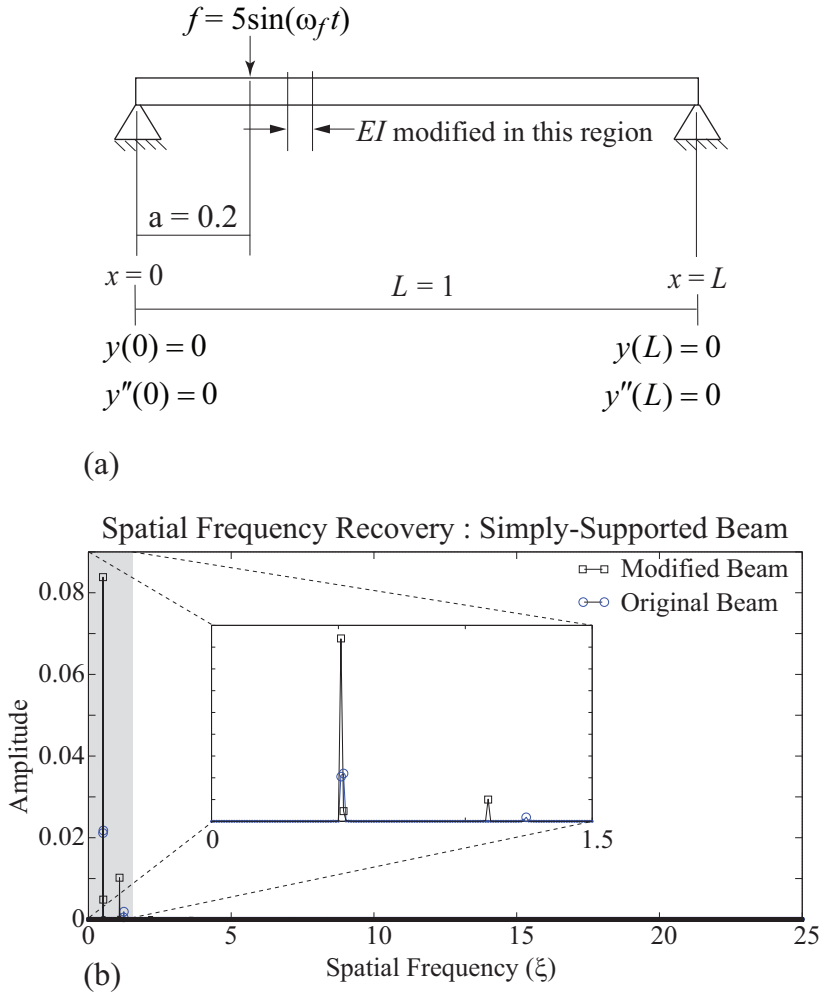

Figure 5.20: (a) Schematic: SS beam with harmonic excitation (b) Spatial frequencies recovered before and after modification of elements

To illustrate the observations made above, we simulate forced vibration of a beam with the following parameters: $L = 1$, $\rho Ar = 1$, $EI = 1$. For the simulation, a finite element model of the beam is used with $N_{el} = 1000$. It is subject to a harmonic excitation force $F = 5\sin(5t)$, which is applied at a distance $a = 0.2$ from the left, as shown in Fig.5.20(a).

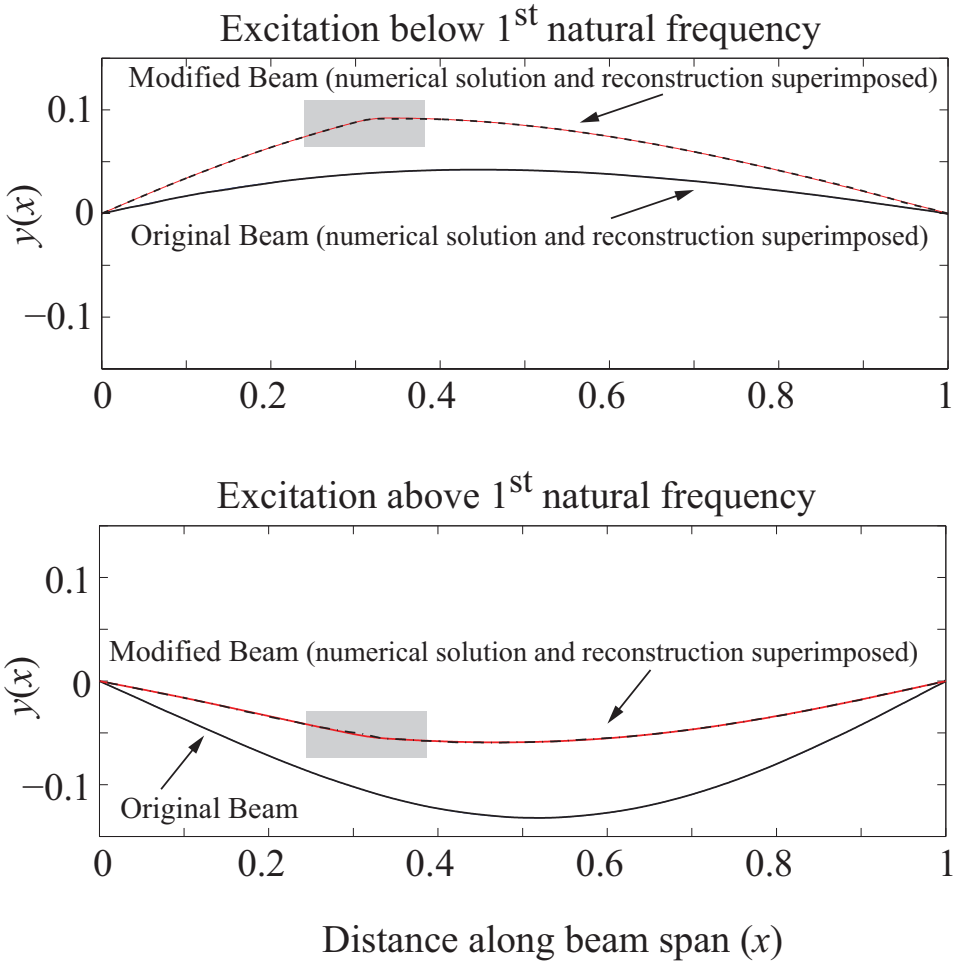

Figure 5.21: Deflections of original and modified beam, with numerical solutions and reconstructed deflections superimposed: (a) ω_f below, and (b) ω_f above the 1^{st} natural frequency

In the original beam, the spatial frequencies ξ_q are $0.5,\ 1,\ 1.5,\ \cdots$, and the corresponding natural frequencies ω_q are $\pi^2,\ 4\pi^2,\ 9\pi^2, \cdots$ rad/s. Since $\omega_f = 5 < \pi^2$, the deflection shape is expected to be mostly dominated by its first mode. To reconstruct the deflection shape, $m = 25$ random dis-

placement samples were collected at a specific time-instant along the beam-span. The ℓ_1 minimum solution of Eq.(5.21) was determined with $n = 2500$, $\xi_l = 0$ and $\xi_h = 25$, implying a frequency resolution of ≈ 0.01, see Eq.(5.21).

The sparse solution for the original beam is shown in Fig.5.20(b), showing the dominant spatial frequency to be at the first mode-shape $\xi = 0.5$, as expected. Next, a fault is introduced by reducing EI from 1 to 0.1, locally in the region $x \in [0.3, 0.35]$, and the ℓ_1 minimum solution was recalculated. The solution is indicated in Fig.5.20(b) as modified beam. The ℓ_1 minimum solutions show shifts in spatial frequencies between the original and modified beam. However, they do not reflect the location of modification (or damage). To determine the location of the damage, the frequencies recovered are used to reconstruct the deflection shape. The reconstruction is shown in Fig.5.21(a) for both the original beam and the modified beam. The accuracy of reconstruction is verified by superimposing the numerical solutions obtained from the finite element model.

For further illustration of shape reconstruction, the forcing frequency was increased $\omega_f = 11$rad/s, which is above the 1^{st} natural frequency of the original beam. The compressive sensing problem was solved to determine the sparse solution in spatial domain and the deflection-shape was reconstructed using the same procedure as above. The results are shown in Fig.5.21(b). In both Figs.5.21(a) and(b), we notice that the region of the defect (or modification) is visually identifiable, and are indicated by the gray squares. In Fig.5.21(a), it was better identifiable due to higher amplitude of oscillation resulting from lower excitation frequency. We clarify that the deflection directions are flipped in Fig.5.21(a) and (b) simply because at the instants at which data were taken, the beams were undergoing positive and negative displacements respectively.

Deflection Shape Reconstruction for Fixed-Fixed Beam

In this section, deflection shape reconstruction, using the idea of compressive sampling, is demonstrated for fixed-fixed beam. The process closely follows the one in Section 5. Both ends of a fixed-fixed beam are constrained to have neither displacement nor slope. The beam-parameters, L, EI and ρA_r, carry their usual meaning. As before, CS based recovery are validated against a finite-element model of the beam of N_{el} elements. Figure 5.22(a) illustrates the beam.

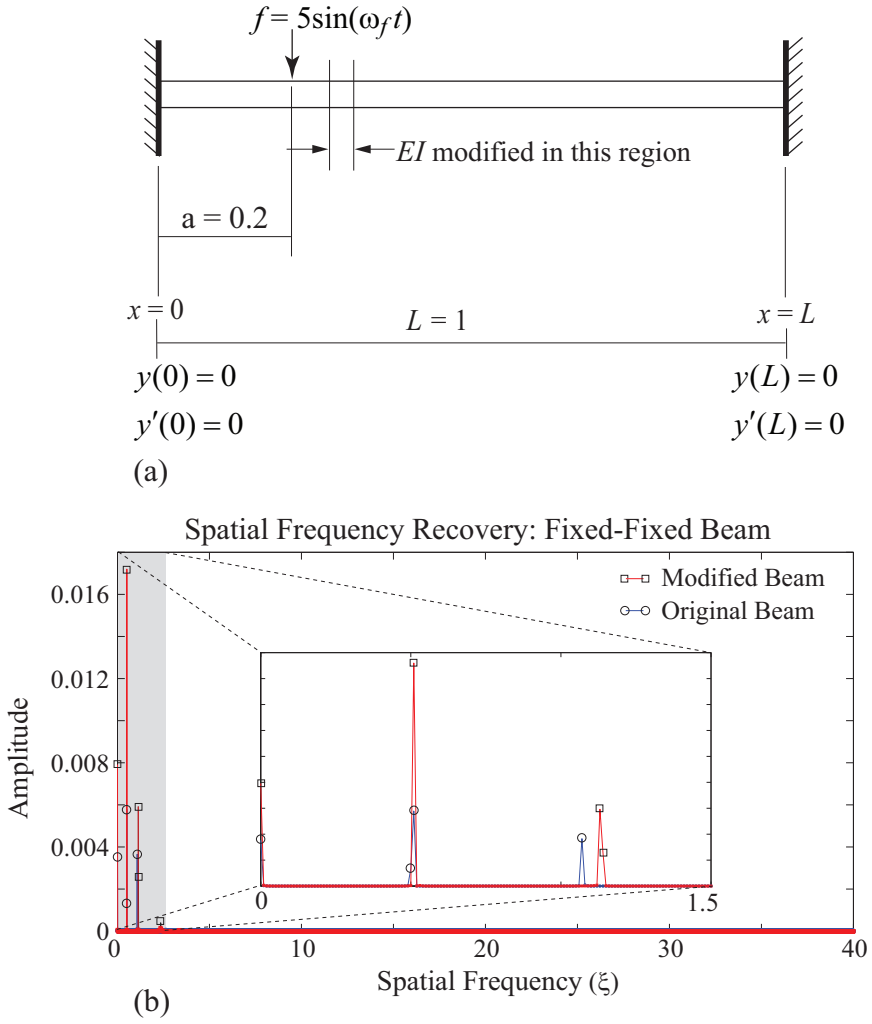

Figure 5.22: (a) Schematic: Fixed-fixed beam with harmonic excitation (b) Spatial frequencies recovered before and after modification of elements

From Eq.(5.18) and [7], the deflection equation for a fixed-fixed beam, at an instant $\bar{t}$ can be expressed as

$$y(x,\bar{t}) = \sum_{q=1}^{\infty} \bar{D}_q(\bar{t}) W_q, \quad W_q = (\sinh \beta_q x - \sin \beta_q x) + \alpha_q(\cosh \beta_q x - \cos \beta_q x), \\ \alpha_q = \frac{\sinh \beta_q L - \sin \beta_q L}{\cos \beta_q L - \cosh \beta_q L}, \quad \cos \beta_q L . \cosh \beta_q L = 1. \tag{5.22}$$

Here the basis is formed by sinusoids and hyperbolic functions. The sinusoids have wavelengths $\lambda_q = 2\pi/\beta_q$, i.e. spatial frequency $\xi_q = \beta_q/2\pi$. For fixed-fixed beams, Eq.(5.22) yields $[\beta_1 L,\ \beta_2 L,\ \beta_3 L,\ \beta_4 L,\ \cdots] = [4.73,\ 7.85,\ 11,\ 14.14,\ \cdots]$. Spatial reconstruction was formulated on similar lines as in Section 5. The following specifications were chosen for the beam: $L = 1$, $\rho A_r = 1$, $EI = 1$ and $N_{el} = 1000$. The beam is harmonically excited at $\omega_f = 20$rad/s which is lower than the first natural frequency of the undamaged beam, $\omega_1 = \beta_1^2 = 22.37$rad/s. The force, of amplitude 5, is applied at a distance $a = 0.2$ from the left, as indicated in Fig.5.22(a). The resulting ODS is expected to resemble a sinusoid of wavelength 2, i.e. $\xi = 0.5$, but with zero deflection and slope near the fixed ends. Structural change is introduced by a reduction in EI from 1 to 0.1 over elements $300 - 340$. The ℓ_1 minimization problem for deflection reconstruction requires a spatial frequency range, as done in Section 5. The range chosen for both the original and modified cases are $\Xi_r = [\xi_l,\ \xi_h] = [0,\ 40]$, with a resolution of 0.01. The measurement vector $z \in R^m$ is generated by taking $m = 25$ measurements y taken at random locations along the length of the beam at an instant $\bar{t}$, $z_j = y(x_j, \bar{t})$, $j = 1, 2, \cdots m$. Based on Eq.(5.22), z_j can be expressed as a function of the basis functions as follows:

$$z_j = \sum_{i}^{n} \big[H_{i,1} \sin(2\pi \xi_i x_j) + H_{i,2} \sinh(2\pi \xi_i x_j) + H_{i,3} \cos(2\pi \xi_i x_j) + H_{i,4} \cosh(2\pi \xi_i x_j) \big], \\ \xi_i = \xi_l + (i-1)\tfrac{(\xi_h - \xi_l)}{n-1}, \quad i = 1,\ 2,\ \cdots n, \tag{5.23}$$

or in a more condensed form, based on Eq.(5.22) as,

$$z_j = \sum_i^n H_i\big[(\sinh(2\pi\xi_i x_j) - \sin(2\pi\xi_i x_j)) + \alpha_i(\cosh(2\pi\xi_i x_j) - \cos(2\pi\xi_i x_j))\big] \\ \alpha_i = \tfrac{\sinh(2\pi\xi_i L) - \sin(2\pi\xi_i L)}{\cos(2\pi\xi_i L) - \cosh(2\pi\xi_i L)}. \tag{5.24}$$

However, trial runs showed poor reconstruction when either of the above sets were used. In contrast, upon using the *sine* and *cosine* functions only

$$z_j = \sum_i^n \big[H_{i,1}\sin(2\pi\xi_i x_j) + H_{i,2}\cos(2\pi\xi_i x_j)\big], \tag{5.25}$$

resulted in significantly better reconstruction. Specifically, the deflection shape was reconstructed by determining the ℓ_1 minimum solution of

$$z = \Phi s, \quad \Phi = \begin{bmatrix} \sin(2\pi\xi_1 x_1) & \cdots & \sin(2\pi\xi_n x_1) & \cos(2\pi\xi_1 x_1) & \cdots & \cos(2\pi\xi_n x_1) \\ \sin(2\pi\xi_1 x_2) & \cdots & \sin(2\pi\xi_n x_2) & \cos(2\pi\xi_1 x_2) & \cdots & \cos(2\pi\xi_n x_2) \\ \vdots & \vdots & \vdots & \vdots & \vdots & \vdots \\ \sin(2\pi\xi_1 x_m) & \cdots & \sin(2\pi\xi_n x_m) & \cos(2\pi\xi_1 x_m) & \cdots & \cos(2\pi\xi_n x_m) \end{bmatrix}, \\ z \in R^m, \quad s = [H_{1,1}\ H_{2,1}\ \cdots H_{n,1}\ H_{1,2}\ H_{2,2}\ \cdots H_{n,2}]^T. \tag{5.26}$$

The reason the formulations of Eqs.(5.25) and (5.26) perform better than those in Eqs.(5.23) and (5.24) is better understood by comparing the *Restricted Isometry Constant* for each case for similar sparsity. As explained in Section 4, this constant is a measure of how well-conditioned the corresponding Φ matrix is. A numerical comparison of the constant, calculated for different sets of basis functions, will be discussed in Section 5. Figure 5.22(b) shows the sparse solution obtained by ℓ_1 minimization. For each frequency, the amplitude is calculated as $\sqrt{H_{i,1}^2 + H_{i,1}^2}$. Because the deflection shape is similar to a sinusoid but with zero slopes at the ends, zero frequency component is also recovered. Furthermore, the fundamental spatial frequency $\xi = 0.5$ is prominent.

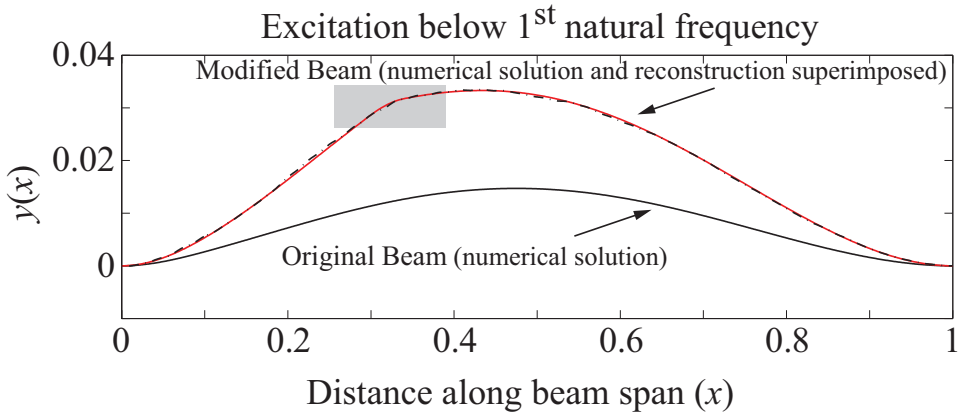

Figure 5.23: Deflections of original and modified beam with superimposed reconstruction

Locating a change/damage requires comparison of the deflection shape before and after introducing structural change in the beam. The reconstructed deflection shape of the modified beam (with EI reduced from 1 to 0.1) is superimposed with the numerical solution in Fig.5.23. Numerical solution of the original deflection is shown on the same plot.

Recall Fig.5.2, where the effectiveness of ℓ_1 minimization was studied by plotting the accuracy of signal recovery in the temporal domain against the number of measurements m. Figure 5.24 illustrates the same, but signal recovery is in the spatial domain for the unmodified fixed-fixed beam described above. In this domain, recovery of spatial frequencies is considered and the signal sparsity is determined by the number of spatial frequencies present in it. Nominally, $n \approx 4000$ and $\Delta\xi = 0.01$ was chosen, thus the frequency range of recovery was $\Xi_r = [0,\ 40]$. Although the highest spatial frequency expected to be recovered is less than 2, this extended frequency range is important for inducing sparsity in the signal, thereby ensuring good deflection reconstruction.

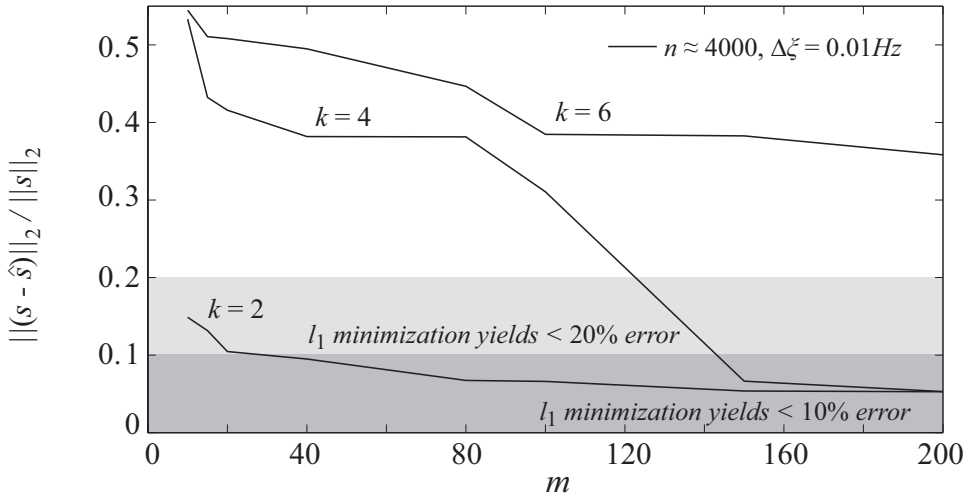

Figure 5.24: Error analysis of ℓ_1 minimization as a function of measurements m for different spatial signal sparsity

The contour $k = 2$ represents the normalized error norm $\|s - \hat{s}\|_2$ when the forced vibration response of the fixed-fixed beam was dominated by the 1^{st} mode, $\xi \approx 0.5$. The contour $k = 4$ represents accuracy of recovery when the first two modes were predominantly present in the response($\xi \approx 0.5$, 1). Similarly, $k = 6$ represents the case when the first 3 modes are predominantly present in the forced response of the beam. Contours in Fig.5.24 match the trend of the contours in Fig.5.2, thus reinforcing the following about ℓ_1 minimization in the spatial domain also: (i) Signal recovery is enhanced with increase in the number of measurements (ii) Higher sparsity benefits signal recovery and reconstruction.

Deflection Shape Reconstruction for Cantilever Beam

In this section, structural changes introduced in a cantilever beam are located by compressive sampling. The process closely follows that explained in the Sections 5 and 5. A schematic representation of a cantilever beam, with its boundary conditions, is shown in Fig.5.25(a).

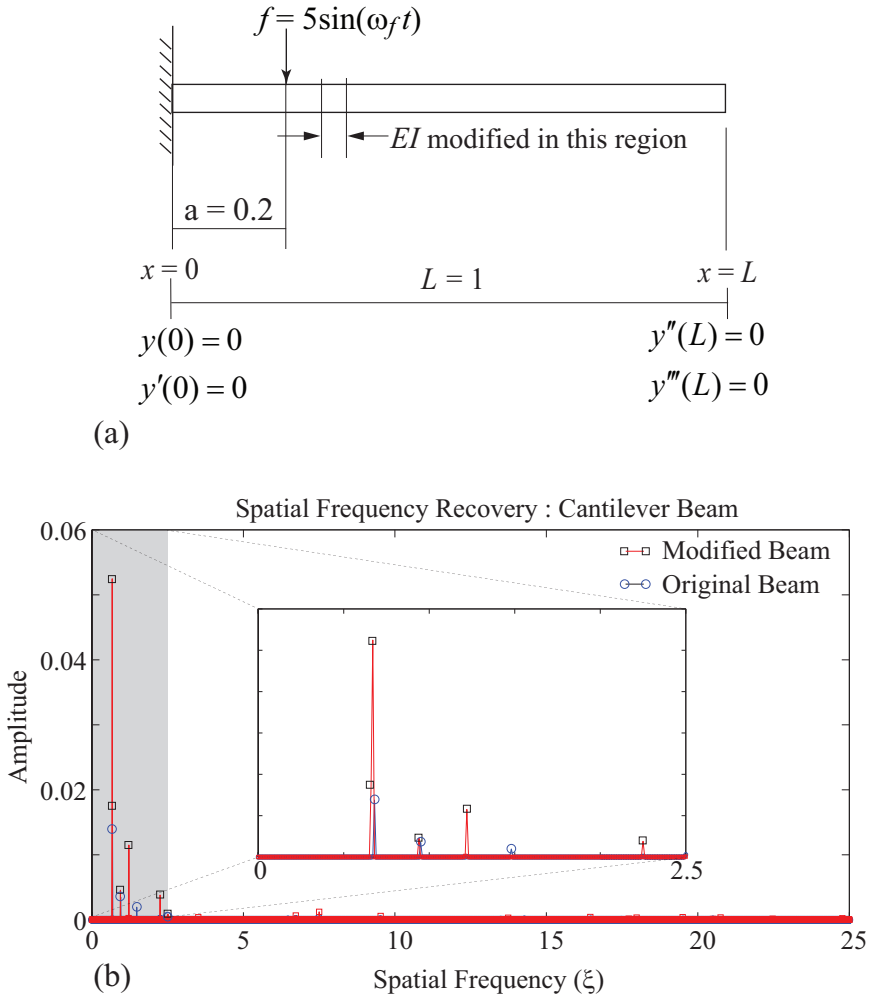

Figure 5.25: (a) Schematic: Cantilever beam, (b) Spatial frequencies recovered from original and modified deflections

Beam parameters retain the same value as prior sections, i.e. $L = 1$, $\rho A_r = 1$, $EI = 1$ and the number of elements in the simulation model is $N_{el} = 1000$. The harmonic force, applied at $a = 0.5$, has a frequency of $\omega_f = 20$rad/s. From Eq.(5.18) and [7], the deflection equation for a

cantilever beam, at any instant $\bar{t}$ can be expressed as

$$y(x,\bar{t}) = \sum_{q=1}^{\infty} \bar{D}_q(\bar{t}) W_q, \quad W_q = (\sin\beta_q x - \sinh\beta_q x) - \alpha_q(\cos\beta_q x - \cosh\beta_q x), \\ \alpha_q = \frac{\sinh\beta_q L + \sin\beta_q L}{\cos\beta_q L + \cosh\beta_q L}, \quad \cos\beta_q L.\cosh\beta_q L = -1. \tag{5.27}$$

For cantilever beams, Eq.(5.27) yields $[\beta_1 L,\ \beta_2 L,\ \beta_3 L,\ \cdots] = [1.88,\ 4.69,\ 7.85,\ \cdots]$. Thus, ω_f is between the first two natural frequencies, $\omega_1 = \beta_1^2 = 3.53$rad/s and $\omega_2 = \beta_2^2 = 22$rad/s. It is also noted that the spatial frequency $\xi_2 = \beta_2/(2\pi) = 0.75$. Based on Eq.(5.27), measurements z_j were expressed as in Eq.(5.23). The spatial frequency range for reconstruction was chosen as $\Xi_r = [\xi_l,\ \xi_h] = [0,\ 25]$, with a resolution of 0.01.

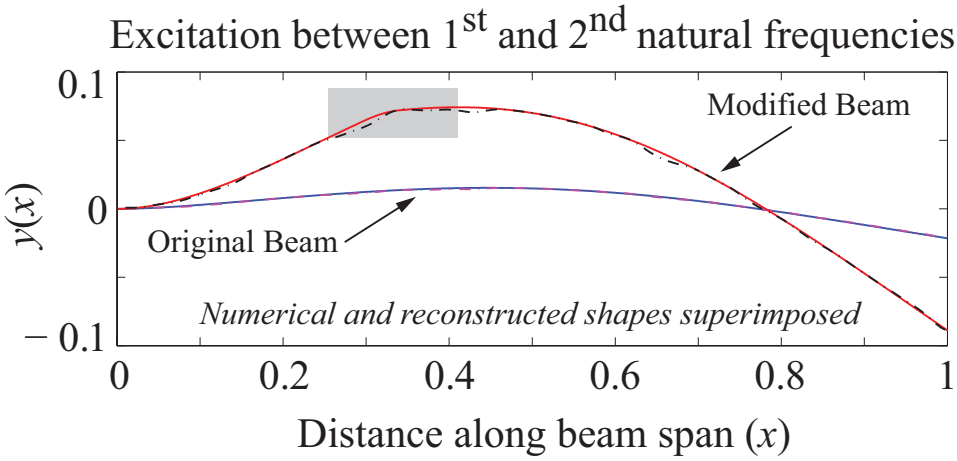

Figure 5.26: Deflection shape reconstruction of original and modified cantilever beam

Unlike fixed-fixed beams where only *sinusoids* were used for the reconstruction, Eqs.(5.25) and (5.26), for cantilever beams consistent reconstruction required inclusion of the *hyperbolic* functions for lower frequencies. For a sub-set $\Xi_{r,h} = [0,\ 2.5]$ of Ξ_r, hyperbolics were included in the basis functions and for the remainder of Ξ_r, only sinusoids were used. The need of hyperbolics is expected for a cantilever beam since its deflections are neither perfectly sinusoidal (e.g. simply-

supported beam), nor approximately sinusoidal (e.g. fixed-fixed beam). To simulate change, the rigidity modulus (EI) was reduced from 1 to 0.1 over elements $300-340$. The sparse solutions of the original and modified beam are shown in Fig.5.25(b) and Fig.5.26 illustrates reconstruction of the original and modified cantilever from the sparse solution. In solving the ℓ_1 minimum solution, the number of samples chosen was $m = 25$ for the original beam and $m = 35$ for the modified beam. Also, the amplitudes plotted in Fig.5.25(b) are $\sqrt{\sum_{j=1}^{4} H_{i,j}^2}$.

Design of Measurement Matrices in the Presence of Hyperbolics

As explained in section 4, the suitability of a measurement matrix Φ, for a given CS problem can be evaluated using the Restricted Isometry Property (RIP). This mathematical aspect of Φ will be discussed in detail in section 5. This section, on the other hand, explores plausible approaches for designing a suitable Φ in the presence of hyperbolic components. Compressive sensing is essentially an ℓ_1 minimization problem that solves an under-determined system of equations to reconstruct the required signal. The measurement matrix Φ, is designed prior to making measurements and is based on the characteristics of the signal to be recovered. One of the most important stages in formulating a CS problem is designing a suitable Φ, with the following characteristics [82]:

1. Well conditioned
2. Enables recovery of sparse coefficients with relative ease and accuracy

Localizing structural changes in a beam makes use of its spatial domain response or operational deflection shape (ODS) that may be expressed as a weighted sum of its modeshapes (Eq.(4.2). Therefore, based on boundary conditions, when hyperbolic components are present in the modeshape of a beam, they appear in the ODS as well as the measurement matrix, which represents the basis for ODS reconstruction. The cantilever beam is a case in point. Fundamental understanding of the nature of mechanical vibrations of standard beams is therefore used as the basis for

formulating Φ when hyperbolic components become inevitable in the response.

Understanding the Behavior of Hyperbolic Components

Depending upon boundary conditions, hyperbolic components such as $sinh$ and $cosh$ appear in the spatial vibration response (ODS) of certain mechanical beams. In certain cases, such as a cantilever beam, these components are indispensable in reconstructing the ODS. It is therefore important to understand the behavior of these components. Figure 5.27 illustrates the variation of $sinh(x)$ and $cosh(x)$ for increasing x.

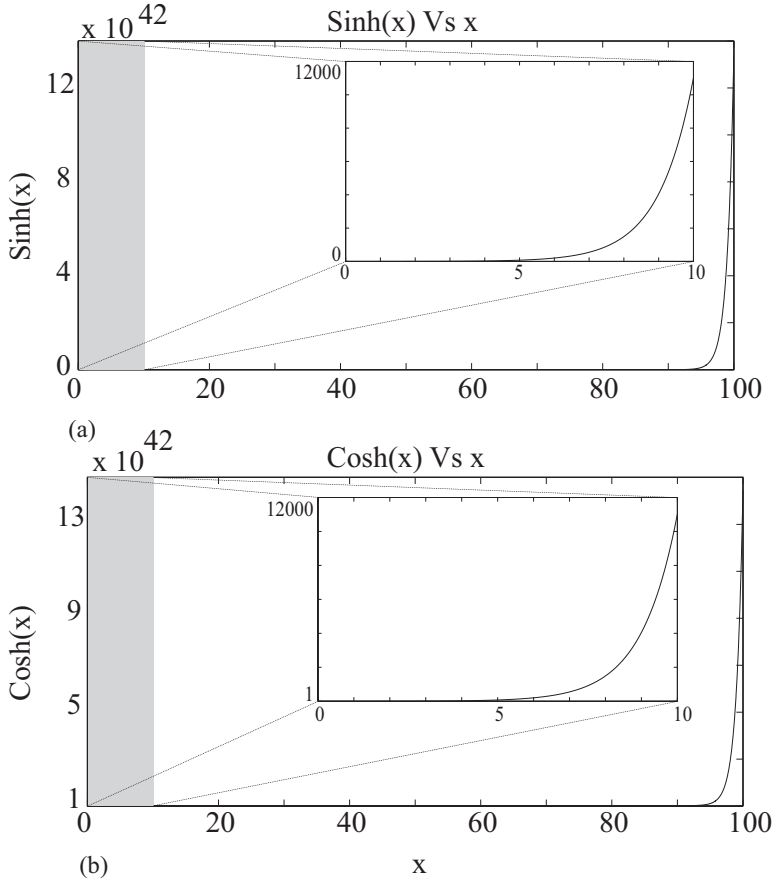

Figure 5.27: Variation of sine and cosine hyperbolic components with increasing x (a) $sinh(x)$ (b) $cosh(x)$

From the figure, it can be observed that values of the hyperbolic components grow almost exponentially with increasing x. Therefore, when such elements are present in the measurement matrix as given below, Φ becomes ill conditioned.

$$\Phi = \begin{bmatrix} \sin(2\pi\xi_1 x_1) & \cdots & \sin(2\pi\xi_n x_1) & \cos(2\pi\xi_1 x_1) & \cdots & \cos(2\pi\xi_n x_1) \\ \sin(2\pi\xi_1 x_2) & \cdots & \sin(2\pi\xi_n x_2) & \cos(2\pi\xi_1 x_2) & \cdots & \cos(2\pi\xi_n x_2) \\ \vdots & \vdots & \vdots & \vdots & \vdots & \vdots \\ \sin(2\pi\xi_1 x_m) & \cdots & \sin(2\pi\xi_n x_m) & \cos(2\pi\xi_1 x_m) & \cdots & \cos(2\pi\xi_n x_m) \end{bmatrix} \cdots$$

$$\cdots \begin{bmatrix} \sinh(2\pi\xi_1 x_1) & \cdots & \sinh(2\pi\xi_n x_1) & \cosh(2\pi\xi_1 x_1) & \cdots & \cosh(2\pi\xi_n x_1) \\ \sinh(2\pi\xi_1 x_2) & \cdots & \sinh(2\pi\xi_n x_2) & \cosh(2\pi\xi_1 x_2) & \cdots & \cosh(2\pi\xi_n x_2) \\ \vdots & \vdots & \vdots & \vdots & \vdots & \vdots \\ \sinh(2\pi\xi_1 x_m) & \cdots & \sinh(2\pi\xi_n x_m) & \cosh(2\pi\xi_1 x_m) & \cdots & \cosh(2\pi\xi_n x_m) \end{bmatrix}. \tag{5.28}$$

While solving the inverse problem using l_1 minimization, such an unbounded Φ poses numerical inconsistencies and difficulties in obtaining a solution and the CS recovery/reconstruction fails. Hence, it is important to devise approaches to design suitable measurement matrices for such cases. In fact, this problem of Φ design presents a wide and viable area for research as an offshoot of this work. Since the use of CS in the field of mechanical vibrations is still in its nascent stages, there isn't very elaborate literature on this topic, thus making it, an important investigation. To avoid numerical inconsistencies, in [83], the authors explain the use of approximate modeshapes for mechanical beams that contain hyperbolic functions. Following this, in our work, two approaches for designing Φ with hyperbolic components are examined:

1. Hyperbolics with restricted spatial frequency range
2. Combined hyperbolic components

Hyperbolic Components Over a Restricted Frequency Range

The modeshape function of a cantilever beam ($W_q(x)$) is expressed by Eq.(5.27). It follows that the corresponding Φ in the CS problem formulation for spatial response reconstruction will be a combination of these four trigonometric components for each frequency. An approach of restricting the $sinh$ and $cosh$ components over a lower frequency range is discussed here. This idea of restricting the frequency range was already introduced in section 5, where, by trial and error, $sinh$ and $cosh$ terms in the measurement matrix were ranging from $0 - 2.5\text{m}^{-1}$, while the sin and cos terms were ranging from $0 - 25\text{m}^{-1}$. A more systematic approach to this restriction is explored here.

In section 5, reconstruction of the cantilever beam ODS is obtained from the recovered spatial frequencies and the reconstruction equation takes the following form:

$$y(x) = a_i sin2\pi fx + b_i cos2\pi fx + c_i sinh2\pi fx + d_i cosh2\pi fx \tag{5.29}$$

where, a_i, b_i, c_i and d_i are the coefficients recovered using el_1 minimization. In this approach, where the hyperbolic and non-hyperbolic components are considered individually in Φ, the difficulty in reconstruction stems from the unbounded nature of $sinh$ and $cosh$ terms. Therefore, one rationale in restricting the frequency range of hyperbolic terms in Φ could be dependent on the relative magnitude between the hyperbolic and non-hyperbolic terms. The ratio of the magnitude of hyperbolic terms to that of the non-hyperbolic terms can be obtained from Eq.(5.30).

$$\begin{gathered} m1 = sinx + cosx, \quad m2 = sinhx + coshx, \\ m_{ratio} = \frac{m2}{m1} \end{gathered} \tag{5.30}$$

Figure 5.28 shows the relative magnitude, m_{ratio}, as a function of increasing frequency ($0 - 0.35$Hz). It can be observed that as the frequency increases, the relative magnitude increases almost exponentially. This is attributed to the exponentially increasing magnitudes of the hyperbolic components. Therefore, restricting the hyperbolic terms to lower frequencies in turn improves the conditioning of the measurement matrix.

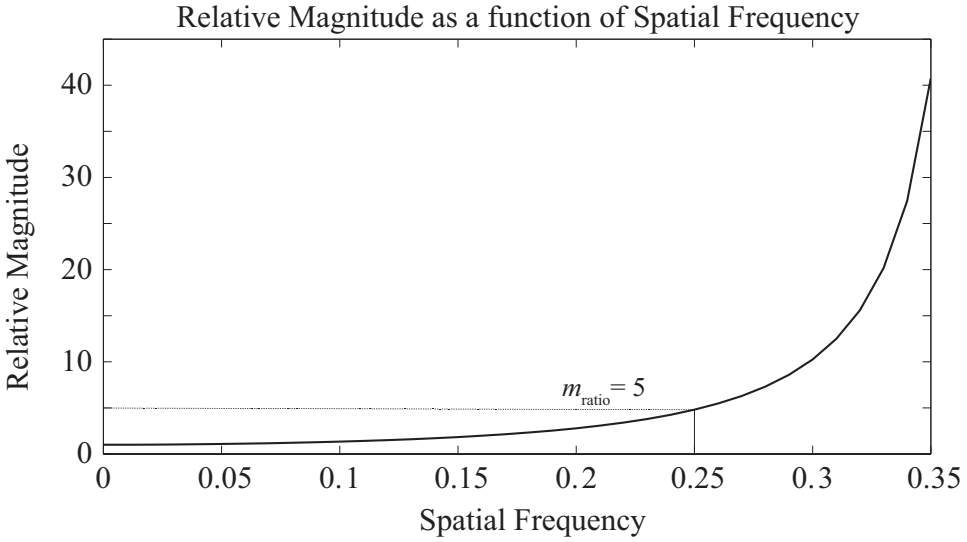

Figure 5.28: Relative magnitude as a function of spatial frequency

Reconstruction of the cantilever ODS with relative magnitude of 5 is illustrated in Fig.5.29(a). It represents relative magnitude of 5, which corresponds to the setup when the complete frequency range of operation is $0 - 25\text{m}^{-1}$ with restricted range $0 - 0.25\text{m}^{-1}$, i,e, scaling factor of 0.01. Case (b) represents a much higher relative magnitude which corresponds a scaling factor of 0.1. Through visual inspection, it can be seen that case (a) and (b) have comparable fidelity. However, the average error reduced from 0.0365 in case (b) to 0.0157 in case (a). In addition, it was observed that the probability of failed reconstruction was reduced with a scaling of 0.01. The performance of such a Φ is examined in sections that follow.

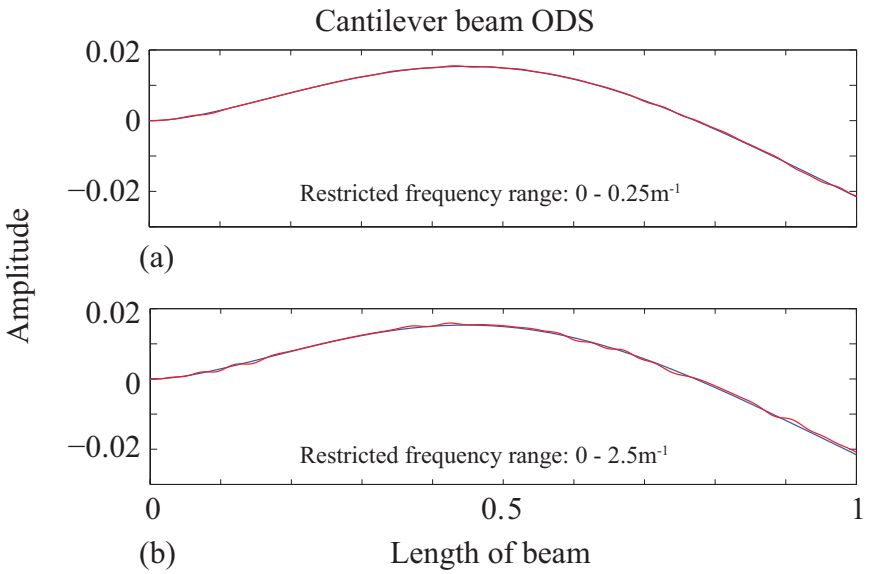

Figure 5.29: Reconstruction of cantilever beam ODS for different cases of frequency restriction (a) 0 - 0.25 (b) 0 - 2.5

While this investigation provided a rationale for restricting the hyperbolic terms to lower frequencies and a potential approach to choosing a suitable scaling factor, it did not help converge on a clear range of spatial frequencies that are to be included in the measurement matrix in the presence of hyperbolic terms. An alternative approach is explored in the following section.

Combined Hyperbolic Components

This section discusses an alternative approach to designing a suitable Φ with hyperbolic terms, without restricting their frequency range. This investigation is important because, although restricting hyperbolic components to lower frequencies did help bypass the numerical inconsistencies in the measurement matrix, it was still difficult to establish a systematic approach. Consider

the modeshape function of a cantilever beam.

$$\begin{aligned} W_q(x) &= (sin\beta_q(x) - sinh\beta_q(x)) - \alpha_q(cos\beta_q(x) - cosh\beta_q(x)) \\ \implies W_q(x) &= [sin\beta_q(x) - \alpha_q cos\beta_q(x)] - [sinh\beta_q(x) - \alpha_q cosh\beta_q(x)] \end{aligned} \tag{5.31}$$

Considering Eq.(5.31) and the nature of $sinh$ and $cosh$ from Fig.5.27, it can be understood that for a given frequency, the two hyperbolic terms may reduce the magnitude of each other. In addition, it is evident that for higher values of x, the magnitudes of $sinh(x)$ and $cosh(x)$ are almost equal to each other, thus possibly eliminating the effect of these hyperbolic functions in the modeshape. This presents an interesting case, because, formulating the measurement matrix, Φ, with these terms combined may therefore help eliminate the numerical inconsistencies encountered earlier with basis functions that contain hyperbolic components. There are several approaches to combining the terms. However, for investigation in this work, such a Φ is formulated as given below. The performance of CS-based ODS reconstruction using this Φ is examined in section 5.

$$\Phi = \begin{bmatrix} \sin(2\pi\xi_1 x_1) - \sinh(2\pi\xi_1 x_1) - \alpha_1 \cos(2\pi\xi_1 x_1) + \alpha_1 \cosh(2\pi\xi_1 x_1) & \cdots \\ \sin(2\pi\xi_1 x_2) - \sinh(2\pi\xi_1 x_2) - \alpha_1 \cos(2\pi\xi_1 x_2) + \alpha_1 \cosh(2\pi\xi_1 x_2) & \cdots \\ \vdots & \vdots \\ \sin(2\pi\xi_1 x_m) - \sinh(2\pi\xi_1 x_m) - \alpha_1 \cos(2\pi\xi_1 x_m) + \alpha_1 \cosh(2\pi\xi_1 x_m) & \cdots \end{bmatrix} \cdots$$

$$\cdots \begin{bmatrix} \cdots & \sin(2\pi\xi_n x_1) - \sinh(2\pi\xi_n x_1) - \alpha_n \cos(2\pi\xi_n x_1) + \alpha_n \cosh(2\pi\xi_n x_1) \\ \cdots & \sin(2\pi\xi_n x_2) - \sinh(2\pi\xi_n x_2) - \alpha_n \cos(2\pi\xi_n x_2) + \alpha_n \cosh(2\pi\xi_n x_2) \\ & \vdots \\ \cdots & \sin(2\pi\xi_n x_m) - \sinh(2\pi\xi_n x_m) - \alpha_n \cos(2\pi\xi_n x_m) + \alpha_n \cosh(2\pi\xi_n x_m) \end{bmatrix}. \tag{5.32}$$

Performance of CS-Based ODS Reconstruction

Sections 5 and 5 discussed two different approaches of designing a potentially suitable (well conditioned) measurement matrix Φ in the presence of hyperbolic components. To recall, these two approaches are: (i) Restricted hyperbolics (ii) Combined hyperbolics. This section evaluates and compares the performance of both the approaches by varying the number of measurements m, and calculating the average l_2 error and probability of successful reconstruction of the cantilever ODS.

Performance evaluation for an undamaged beam

The cantilever beam used for analysis in this section is considered to be undamaged, i.e. the specifications are that of the original beam without any structural changes. The specifications of such a beam and the CS problem setup are as follows:

Beam Specifications:

$L = 1$, $\rho A = 1$, $EI = 1$, $N_{el} = 1000$

CS Problem Setup:

$f(t) = f_0 sin\omega_f t$, $\omega_f = 20\text{rads}^{-1}$, $f_0 = 5$

$a = 0.2$, $\Xi_r = [\xi_l,\ \xi_h] = [0,\ 25]$, *Scaling = 0.01*

Figure 5.30 (a) and (b) illustrate the variation of probability of success (PS) and average l_2 error of the cantilever beam ODS reconstruction using two different measurement matrices designed using combined and restricted hyperbolic components respectively. Recall that while the restricted frequency approach has a scaling factor of 0.01 for hyperbolic terms, the combined hyperbolic approach was formulated to eliminate the need for restriction of $sinh$ and $cosh$ terms to lower frequencies. An increase in the number of measurements is accompanied by decreasing reconstruc-

tion error and increasing PS. This behavior is consistent with the results observed in the previous sections. Because the reconstruction error provides a quantitative measure of the performance of Φ, the rest of the discussion will be based on Fig.5.30 (b).

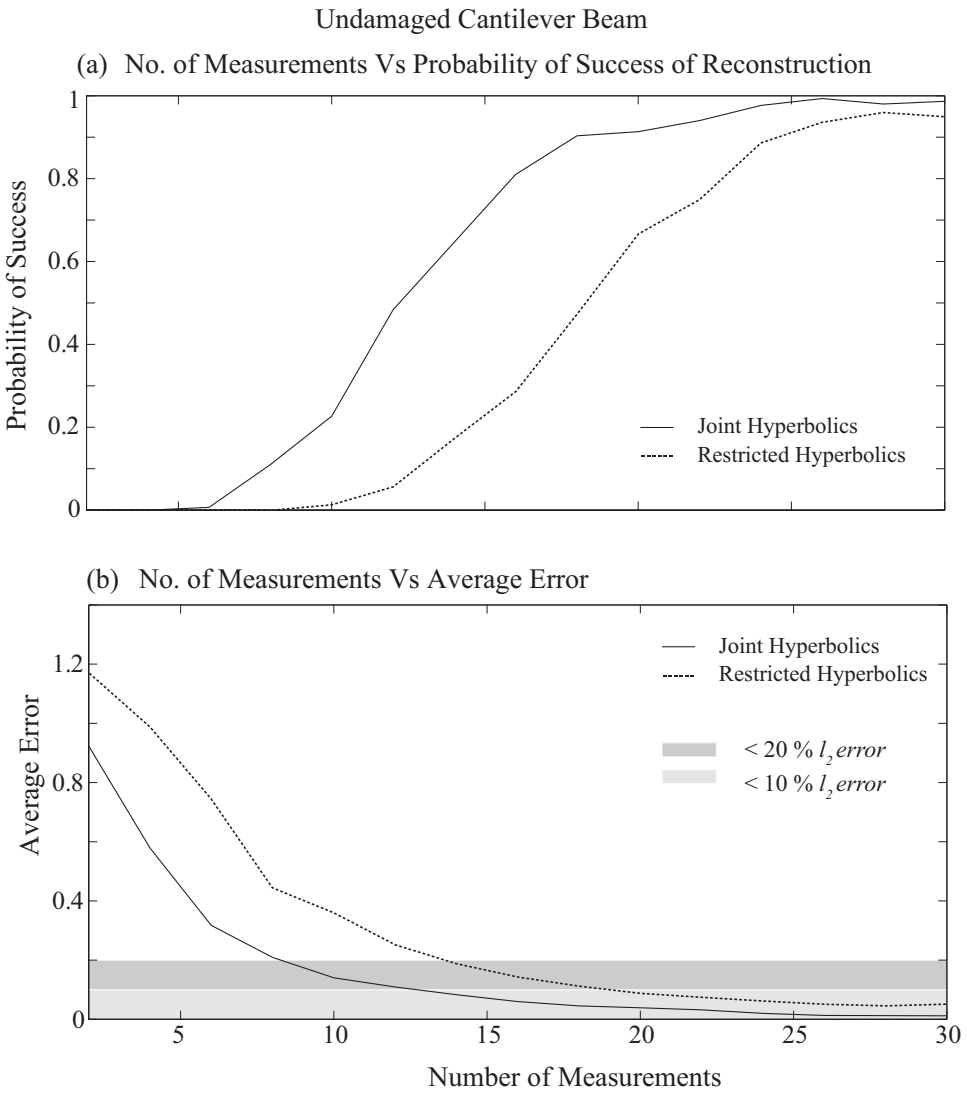

Figure 5.30: Comparing restricted and combined hyperbolics (a) Variation of probability of successful reconstruction with number of measurements (b) Variation of average l_2 error with number of measurements

It can be seen that the average l_2 error of reconstruction using either Φ falls within below 10% error

for a modest number of measurements. However, in comparison to using restricted frequency range for hyperbolic components, the combined hyperbolic approach exhibits better performance. For instance, while the average reconstruction error falls below 10% for about $m = 15$ for Φ with combined hyperbolic terms, $m = 20$ (approximately) for achieving less than 10% error for Φ with restricted hyperbolic terms. Fig.5.31 compares the ODS reconstruction for $m = 10$ and 20 for both cases of Φ. Table 5.13 lists the $\%$ drop in reconstruction error for Φ designed using both approaches.

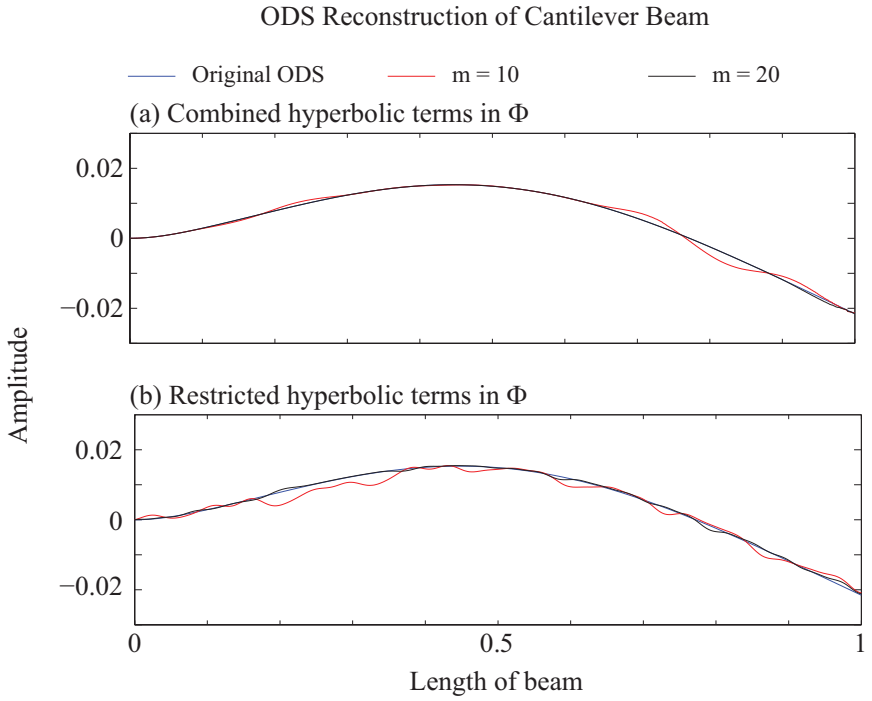

Figure 5.31: Reconstructed ODS of cantilever beam for different l_2 errors (a) Φ with combined hyperbolics (b) Φ with restricted hyperbolics

Table 5.13: l_2 Reconstruction Error for Φ with Combined and Restricted hyperbolics

No. of Measurements	Combined Hyperbolics	Restricted Hyperbolics	% Drop in l_2 error
15	0.08	0.17	9
30	0.01	0.05	4

Performance evaluation for damaged beam

The real importance of ODS reconstruction lies in localization of structural change. This section therefore examines the CS performance using both types of measurement matrices in the presence of damage in the cantilever beam. Specifically, the CS-based reconstruction is evaluated under three levels of damage: (i) Low severity (EI' = 0.9) (ii) Medium severity (EI' = 0.5) (iii) High severity (EI' = 0.1). Figure 5.32 illustrates the variation of reconstruction error for increasing number of measurements.

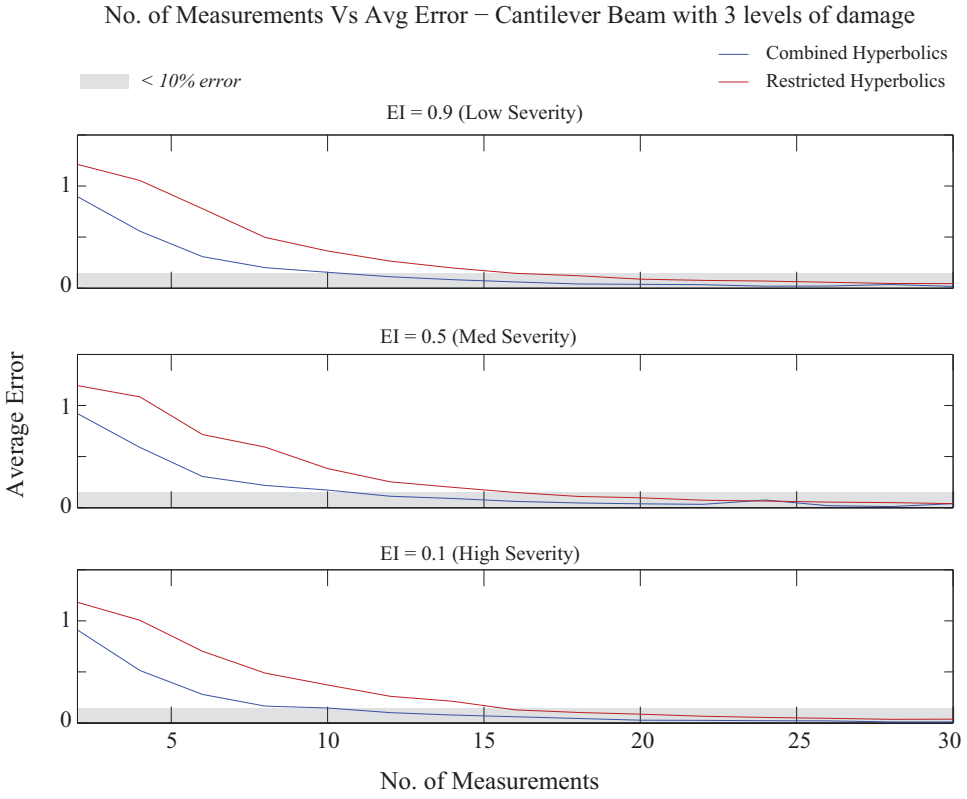

Figure 5.32: Reconstruction error vs no. of measurements: (a) Low severity damage (b) Medium severity damage (c) High severity damage

Consistent with the performance results in section 5, it can be observed that the CS-based ODS reconstruction using Φ with combined hyperbolic components has lower reconstruction error for

a given number of measurements when compared to using Φ with restricted hyperbolic terms. Examining the reconstruction errors and performance results obtained in the current and previous sections (cantilever beam with and without structural changes), it may be understood that for CS-based recovery and reconstruction in the presence of hyperbolic terms, employing a Φ where the these terms are combined is potentially effective. To reiterate, reconstruction of cantilever-type ODS (free end), hyperbolic terms play an indispensable role. Therefore, combining these terms in such a way that their overall magnitude is reduced helps to overcome the numerical inconsistencies (ill-conditioning of Φ) while still drawing required contribution from these terms. As an alternate representation, variation of probability of successful reconstruction with increasing number of measurements is shown in Fig.5.33.

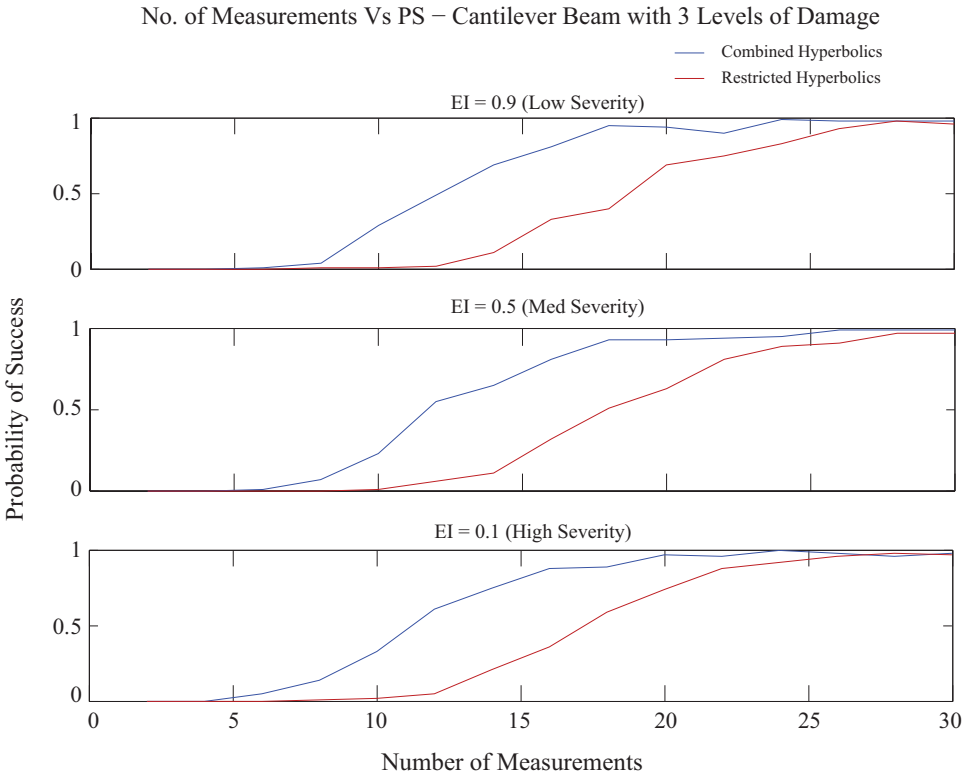

Figure 5.33: %PS vs no. of measurements: (a) Low severity damage (b) Medium severity damage (c) High severity damage

Section 5 in this chapter, described the formulation and reconstruction results for locating changes in the ODS of simply-supported, fixed-fixed and cantilever beams using compressive sampling. Formulation of the CS-based vibration problem in the spatial domain may be considered as a novel and important extension of the capability of CS from the temporal domain. The fundamental vibration characteristics of mechanical beams, i.e. their modeshapes, are used as the foundation for developing the corresponding measurement matrices. The boundary conditions of simply-supported, fixed-fixed and cantilever beams and hence their mode shape functions of these beams become increasingly complicated in that order [7]. The simply-supported beam only contains sinusoidal components in its mode shapes. Its measurement matrix Φ, shown in Eq.(5.21), therefore is composed of only sine components of those frequencies considered in the CS problem setup. Consequently, it produces consistent reconstruction in terms of fidelity and probability. However, it was observed that presence of hyperbolic functions in the measurement matrix attributed to its ill-conditioning. In fact, as hyperbolic functions become more prominent in mode shapes, the spatial data requirement increases for high quality reconstruction. As seen in Section 5, for the ODS of a fixed-fixed beam, Φ (see Eq.(5.26)) could be manipulated to containing only non-hyperbolic components. This is due to the nature of its ODS, which may be approximated to that of a simply-supported beam.

On the other hand, for a cantilever beam, these hyperbolic functions became indispensable in the measurement matrix. This dependency may stem from the free-end boundary condition of the beam that has both zero deflection and slope. For improving the condition of such a Φ that contains hyperbolic components, it was important to either eliminate them or reduce the frequency range over which hyperbolic basis functions were used. Evidently, the non-periodic and unbounded nature of the hyperbolic functions makes the Φ matrix ill-conditioned. As a result, when these com-

ponents are included in the Φ matrix without any restrictions, ℓ_1 minimization fails to produce an acceptable frequency recovery and signal reconstruction. This can be linked to the requirement of Restricted Isometry Property (RIP) discussed in Section 4. Using Eq.(4.10), the Restricted Isometry Constant δ_k is calculated for Φ matrices with and without hyperbolic components. In addition, it is calculated for the Φ matrix of the cantilever beam, that is developed from a combination of the non-hyperbolic and hyperbolic terms.

It is important to note that the standard results on l_1 recovery usually involve $2K-RIC$. From [66] and [74], it may be understood that these bounds on RIP help to guarantee signal recovery and reconstruction with overwhelming probability. Hence, while $2K - RIC$ is the standard bound, $K - RIC$ is not forbidden. In addition, the results involving $2K - RIC$ were derived for random matrices. In our application, the measurement matrix Φ is determined based on the response of the beam in temporal and spatial domains. Hence, the $K - RIC$ result is used as a guiding factor in analyzing the probability of reconstruction and not as a strict matrix deciding factor. From Eq.(4.10), it is understood that calculating δ_k for any $m \times n$ matrix is a combinatorial task that becomes computationally intensive when n is large. However, to get an understanding of how the Φ matrices compare to one another with respect to probability of reconstruction (spatial domain), n is kept small and δ_k is numerically calculated for $k = 1, \cdots 4$. Specifically, $\Xi = [0,\, 5]\text{m}^{-1}$ is chosen as the frequency range with a resolution of 0.01m^{-1}. The individual spatial frequencies are therefore, $\xi_i = 5\,(i-1)/(n-1)$, $n = 51$, $i = 1, 2, \cdots n$. The measurement matrices are: $\Phi_1 \in R^{m\times n}$ containing only $sine$ functions, $\Phi_2 \in R^{m\times 2n}$ containing both $sine$ and $cosine$ functions, and (Φ_3 and Φ_4) $\in R^{m\times 4n}$ containing $sine$, $cosine$, $sinh$ and $cosh$ functions. The Φ_3 and Φ_4

matrices are constructed as follows:

$$\Phi_3 = \begin{bmatrix} \sin(2\pi\xi_1 x_1) & \cdots & \sin(2\pi\xi_n x_1) & \cos(2\pi\xi_1 x_1) & \cdots & \cos(2\pi\xi_n x_1) & \\ \sin(2\pi\xi_1 x_2) & \cdots & \sin(2\pi\xi_n x_2) & \cos(2\pi\xi_1 x_2) & \cdots & \cos(2\pi\xi_n x_2) & \cdots \\ \vdots & \vdots & \vdots & \vdots & \vdots & \vdots & \\ \sin(2\pi\xi_1 x_m) & \cdots & \sin(2\pi\xi_n x_m) & \cos(2\pi\xi_1 x_m) & \cdots & \cos(2\pi\xi_n x_m) & \end{bmatrix}$$

$$\cdots \begin{bmatrix} \sinh(2\pi\xi_1 x_1) & \cdots & \sinh(2\pi\xi_n x_1) & \cosh(2\pi\xi_1 x_1) & \cdots & \cosh(2\pi\xi_n x_1) \\ \sinh(2\pi\xi_1 x_2) & \cdots & \sinh(2\pi\xi_n x_2) & \cosh(2\pi\xi_1 x_2) & \cdots & \cosh(2\pi\xi_n x_2) \\ \vdots & \vdots & \vdots & \vdots & \vdots & \vdots \\ \sinh(2\pi\xi_1 x_m) & \cdots & \sinh(2\pi\xi_n x_m) & \cosh(2\pi\xi_1 x_m) & \cdots & \cosh(2\pi\xi_n x_m) \end{bmatrix}. \tag{5.33}$$

$$\Phi_4 = \begin{bmatrix} \sin(2\pi\xi_1 x_1) - \sinh(2\pi\xi_1 x_1) - \cos(2\pi\xi_1 x_1) + \cosh(2\pi\xi_1 x_1) & \cdots & \\ \sin(2\pi\xi_1 x_2) - \sinh(2\pi\xi_1 x_2) - \cos(2\pi\xi_1 x_2) + \cosh(2\pi\xi_1 x_2) & \cdots & \cdots \\ \vdots & \vdots & \\ \sin(2\pi\xi_1 x_m) - \sinh(2\pi\xi_1 x_m) - \cos(2\pi\xi_1 x_m) + \cosh(2\pi\xi_1 x_m) & \cdots & \end{bmatrix}$$

$$\cdots \begin{bmatrix} \cdots & \sin(2\pi\xi_n x_1) - \sinh(2\pi\xi_n x_1) - \cos(2\pi\xi_n x_1) + \cosh(2\pi\xi_n x_1) \\ \cdots & \sin(2\pi\xi_n x_2) - \sinh(2\pi\xi_n x_2) - \cos(2\pi\xi_n x_2) + \cosh(2\pi\xi_n x_2) \\ \vdots & \\ \cdots & \sin(2\pi\xi_n x_m) - \sinh(2\pi\xi_n x_m) - \cos(2\pi\xi_n x_m) + \cosh(2\pi\xi_n x_m) \end{bmatrix}. \tag{5.34}$$

The results of δ_k for k ranging from 1 to 4, i.e. sparse vectors that have from 1 to 4 non-zero entries are illustrated in Fig.(5.34). In each case, although the number of frequencies remains the same, the size of Φ varies. In the first case, Φ_1 contains only sine components of all the frequencies. The matrix is well conditioned with δ_k showing steady reduction as the number of random samples m increases. This led to high probability of accurate ODS reconstruction for a simply-supported

beam with few data points. The performance of Φ_2 is very similar to that of Φ_1. This is expected since $sine$ and $cosine$ functions are bounded and periodic with similar magnitudes.

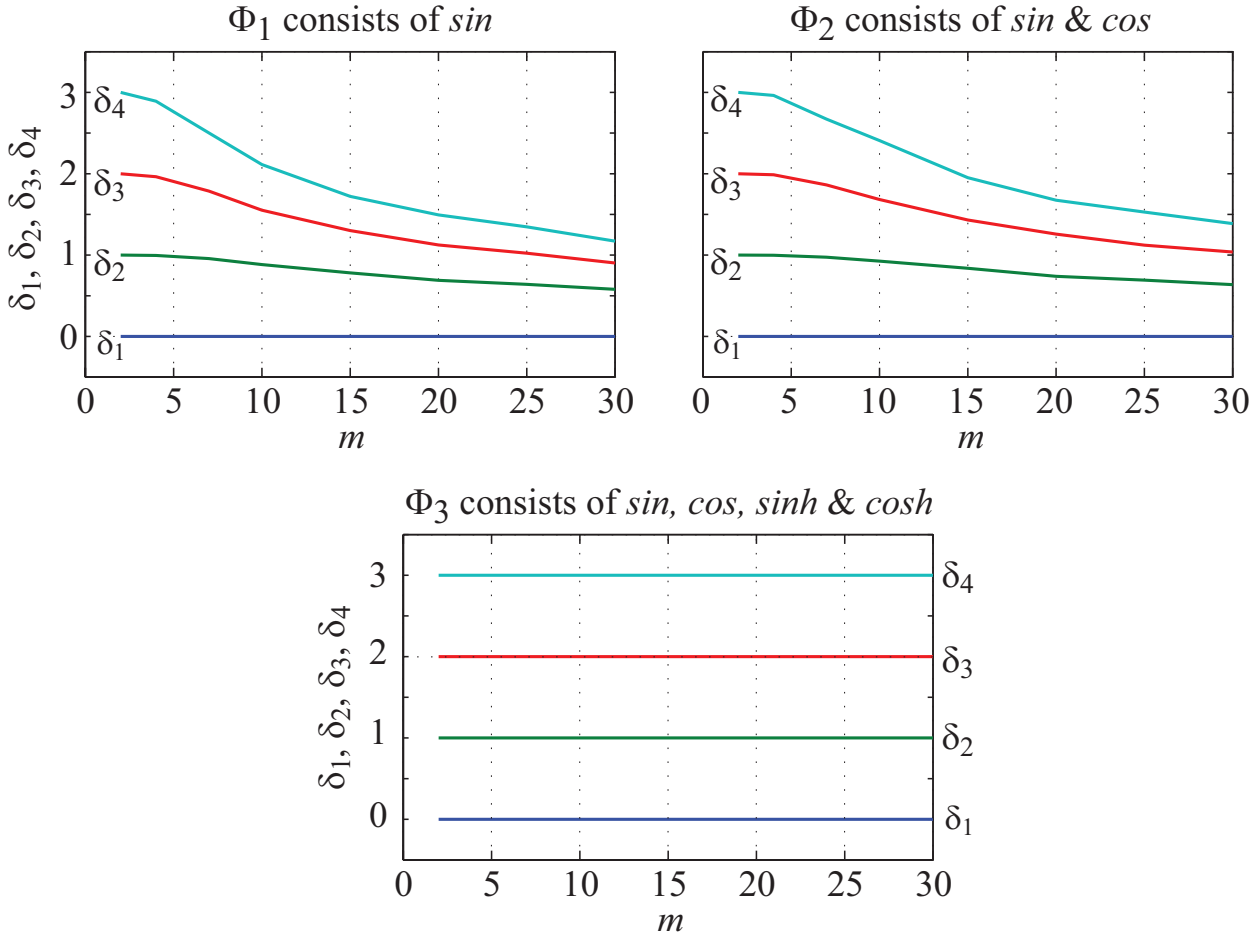

Figure 5.34: Variation of δ_k with m for different measurement matrix Φ

The matrix Φ_3 presents a more complicated case. It can be observed that in contrast to Φ_1 and Φ_2, all the calculated δ_k's are integer values and non-decreasing, indicating a computational shortcoming. This can be attributed to the presence of hyperbolic components in Φ_3. These unbounded and non-periodic functions contribute to the ill-conditioning of the matrix, thus leading to inexact or failure of reconstruction in the ODS reconstruction of a cantilever beam. Recall from Section 5

that for the cantilever beam, the frequency range of the hyperbolic functions was reduced and this helped in improving the probability of accurate reconstruction.

Effects of Incorporating Boundary Conditions in CS-Based Vibration Problem

This section explores the use of boundary conditions to potentially reduce the number of data points in reconstructing the ODS of a given beam. Consider a fixed-fixed (FF) beam as shown in Fig.5.35. It is harmonically excited at $a = 0.2$ by a harmonic forcing, $f(t) = 5sin20t$.

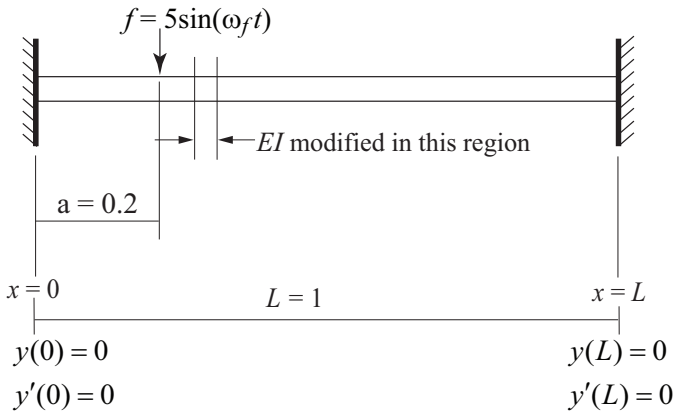

Figure 5.35: FF Beam schematic representation

Any given beam has four boundary conditions that govern its characteristic equation. For the FF beam represented above, the boundary conditions (BCs) are listed on the schematic itself. These BCs imply that either end of the FF beam have zero displacement and zero slope. When incorporated into the standard beam equation, the BCs give rise to a set of four equations. These are listed below:

$$W_n(x) = C_1 sin\beta_n x + C_2 cos\beta_n x + C_3 sinh\beta_n x + C_4 cosh\beta_n x \tag{5.35}$$

At $x = 0$ of the beam,

$$W_n(0) = C_1 sin\beta_n 0 + C_2 cos\beta_n 0 + C_3 sinh\beta_n 0 + C_4 cosh\beta_n 0 = 0 \tag{5.36}$$

$$W'_n(0) = C_1\beta_n cos\beta_n 0 - C_2\beta_n sin\beta_n 0 + C_3\beta_n cosh\beta_n 0 + C_4\beta_n sinh\beta_n 0 = 0 \tag{5.37}$$

At $x = L$ of the beam,

$$W_n(L) = C_1 sin\beta_n L + C_2 cos\beta_n L + C_3 sinh\beta_n L + C_4 cosh\beta_n L = 0 \tag{5.38}$$

$$W'_n(L) = C_1\beta_n cos\beta_n L - C_2\beta_n sin\beta_n L + C_3\beta_n cosh\beta_n L + C_4\beta_n sinh\beta_n L = 0 \tag{5.39}$$

Recall that the CS problem is essentially the l_1 minimization of an under-sampled signal from random, linear and non-adaptive measurements. In other words, for a system represented by an under-determined set of equations (where the number of equations are less than the number of unknowns), the solution to CS problem is one that has the least l_1 norm. As seen previously on numerous occasions, as the number of measurements increase, the reconstruction error drops, owing to the probabilistic solution tending toward a more definitive one. In this context, the information from boundary conditions may be treated as four measurements in addition to those taken at random points along the length of the beam. In the spatial domain, each measurement corresponds to a sensor placed on the beam. Hence, this investigation is important because it allows for four additional measurements without the use of four more sensors. The corresponding measurement matrix Φ and measurement vector z are as given below:
s

$$z = \begin{bmatrix} 0(y(0)) & z_1 & z_2 & \cdots z_m & 0(y(L)) & 0(y'(0)) & 0(y'(L)) \end{bmatrix} \tag{5.40}$$

$$\Phi = \begin{bmatrix} \sin(2\pi\xi_1 x_1) & \cdots & \sin(2\pi\xi_n x_1) & \cos(2\pi\xi_1 x_1) & \cdots & \cos(2\pi\xi_n x_1) \\ \sin(2\pi\xi_1 x_2) & \cdots & \sin(2\pi\xi_n x_2) & \cos(2\pi\xi_1 x_2) & \cdots & \cos(2\pi\xi_n x_2) \\ \vdots & \vdots & \vdots & \vdots & \vdots & \vdots \\ \sin(2\pi\xi_1 x_m) & \cdots & \sin(2\pi\xi_n x_m) & \cos(2\pi\xi_1 x_m) & \cdots & \cos(2\pi\xi_n x_m) \\ 0 & \cdots & 0 & 2\pi\xi_1 & \cdots & 2\pi\xi_n \\ -2\pi\xi_1 sin(2\pi\xi_1 L) & \cdots & -2\pi\xi_n sin(2\pi\xi_n L) & 2\pi\xi_1 cos(2\pi\xi_1 L) & \cdots & 2\pi\xi_n cos(2\pi\xi_n L) \end{bmatrix} \tag{5.41}$$

Figure 5.36 shows four plots, each illustrating the effect of incorporating boundary conditions of the FF beam while solving the CS problem. Four cases of ODS reconstruction were examined - FF beam without structural changes and FF beam with three degrees of severity of structural change. Recall that structural change in the FF beam is introduced by simulating change in stiffness coefficient (EI) over certain number of elements of the finite element model. For each of the four cases, the ODS was reconstructed for varying number of measurements and the average l_2 error was calculated over 100 trials. It is important to note that the CS problem (ODS reconstruction) with BCs included always had four more measurements. For instance, for the CS problem without BCs, when $m = 10$, the same problem with BCs was solved using $m = 10 + 4$ measurements. From Fig.5.36, it can be observed that incorporating BCs did not greatly influence in bringing down the reconstruction error. In fact, while setting up this exploration, it was expected that the BCs may not play a significant role when the number of measurements was already sufficient or sufficiently high to solve the CS problem. The region of focus was, therefore, when the number of measurements was lower than optimal, i.e. when $m < kln(\frac{n}{k})$. Specifically, with respect to the FF beam considered here, the minimum number of measurements is approximated at $m \approx 15$. And, for $m < 15$, including BCs for solving the CS problem does help in reducing the reconstruction error, because it essentially increases the number of measurements without actually having to "measure" the amplitude at those points. However, this reduction in error is not significant enough to noticeably improve the ODS reconstruction.

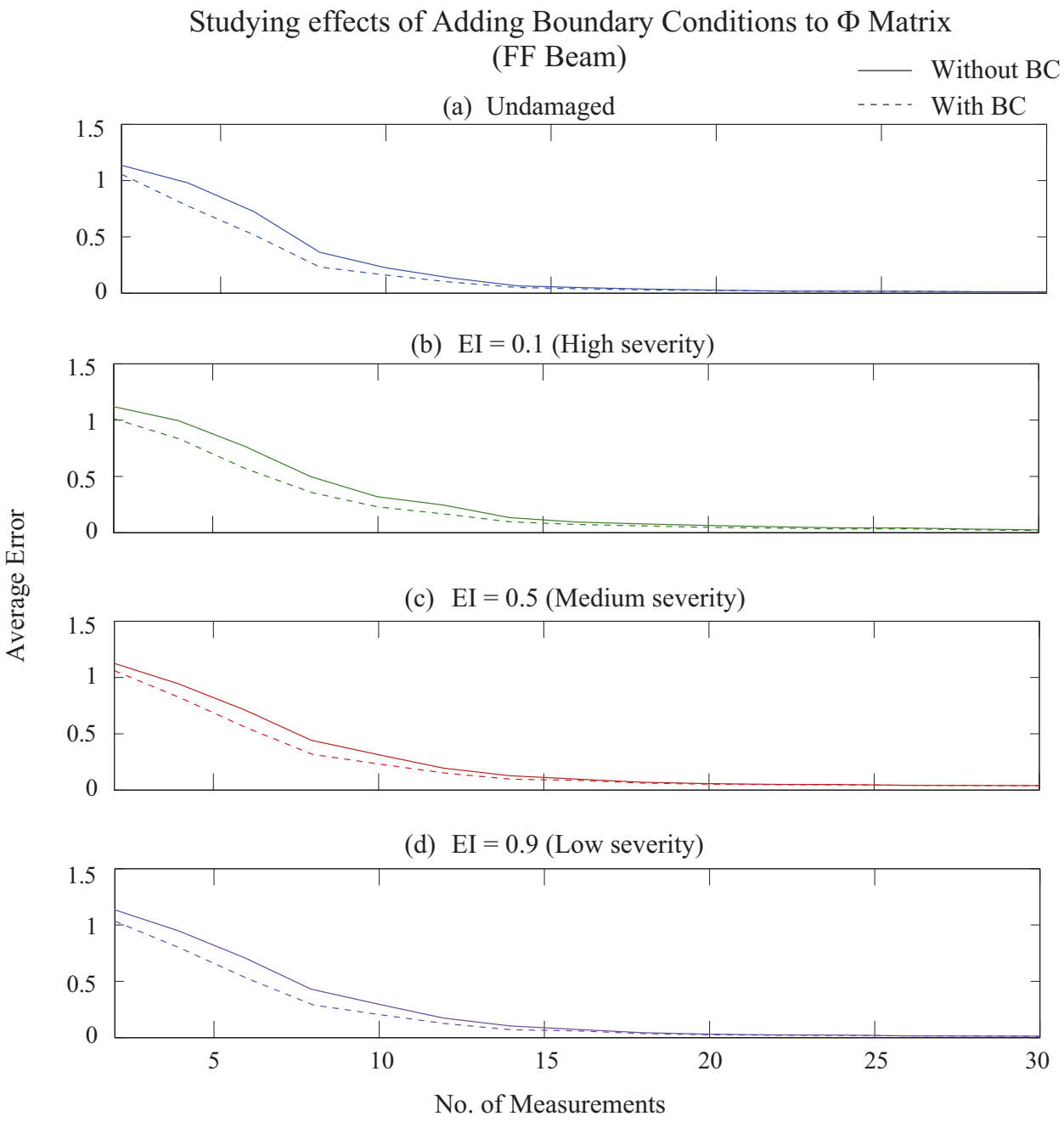

Figure 5.36: Effect of incorporating boundary conditions on ODS reconstruction error of fixed-fixed beam (a) Undamaged (b) High severity (c) Medium severity (d) Low severity

CHAPTER 6: CONCLUSION

This research shows the application of CS in vibration-based monitoring of mechanical structures. To demonstrate its viability, this study focuses on lateral vibration of fundamental beams such as simply-supported, fixed-fixed and cantilever beams. Recovery of natural frequencies from free vibration data using CS is demonstrated, which enables detecting structural changes in the corresponding beam. The inherent sparsity in frequency domain is exploited by CS to enable accurate recovery from random and under-sampled data. Subsequently, CS is extended to spatial domain and used to reconstruct ODS from random spatially distributed vibration data. This step can potentially help localize any structural change. Here again, sparsity of mode shapes is utilized by CS to deliver accurate reconstruction with limited sensing.

In addition to simulation results that demonstrated the feasibility of CS-based detection and localization of structural changes, preliminary experimental validation for detecting shift in natural frequencies of a cantilever beam is presented. CS-based recovery was tested for two configurations of structural change (tip and mid-length), each with six different values of added mass. The shift in natural frequencies thus produced, followed a trend similar to that expected due to varying levels of damage/structural change. In these experiments, CS based recovery was feasible without explicit formulation for handling of noise in the ℓ_1 minimization problem. Also, filtering of noise was not required. However, more complex structures may have amplitudes of vibration comparable to noise, which might warrant explicit formulation of noise in the ℓ_1 minimization problem.

With this in view, the performance of CS-based recovery and reconstruction with a formulation for handling noise was examined for three cases - sinusoidal signal with multiple frequencies (simulation), SS beam temporal domain free vibration response (simulation) and cantilever beam temporal free vibration response (experimental). In simulation, the effect of noise formulation was evalu-

ated by varying the SNR, while in the experimental result, the effect was evaluated by varying the number of measurements. This provided a quantitative understanding of including noise handling. Boundary conditions of a beam provide valuable information about its configuration and play a decisive role in its characteristic equation. The effect of incorporating this information while solving the CS problem is also explored, using a FF beam.

Designing a suitable measurement matrix is an important part of successfully solving any CS problem. When extended to the spatial domain or ODS reconstruction, the measurement matrix will depend on the boundary conditions of the beam under consideration. In the presence of hyperbolic components in the spatial domain response, the measurement matrix Φ has to be modified to handle numerical inconsistencies that stem from the unboundedness of such terms. Following this, two approaches for designing a suitable Φ for reconstructing the ODS of a cantilever beam was investigated.

Future Scope of this Research

Formulation of compressive sensing for mechanical vibrations is in its nascent stages. In fact, during this research, it was quite evident that the literature on this topic and related challenges was scarce. This work provides a fundamental and initial effort in formulation of CS-based vibration monitoring and diagnostics, and further research is needed in many fronts. Listed below are some aspects of CS and CS-based vibration monitoring problems that will be examined as an extension of this work. Some of this work was derived from an NSF proposal that was submitted as a result of this research.

Improving the Restricted Isometry Property (RIP) of measurement matrix in the presence of hyperbolic components: In section 5, two approaches to designing a suitable measurement matrix Φ were discussed in detail. However, investigation into these approaches opened a wider avenue

of research. Further exploration of different ways of combining the hyperbolic terms in formulating the Φ will be discussed and their performance evaluated. Approximation of the modeshape equation for a cantilever beam will also be looked into.

Extension to complicated structures: The work in this dissertation was focused on developing the fundamental framework for CS-based vibration monitoring and diagnostics for mechanical structures. While this work entailed standard beams (simply supported, fixed-fixed and cantilever), realization of this work outside laboratory environment mandates its extension to more complicated structures. This will be an important aspect of future work.

Quantifying the location of structural change: A standard procedure for locating fault from deflection must be established. One way is to numerically compute the absolute curvature along the beam-span, $\kappa = |y''|/(1 + y'^2)^{3/2}$, from the reconstructed deflection and identify peaks in its distribution.

Synchronization of sensor-data by using data-packets: As mentioned before, spatial data will inevitably be staggered in time, at least to a small extent. This will be a source of reconstruction error. One way to address this, without significantly increasing the volume of data, is for sensors to transmit a small packet of equispaced data instead of a single value. Then, by finding the overlapped interval $[t_1, t_2]$ from all data-packets, the deflection at each sensor-location at $\bar{t} \in [t_1, t_2]$ can be found by averaging.

A Unified Spatio-temporal Compressive Sensing Framework: The goal of this task is to address the temporal (frequency recovery) and spatial (deflection reconstruction) problems within a unified framework. The approach will allow a greater flexibility in the use of data from sensors that are spatially distributed along a structure. The framework will be particularly useful when data obtained are simultaneously randomized in space and time.

LIST OF REFERENCES

[1] Shi, Z. Y., Law, S. S., and Zhang, L. M., 2000. "Structural damage detection from modal strain energy change". *Journal of Engineering Mechanics,* **126**(12), pp. 1216–1223.

[2] About america's infrastructure. American Society of Civil Engineers, 2013.

[3] Tandon, N., and Choudhury, A., 1999. "A review of vibration and acoustic measurement methods for the detection of defects in rolling element bearings". *Tribology international,* **32**(8), pp. 469–480.

[4] Ghoshal, A., Sundaresan, M. J., Schulz, M. J., and Pai, P. F., 2000. "Structural health monitoring techniques for wind turbine blades". *Journal of Wind Engineering and Industrial Aerodynamics,* **85**(3), pp. 309–324.

[5] Raghavan, A., and Cesnik, C. E. S., 2007. "Review of guided-wave structural health monitoring". *The Shock and Vibration Digest,* **39**, pp. 91–114.

[6] Doebling, S. W., Farrar, C. R., Prime, M. B., and Shevitz, D. W., 1996. Damage identification and health monitoring of structural and mechanical systems from changes in their vibration characteristics: A literature review. Tech. rep., Los Alamos National Lab., NM, USA.

[7] Rao, S. S., 2011. *Mechanical vibrations*, 5 ed. Prentice Hall.

[8] Inman, D. J., 1996. *Engineering Vibration*. Prentice Hall.

[9] Aktan, A. E., Catbas, F. N., Grimmelsman, K. A., and Tsikos, C. J., 2000. "Issues in infrastructure health monitoring for management". *Journal of Engineering Mechanics,* **126**(7), pp. 711–724.

[10] Catbas, F. N., and Aktan, A. E., 2002. "Condition and damage assessment: issues and some promising indices". *Journal of Structural Engineering,* **128**(8), pp. 1026–1036.

[11] Catbas, F. N., Gokce, H. B., and Gul, M., 2012. "Nonparametric analysis of structural health monitoring data for identification and localization of changes: Concept, lab, and real-life studies". *Structural Health Monitoring,* **11**(5), pp. 613–626.

[12] Unser, M., 2000. "Sampling-50 years after shannon". *Proceedings of the IEEE,* **88**(4), pp. 569–587.

[13] Baraniuk, R. G., 2011. "More is less: signal processing and the data deluge". *Science,* **331**(6018), pp. 717–719.

[14] Carden, E. P., and Fanning, P., 2004. "Vibration based condition monitoring: A review". *Structural Health Monitoring,* **3**(4), pp. 355–377.

[15] Farrar, C. R., and Doebling, S. W., 1999. "Damage detection and evaluation ii: Field applications to large structures". In *Modal Analysis and Testing*, J. M. M. Silva and N. M. M. Maia, eds. Springer.

[16] Adams, R. D., Cawley, P., Pye, C. J., and Stone, B. J., 1978. "A vibration technique for non-destructively assessing the integrity of structures". *Journal of Mechanical Engineering Science,* **20**(2), pp. 93–100.

[17] Samman, M. M., and Biswas, M., 1994. "Vibration testing for nondestructive evaluation of bridges. i: Theory". *Journal of Structural Engineering,* **120**(1), pp. 269–289.

[18] Samman, M. M., and Biswas, M., 1994. "Vibration testing for nondestructive evaluation of bridges. ii: Results". *Journal of Structural Engineering,* **120**(1), pp. 290–306.

[19] Aktan, A. E., Farhey, D. N., Helmicki, A. J., Brown, D. L., Hunt, V. J., Lee, K.-L., and Levi, A., 1997. "Structural identification for condition assessment: Experimental arts". *Journal of Structural Engineering,* **123**(12), pp. 1674–1684.

[20] Maia, N. M. M., and Silva, J. M. M., 1997. *Theoretical and experimental modal analysis*. Research Studies Press Ltd.

[21] Cawley, P., and Adams, R. D., 1979. "The location of defects in structures from measurements of natural frequencies". *The Journal of Strain Analysis for Engineering Design,* **14**(2), pp. 49–57.

[22] Salawu, O. S., 1997. "Detection of structural damage through changes in frequency: A review". *Engineering structures,* **19**(9), pp. 718–723.

[23] Banks, H. T., Inman, D. J., Leo, D. J., and Wang, Y., 1996. "An experimentally validated damage detection theory in smart structures". *Journal of Sound and Vibration,* **191**(5), pp. 859–880.

[24] Kessler, S. S., Spearing, S. M., Atalla, M. J., Cesnik, C. E. S., and Soutis, C., 2002. "Damage detection in composite materials using frequency response methods". *Composites Part B: Engineering,* **33**(1), pp. 87–95.

[25] Chen, H. L., Spyrakos, C. C., and Venkatesh, G., 1995. "Evaluating structural deterioration by dynamic response". *Journal of Structural Engineering,* **121**(8), pp. 1197–1204.

[26] Chang, P. C., Faltau, A., and Liu, S., 2003. "Review paper: Health monitoring of civil infrastructure". *Structural Health Monitoring,* **2**(3), pp. 257–267.

[27] Farrar, C. R., Baker, W. E., Bell, T. M., Cone, K. M., Darling, T. W., Duffey, T. A., Eklund, A., and Migliori, A., 1994. Dynamic characterization and damage detection in the i-40 bridge over the rio grande. Tech. rep., Los Alamos National Lab., NM (United States).

[28] Law, S. S., Ward, H. S., Shi, G. B., Chen, R. Z., Waldron, P., and Taylor, C., 1995. "Dynamic assessment of bridge load-carrying capacities. i". *Journal of Structural Engineering,* **121**(3), pp. 478–487.

[29] Law, S. S., Ward, H. S., Shi, G. B., Chen, R. Z., Waldron, P., and Taylor, C., 1995. "Dynamic assessment of bridge load-carrying capacities. ii". *Journal of Structural Engineering,* **121**(3), pp. 488–495.

[30] Pereira, J. A., Heylen, W., Lammens, S., and Sas, P., 1995. "Influence of the number of frequency points and resonance frequencies on modal updating techniques for health condition monitoring and damage detection of flexible structure". In Proceedings-SPIE The International Society for Optical Engineering, pp. 1273–1273.

[31] Pereira, J. A., Heylen, W., Lammens, S., and Sas, P., 1994. "Model updating and failure detection based on experimental frf's: Case study on a space frame structure". In Proceedings of the International Conference on Noise and Vibration Engineering, pp. 669–681.

[32] Mannan, M. A., and Richardson, M. H., 1990. "Detection and location of structural cracks using FRF measurements". In Proc. of the 8th International Modal Analysis Conference, Vol. 1, pp. 652–657.

[33] Morassi, A., 2001. "Identification of a crack in a rod based on changes in a pair of natural frequencies". *Journal of Sound and Vibration,* **242**(4), pp. 577–596.

[34] Trendafilova, I., and Heylen, W., 1998. "Fault localization in structures from remote frf measurements. influence of the measurement points". In Proceedings of the International Conference on Noise and Vibration Engineering, Leuven, Belgium, pp. 149–156.

[35] Johnson, T. J., and Adams, D. E., 2002. "Transmissibility as a differential indicator of structural damage". *Journal of Vibration and Acoustics,* **124**(4), pp. 634–641.

[36] Ewins, D. J., 2000. *Modal testing: Theory and practice*, 2 ed. Research Studies Press Ltd.

[37] Allemang, R. J., and Brown, D. L., 1982. "A correlation coefficient for modal vector analysis". In Proceedings of the 1st International Modal Analysis Conference, Orlando, FL, Vol. 1, pp. 110–116.

[38] Lieven, N. A. J., and Ewins, D. J., 1988. "Spatial correlation of mode shapes, the coordinate modal assurance criterion (COMAC)". In Proceedings of the 4th International Modal Analysis Conference, Vol. 1, pp. 690–695.

[39] Frỳba, L., and Pirner, M., 2001. "Load tests and modal analysis of bridges". *Engineering Structures,* **23**(1), pp. 102–109.

[40] Chance, J., Tomlinson, J. R., and Worden, K., 1994. "A simplified approach to the numerical and experimental modelling of the dynamics of a cracked beam". *Proc. SPIE Vol. 2251, Proceedings of the 12th International Modal Analysis Conference*, pp. 778–785.

[41] Ren, W.-X., and De Roeck, G., 2002. "Structural damage identification using modal data. i: Simulation verification". *Journal of Structural Engineering,* **128**(1), pp. 87–95.

[42] Ren, W.-X., and De Roeck, G., 2002. "Structural damage identification using modal data. ii: Test verification". *Journal of Structural Engineering,* **128**(1), pp. 96–104.

[43] Alampalli, S., Fu, G., and Dillon, E. W., 1997. "Signal versus noise in damage detection by experimental modal analysis". *Journal of Structural Engineering,* **123**(2), pp. 237–245.

[44] Ratcliffe, C. P., and Bagaria, W. J., 1998. "Vibration technique for locating delamination in a composite beam". *AIAA journal,* **36**(6), pp. 1074–1077.

[45] Wahab, M. M. A., and De Roeck, G., 1999. "Damage detection in bridges using modal curvatures: application to a real damage scenario". *Journal of Sound and Vibration,* **226**(2), pp. 217–235.

[46] Oh, B., and Jung, B., 1998. "Structural damage assessment with combined data of static and modal tests". *Journal of Structural Engineering,* **124**(8), pp. 956–965.

[47] Wahab, M. M. A., 2001. "Effect of modal curvatures on damage detection using model updating". *Mechanical Systems and Signal Processing,* **15**(2), pp. 439–445.

[48] Sampaio, R. P. C., Maia, N. M. M., and Silva, J. M. M., 1999. "Damage detection using the frequency-response-function curvature method". *Journal of Sound and Vibration,* **226**(5), pp. 1029–1042.

[49] Kim, J.-T., and Stubbs, N., 1995. "Model-uncertainty impact and damage-detection accuracy in plate girder". *Journal of Structural Engineering,* **121**(10), pp. 1409–1417.

[50] Salawu, O. S., and Williams, C., 1995. "Bridge assessment using forced-vibration testing". *Journal of structural engineering,* **121**(2), pp. 161–173.

[51] Shi, Z. Y., Law, S. S., and Zhang, L. M., 2000. "Damage localization by directly using incomplete mode shapes". *Journal of Engineering Mechanics,* **126**(6), pp. 656–660.

[52] Kim, J.-T., and Stubbs, N., 2002. "Improved damage identification method based on modal information". *Journal of Sound and Vibration,* **252**(2), pp. 223–238.

[53] Chen, H.-L. R., and Kiriakidis, A. C., 2000. "Stiffness evaluation and damage detection of ceramic candle filters". *Journal of engineering mechanics,* **126**(3), pp. 308–319.

[54] Stubbs, N., and Kim, J.-T., 1996. "Damage localization in structures without baseline modal parameters". *Aiaa Journal,* **34**(8), pp. 1644–1649.

[55] Catbas, F. N., Gokce, H. B., and Gul, M., 2012. "Nonparametric analysis of structural health monitoring data for identification and localization of changes: Concept, lab, and real-life studies". *Structural Health Monitoring*, p. 1475921712451955.

[56] Pai, P. F., and Young, L. G., 2001. "Damage detection of beams using operational deflection shapes". *International journal of solids and structures,* **38**(18), pp. 3161–3192.

[57] Waldron, K., Ghoshal, A., Schulz, M. J., Sundaresan, M. J., Ferguson, F., Pai, P. F., and Chung, J. H., 2002. "Damage detection using finite element and laser operational deflection shapes". *Finite Elements in Analysis and Design,* **38**(3), pp. 193–226.

[58] Wu, M., Chen, X., and Liu, C. R., 2002. "Highway crack monitoring system". In SPIE's 9th Annual International Symposium on Smart Structures and Materials, pp. 293–299.

[59] Solís, M., Algaba, M., and Galvín, P., 2013. "Continuous wavelet analysis of mode shapes differences for damage detection". *Mechanical Systems and Signal Processing,* **40**(2), pp. 645–666.

[60] Rucka, M., and Wilde, K., 2006. "Crack identification using wavelets on experimental static deflection profiles". *Engineering structures,* **28**(2), pp. 279–288.

[61] Poudel, U. P., Fu, G., and Ye, J., 2005. "Structural damage detection using digital video imaging technique and wavelet transformation". *Journal of Sound and Vibration,* **286**(4), pp. 869–895.

[62] Messina, A., 2008. "Refinements of damage detection methods based on wavelet analysis of dynamical shapes". *International Journal of Solids and Structures,* **45**(14), pp. 4068–4097.

[63] Wang, Q., and Deng, X., 1999. "Damage detection with spatial wavelets". *International journal of solids and structures,* **36**(23), pp. 3443–3468.

[64] Montanari, L., Basu, B., Spagnoli, A., and Broderick, B. M., 2015. "A padding method to reduce edge effects for enhanced damage identification using wavelet analysis". *Mechanical Systems and Signal Processing,* **52**, pp. 264–277.

[65] Montanari, L., Spagnoli, A., Basu, B., and Broderick, B., 2015. "On the effect of spatial sampling in damage detection of cracked beams by continuous wavelet transform". *Journal of Sound and Vibration,* **345**, pp. 233–249.

[66] Fornasier, M., and Rauhut, H., 2011. "Compressive sensing". In *Handbook of mathematical methods in imaging*. Springer, pp. 187–228.

[67] Bao, Y., Beck, J. L., and Li, H., 2010. "Compressive sampling for accelerometer signals in structural health monitoring". *Structural Health Monitoring*.

[68] Chardon, G., Leblanc, A., and Daudet, L., 2011. "Plate impulse response spatial interpolation with sub-nyquist sampling". *Journal of sound and vibration,* **330**(23), pp. 5678–5689.

[69] Dokmanić, I., and Vetterli, M., 2012. "Room helps: Acoustic localization with finite elements". In 2012 IEEE International Conference on Acoustics, Speech and Signal Processing (ICASSP), Ieee, pp. 2617–2620.

[70] Chardon, G., Nowakowski, T., De Rosny, J., and Daudet, L., 2015. "A blind dereverberation method for narrowband source localization". *IEEE Journal of Selected Topics in Signal Processing,* **9**(5), pp. 815–824.

[71] Sanandaji, B. M., Vincent, T. L., Poolla, K., and Wakin, M. B., 2012. "A tutorial on recovery conditions for compressive system identification of sparse channels". In 2012 IEEE 51st Annual Conference on Decision and Control (CDC), IEEE, pp. 6277–6283.

[72] Boyd, S., and Vandenberghe, L., 2004. *Convex optimization*. Cambridge university press.

[73] Candès, E. J., 2006. "Compressive sampling". In Proceedings of the International Congress of Mathematicians, Vol. 3, Madrid, Spain, pp. 1433–1452.

[74] Foucart, S., and Rauhut, H., 2013. *A mathematical introduction to compressive sensing*. Springer.

[75] Ganesan, V., Das, T., Rahnavard, N., and Kauffman, J. L., 2017. "Vibration-based monitoring and diagnostics using compressive sensing". *Journal of Sound and Vibration,* **394**, pp. 612–630.

[76] Ganesan, V., Das, T., Kauffman, J. L., and Rahnavard, N. "Including vibration characteristics within compressive sensing formulations for structural monitoring of beams". *Proceedings of the 2017 ASME Dynamic Systems and Controls Conference, Accepted*.

[77] Daubechies, I., Defrise, M., and De Mol, C., 2004. "An iterative thresholding algorithm for linear inverse problems with a sparsity constraint". *Communications on pure and applied mathematics,* **57**(11), pp. 1413–1457.

[78] Ramlau, R., and Teschke, G., 2010. "Sparse recovery in inverse problems". *Theoretical foundations and numerical methods for sparse recovery,* **9**, pp. 201–262.

[79] ElShahaby, F. E. A., Landman, B. A., and Prince, J. L., 2011. "Effect of regularization parameter and scan time on crossing fibers with constrained compressed sensing". In SPIE Medical Imaging, International Society for Optics and Photonics, pp. 79624J–79624J.

[80] Xiao, P., Li, C., and Ze, Y., 2011. "Effects of noise, sampling rate and signal sparsity for compressed sensing synthetic aperture radar pulse compression". In Geoscience and Remote Sensing Symposium (IGARSS), 2011 IEEE International, IEEE, pp. 656–659.

[81] Boufounos, P., Duarte, M. F., and Baraniuk, R. G., 2007. "Sparse signal reconstruction from noisy compressive measurements using cross validation". In Statistical Signal Processing, 2007. SSP'07. IEEE/SP 14th Workshop on, IEEE, pp. 299–303.

[82] Baraniuk, R. G., 2007. "Compressive sensing". *IEEE signal processing magazine,* **24**(4).

[83] Sugino, C., Xia, Y., Leadenham, S., Ruzzene, M., and Erturk, A., 2016. "A general theory for bandgap estimation in locally resonant metastructures". *arXiv preprint arXiv:1612.03130*.